Isolation and Characterization of Oxidized Lysozyme Variants Produced by a Copper (II)/Hydrogen Peroxide Metal-Catalyzed Oxidation System

by

Cory E. Muraco

Submitted in Partial Fulfillment of the Requirements

for the Degree of

Master of Science

in the

Chemistry

Program

YOUNGSTOWN STATE UNIVERSITY

May, 2013

Isolation and Characterization of Oxidized Lysozyme Variants Produced by a Copper (II)/Hydrogen Peroxide Metal-Catalyzed Oxidation System

Cory E. Muraco

I hereby release this thesis to the public. I understand that this thesis will be made available from the OhioLINK ETD Center and the Maag Library Circulation Desk for public access. I also authorize the University or other individuals to make copies of this thesis as needed for scholarly research.

Signature:

_____

Cory E. Muraco, Student Date

Approvals:

_____

Dr. Michael A. Serra, Thesis Advisor Date

_____

Dr. Nina V. Stourman, Committee Member Date

_____

Dr. Gary R Walker, Committee Member Date

_____

Bryan DePoy, Interim Dean of School of Graduate Studies and Research Date

ABSTRACT

Protein oxidation has been correlated with several chronic diseases including Alzheimer's disease, Parkinson's disease, and cataractogenesis. The purpose of this project was to isolate and characterize the various oxidized forms of hen egg white lysozyme that were produced by a copper(II)/hydrogen peroxide metal-catalyzed oxidation system. Five oxidized protein variants were purified using high performance liquid chromatography on a cation-exchange column. Tandem mass spectrometry determined that several amino acids were oxidized in each variant with histidine 15 being the most readily oxidized residue. Bacteriolytic assays showed decreased activity of Peaks IB, IIB, and III (31.4%, 61.2%, and 86.5%, respectively) relative to native enzyme while the activity for Peaks IV and V was greater than that of native enzyme (215% and 308%, respectively). Crystals of Peaks IB, III, IV, and V were grown, but attempts to determine the crystal structure were unsuccessful.

ACKNOWLEDGEMENTS

I would like to first thank my advisor and mentor, Dr. Michael Serra, for his help and guidance throughout the entirety of this project. He is an amazing professor and a wonderful person, and I have become a better scientist through his guidance and support. I would also like to thank Dr. Nina Stourman and Dr. Gary Walker for taking the time to be on my thesis defense committee and for their helpful comments throughout writing this thesis. I also extend my gratitude to the other members of the Serra Research Group, especially Nichole Patton, Roger Raby, and Praneeth Samalla, for helping me with this project and for the excellent, and sometimes off-topic, conversations that would brighten my day. Finally, I would like to acknowledge the Youngstown State University Department of Chemistry for supporting this project.

I would like to also thank Dr. Andrew Alpert at Poly LC Inc. for assistance in analyzing the HPLC results, Dr. Vivian Yee at Case Western Reserve University for attempting to determine the crystal structure of the oxidized protein variants and Dr. Kari Green at The Ohio State University for assistance in analyzing the tandem mass spectrometry results. I would also like to extend my gratitude to Dr. Jackob Moskovitz at Kansas State University for providing the M15 *E. coli* cells used in the MsrA work.

Finally, I would like to extend my deepest gratitude to my mom, Lori Muraco, my dad, Jerry Muraco, and my brother, Logan Muraco, for their love and support during my time working on this project. They always encouraged me and told me to never give up, even in my darkest hours, and without their support, this thesis would not have been possible.

TABLE OF CONTENTS

LIST OF FIGURES

LIST OF EQUATIONS

LIST OF TABLES

LIST OF ABBREVIATIONS

Arg	Arginine
Asp	Aspartate
BLAST	Basic local alignment search tool
Cys	Cysteine
DNA	Deoxyribonucleic acid
DTT	Dithiotheritol
EDTA	Ethylenediaminetetraacetic acid
ESI	Electrospray ionization
fRMsr	Free methionine sulfoxide reductase B
GEWL	Goose egg white lysozyme
Glu	Glutamate
GSH	Glutathione
GSSG	Glutathione disulfide
H_2O_2	Hydrogen peroxide
HEWL	Hen egg white lysozyme
His (H)	Histidine
$HO^{\bullet}$	Hydroxyl radical
HPLC	High performance liquid chromatography
IPTG	Isopropyl-β-D-thiogalactopyranoside
K_a	Acid dissociation constant
K_d	Dissociation constant
KP_i	Potassium phosphate
LB	Luria-Bertini
LC	Liquid chromatography
Leu	Leucine
Lys	Lysine
MCO	Metal-catalyzed oxidation
Met (M)	Methionine
MetO	Methionine sulfoxide
MS	Mass spectrometry
MsrA	Methionine sulfoxide reductase A
MsrB	Methionine sulfoxide reductase B
NADPH	Reduced nicotinamide adenine dinucleotide phosphate
NAG	*N*-acetylglucosamine
NAM	*N*-acetylmuramic acid
NaP_i	Sodium phosphate
$O_2^{\bullet-}$	Superoxide anion
PEG	Polyethylene glycol
Pro	Proline

ROS	Reactive oxygen species
SDS-PAGE	Sodium dodecyl sulfate-polyacrylamide gel electrophoresis
TFA	Trifluoroacetic acid
Thr	Threonine
TjL	*Tapes japonica* lysozyme
Trp (W)	Tryptophan
Tyr	Tyrosine
UV-VIS	Ultraviolet-Visible

CHAPTER 1: INTRODUCTION

Reactive Oxygen Species

Oxygen is an essential molecule for aerobic organisms. Oxygen serves several functions once it enters an organism. These functions include acting as the final electron acceptor in the electron transport chain in oxidative phosphorylation as well as providing a source of oxygen for biochemical processes such as the exchange of oxygen for carbon dioxide in vertebrates and photosynthesis in autotrophs. However, oxygen can become a hazard to cells if it gets reduced and becomes more reactive. Oxygen, during its complete reduction to water, forms several reactive oxygen species (ROS) that can cause oxidative damage to all classes of biological molecules. This reduction sequence is summarized in Equation 1-1:

$$O_2 \xrightarrow{e^-} O_2^{\bullet -} \xrightarrow{e^- + 2\,H^+} H_2O_2 \xrightarrow{e^-} OH^{\bullet} \xrightarrow{e^- + H^+} H_2O \qquad \text{(Equation 1-1)}$$

where $O_2^{\bullet -}$ is the superoxide anion, H_2O_2 is hydrogen peroxide, and $OH^{\bullet}$ is the hydroxyl radical. The electrons in the above reactions can come from several sources including electron leakage from the electron transport chain in mitochondria, transition metals, and exogenous sources such as cigarette smoke, smog, and radiation. Kinetic studies have shown that $OH^{\bullet}$ is the most reactive ROS, reacting at diffusion controlled rates.[1]

Oxidative Damage Caused by ROS

Once a reactive oxygen species enters the cell, it can cause extensive damage to proteins, nucleic acids, and lipids. Unsaturated fatty acids, which contain one or more carbon-carbon double bonds, can be oxidized by the hydroxyl radical resulting in lipid peroxidation. This peroxidation is due to the easy abstraction of methylene group hydrogens that are adjacent to the double bond.[1]

ROS can cause oxidative damage to both nuclear and mitochondrial DNA. The hydroxyl radical can cause oxidation and modification of the nitrogenous bases of DNA such as the C-8 hydroxylation of guanine to form 8-oxo-7,8-dihydro-2′-deoxyguanosine as well as the formation of other oxidized bases such as 8-hydroxyadenine, and 2,6-diamino-4-hydroxy-5-formaminodipyrimidine. These modified nitrogenous bases can cause mismatches in the base pairing of the nucleotides, thus creating errors in transcription and translation.[1] As an example of how detrimental these modifications can be, Hussain *et al.* has shown that such mutations can lead to the suppression of the *p53* tumor-suppressor gene, which is an essential gene for maintaining the cell cycle.[2]

Oxidation of proteins occurs mostly by the oxidation of amino acid side chains. These modifications can cause structural changes that alter the catalytic efficiency in some enzymes. However, protein oxidation can also result in oxidation of the protein backbone, protein fragmentation, formation of protein carbonyl derivatives, and the general accumulation of oxidized proteins in a cell.[3] Due to these processes, many researchers have postulated a positive correlation between the accumulation of oxidized proteins in the cell and several diseases such as Alzheimer's disease, cancer, and Parkinson's disease.[1]

a. Oxidation of the Protein Backbone

Oxidation of the protein backbone requires the action of the hydroxyl radical generated by either the radiolysis of water via X-rays, or, more commonly, the action of transition metals on H_2O_2. The hydroxyl radical abstracts the α-hydrogen atom of an amino acid residue to form a carbon-centered radical. This reaction is presented in Figure 1-1 below.

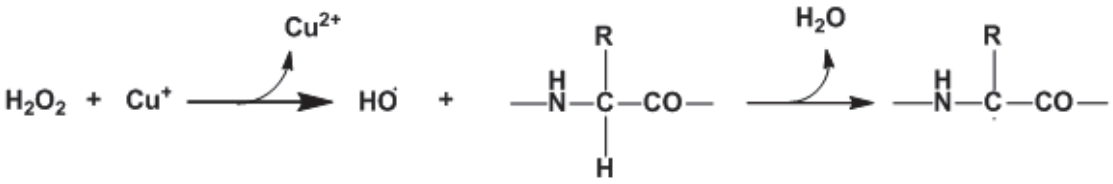

Figure 1-1: Formation of a carbon-centered radical via metal-catalyzed oxidation.

If the reaction occurs in an area of low oxygen concentration, the carbon-centered radical can attack other amino acid residues in adjacent proteins, thus forming more carbon-centered radicals or forming protein cross-links.[3]

b. Protein Fragmentation

If oxygen is present in the region where the oxidation of the amino acid occurred, further reaction with oxygen will occur as diagramed in Figure 1-2. The carbon-centered radical formed from the reaction with $HO^{\bullet}$ rapidly reacts with oxygen to form an alkylperoxyl radical intermediate which then becomes an alkylperoxide. The alkylperoxide undergoes further reaction with the perhydroxyl radical to form an alkoxyl radical, which sets the stage for peptide bond cleavage.[3]

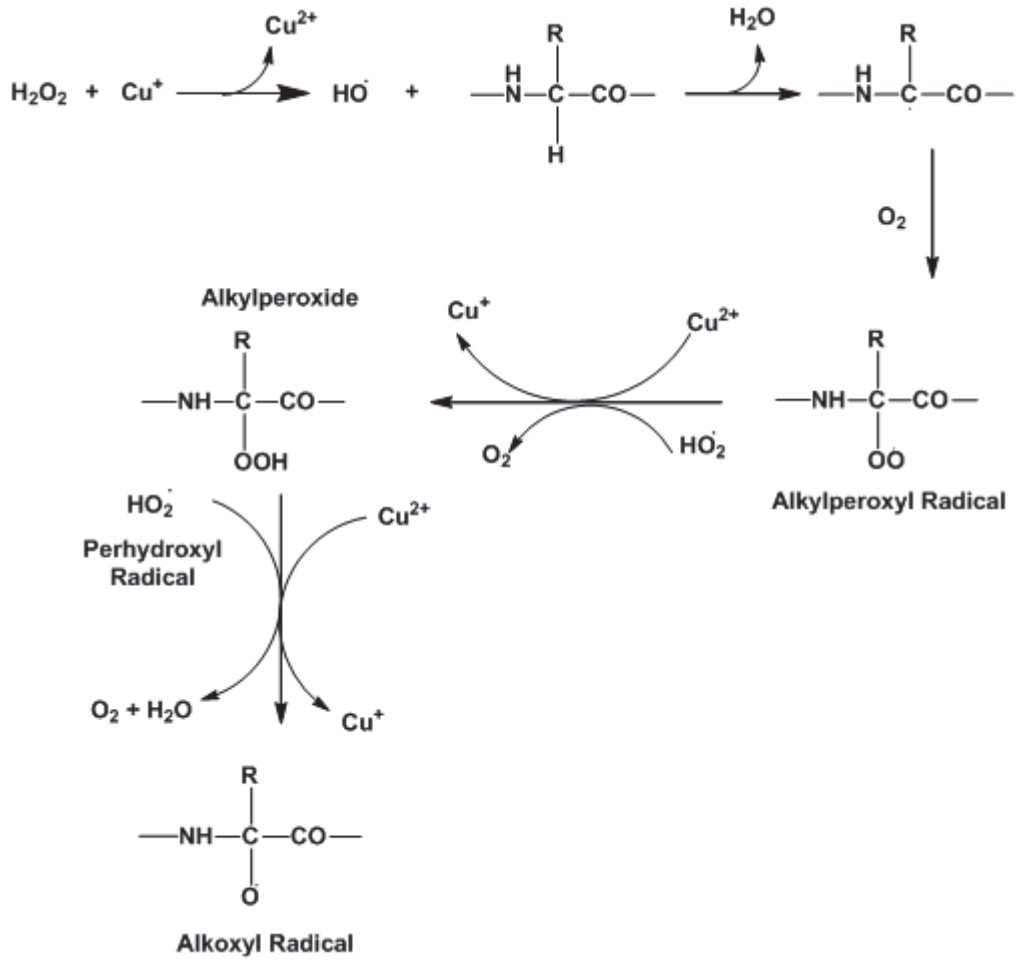

Figure 1-2: Formation of an alkoxyl radical from amino acids in a polypeptide.

Once the alkoxyl radical is formed, peptide bond cleavage can occur via one of two pathways. In the first pathway (pathway A, Figure 1-3), the peptide fragment that came from the N-terminal portion of the parent protein possesses a diamide structure at the C-terminal end, whereas the peptide from the C-terminal end of the parent protein possesses an isocyanate structure at its N-terminal end. This pathway is called the diamide pathway. In the second pathway (pathway B, Figure 1-3), α-amidation occurs where the N-terminal residue possesses an amide group at its C-terminal end, whereas the N-terminal residue derived from the C-

terminal end of the parent protein exists as an *N*-α-ketoacyl derivative. This pathway is known as the α-amidation pathway. Notice that the peptide bond is cleaved in both instances.[3]

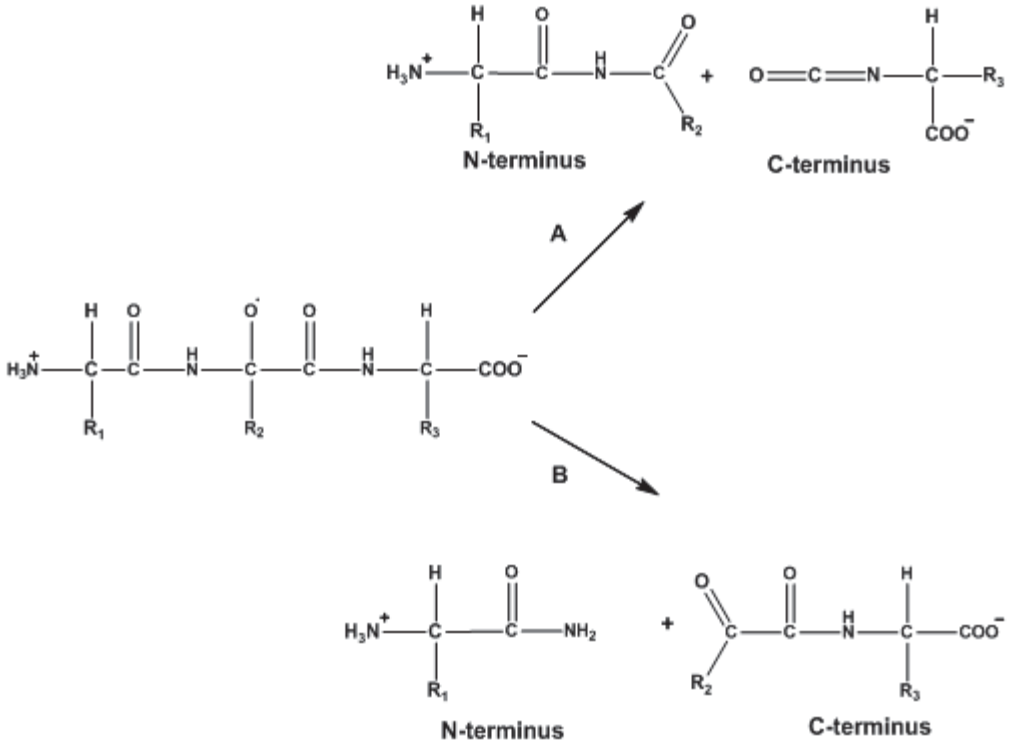

Figure 1-3: The diamide, A, and the α-amidation, B, pathways leading to peptide bond cleavage.

c. Generation of Carbonyl Derivatives

Oxidation of biological molecules can result in the formation of carbonyl derivatives. Carbonyl formation can be brought about by the direct oxidation of amino acid side chains, reactions with aldehydes during lipid peroxidation, or by reactive carbonyl derivatives generated by reducing sugars after reaction with amino acid side chains (glycation and glycooxidation reactions). An important consequence of forming protein carbonyl derivatives is the fact that the cell has proteases that degrade proteins with an excessive amount of carbonyl functional groups. Based on work by Stadtman *et al.*, it has been shown that the rate

of formation of carbonyl functional groups increases with aging, oxidative stress, and in association with several diseases.[4]

d. Accumulation of Oxidized Protein

A useful clinical test to determine the extent of oxidative damage in the cell is to assay cells for carbonyl compounds. One such test uses radioactive $NaBH_4$ to reduce the carbonyl to the hydroxyl and assay the cell for radioactivity. If the number of carbonyl functional groups produced is greater than the number that can be reduced by either exogenous or endogenous antioxidants, then the cell is marked for degradation by proteases. However, some oxidized forms of proteins, like protein-protein cross-links, are not only resistant to proteolysis, but can also inhibit the ability of proteases to degrade the oxidized forms of other proteins. This "immortality" that has been bestowed upon some oxidized proteins can cause devastating effects within and between cells by inhibiting proteases and thus allowing free radical oxidation to continue modifying proteins.[4]

Metal-Catalyzed Oxidation

Metal-catalyzed oxidation (MCO) is the reaction of a metal cation with O_2^- or H_2O_2 to eventually form the hydroxyl radical. An example of an MCO system is the Haber-Weiss reactions shown below:

$$M(n) + O_2^- \longrightarrow M(n-1) + O_2 \qquad \text{(Equation 1-2)}$$

$$M(n-1) + H_2O_2 \longrightarrow M(n) + HO^\bullet + HO^- \qquad \text{(Equation 1-3)}$$

where M denotes any metal ion and n denotes the oxidation state of the metal ion. The Haber-Weiss process occurs most frequently in neutrophils and thus can release radicals if the neutrophil is phagocytosed by a lysosome.[5] An example of an MCO system using Fe (II) is shown below:

$$Fe\ (II) + H_2O_2 \longrightarrow Fe\ (III) + {}^{\bullet}OH + OH^{-} \qquad \text{(Equation 1-4)}$$

This redox reaction, known as the Fenton reaction, directly produces the hydroxyl radical upon oxidation of Fe (II) to Fe (III).[6]

Some skepticism exists in regards to the prevalence of a redox reaction using Fe (II) occurring *in vivo*. The major criticisms of this reaction occurring are that the rate constant for this reaction is too low to cause significant generation of the hydroxyl radical and that there is far less free iron as compared to free copper in biological systems. Nonetheless, this reaction has been shown to occur *in vivo* due to the degeneration and release of free iron from ferritin.[5]

Metal catalyzed oxidation can be considered site-specific since it occurs at certain amino acid side chains at or near metal-binding sites on proteins. Since transition metals are commonly seen in the active sites of enzymes, metal catalyzed oxidation of catalytic amino acids can cause inhibition of the enzyme or structural changes in the protein. Amino acids that are most susceptible to site-specific oxidation include arginine (Arg), lysine (Lys), proline (Pro), cysteine (Cys), threonine (Thr), leucine (Leu), histidine (His), tyrosine (Tyr), and methionine (Met). For example, oxidation of histidine can produce 2-oxo histidine and oxidation of tryptophan can produce *N*-formylkynurenine and, if two oxidation events occur, kynurenine. Figure 1-4 shows the structures of these oxidized amino acids.[7]

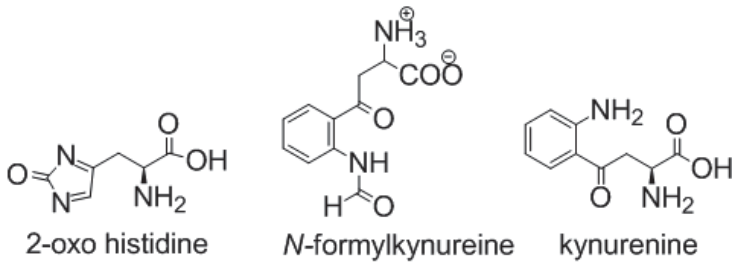

Figure 1-4: Structures of 2-oxo histidine, *N*-formylkynureine, and kynureine.

Oxidative damage by MCO systems may occur by a "caged" reaction. The free radical is generated by the creation of the hydroxyl radical in the metal-binding pocket of the protein through reaction of the metal ion with H_2O_2. The free radical then reacts with all nearby, susceptible, amino acid residues. During this "caged" reaction, the free radical is protected from scavengers or antioxidants. This explains why MCO systems are immune to free radical scavengers since these scavengers do not react with free radicals that are protected in a pocket of the protein.[8] This also emphasizes the point that tertiary structure, the three dimensional structure of the protein, may play a prominent role in the pattern of protein oxidation as opposed to just primary sequence, which provides metal-chelating residues.

Oxidation of Methionine Residues

The thioether group of Met residues is one of the most readily oxidized side chains of all 20 standard amino acids. Oxidation of Met residues results primarily in the production of methionine sulfoxide (MetO), but harsher oxidizing conditions (X-ray induced oxidation) can produce methionine sulfone. This conversion process is diagrammed in Figure 1-5.[8]

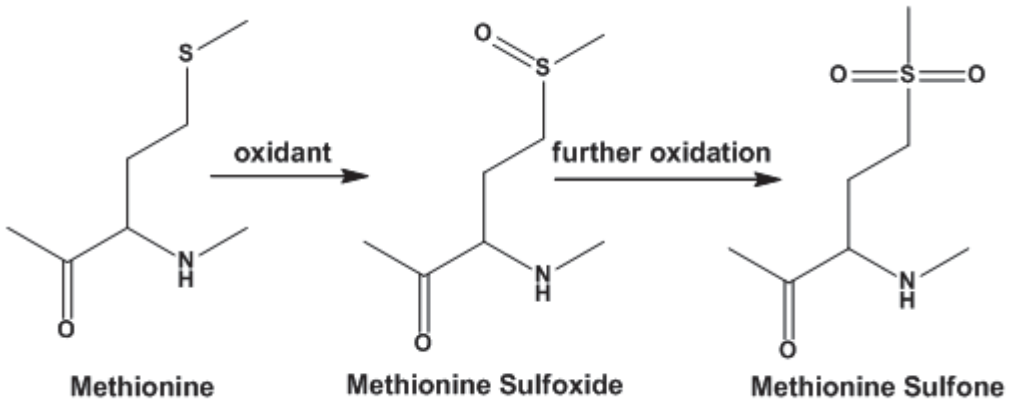

Figure 1-5: Sequential oxidation of a Met residue to produce first the sulfoxide then the sulfone.

One of the crucial aspects of Met oxidation is that the generation of MetO produces two stereoisomers. By considering the lone pair of electrons as the lowest priority group, an assignment of the R and S-enantiomers can be made. Figure 1-6 shows the structures of the two enantiomers.

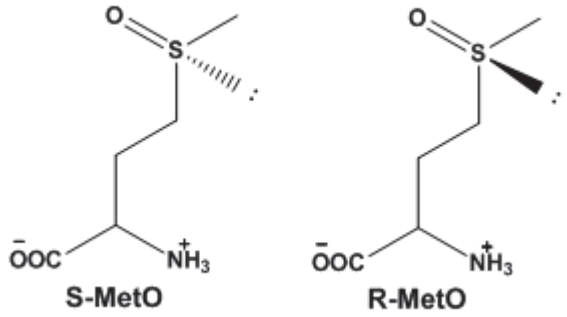

Figure 1-6: Structures of S-MetO and R-MetO.

The formation of the sulfoxide has been described as an addition reaction to the sulfur atom. The hydroxyl radical attacks the sulfur atom to form a transient R-$^{\bullet}$S(OH)-R hydroxyl sulfuranyl adduct species. Further oxidation results in the sulfoxide. Current methods in trying to elucidate the exact steps of this conversion have not come up with a conclusive mechanism; however, research shows that a stabilizing, two-center, three-electron bond can form between S-N, S-O, and S-X where X is a halide atom. This stabilizing system is dependent on the neighboring atoms and the sequence of the polypeptide.[9]

As was discussed previously, oxidation of proteins can alter the structure of peptides by breaking peptide bonds and forming protein-protein cross-links. It has also been shown that oxidation of amino acid side chains, like Met, can alter the tertiary structure of the protein. Surface-exposed amino acids are oxidized most readily and have little, if any, effect on the tertiary structure of the protein. Oxidation of buried residues has been shown to cause

conformational changes in the structure of the protein. Oxidation of the Met side chain increases the hydrophilicity of the residue. By becoming oxidized, the side chains of MetO have a greater dipole moment and can more readily participate in hydrogen bonding with solvent molecules. Thus, there is a driving force for a change in protein conformation since these residues prefer an external, water-accessible surface.[9]

Antioxidant Defense Against ROS Damage

Reactive oxygen species, like all free radicals, can be terminated by reactions with other radicals or by radical scavengers. In most MCO systems, the free radicals react with each other to form addition and cross-linked products. These products, as mentioned previously, are damaging to other proteins; however, there are several exogenous and endogenous systems to quench free radicals. Bandyopadhyay, *et al.* categorizes antioxidant defense strategies as primary and secondary, with primary being the antioxidant enzymes and secondary being free radical scavengers.[1]

a. Catalytic Removal of ROS by Antioxidant Enzymes

There are several enzymes within the cell that can quench free radicals and prevent them from modifying proteins. These enzymes include superoxide dismutase, heme peroxidase, and catalase. Catalase and heme peroxidase, both of which catalyze the removal of H_2O_2 with the concomitant production of water and oxygen, remove excess H_2O_2 from the cell. Superoxide dismutase catalyzes the removal of O_2^- from the cell by converting it to H_2O_2 using either a copper- or zinc-catalyzed reaction.[1]

b. Catalytic Removal of ROS by Free Radical Scavengers

Free radical scavengers are small molecules which react with free radicals to form either stable complexes that can be removed from the cell or another radical that can be quenched by an enzyme or other molecule. Two of the most common free radical scavengers that are

physiologically relevant include α-tocopherol and ascorbate. The general scheme of free radical scavengers is to transfer its unshared electron to an antioxidant enzyme like glutathione peroxidase (GSH) or methionine sulfoxide reductase (Msr). For example, α-tocopherol is used to quench DNA chain-breaking radicals. Once the tocopherol radical is formed, it is transferred to the cell membrane surface and gets reduced to α-tocopherol with the concomitant oxidation of GSH to GSSG (oxidized glutathione peroxidase). The GSH is regenerated by use of an NADPH-glutathione reductase system.[1]

Methionine Sulfoxide Reductase

Since Met oxidation is a facile process intra and extracellularly, a process to repair Met residues is present in living organisms in the form of methionine sulfoxide reductases (Msr).[10] There are three types of Msr: MsrA, MsrB, and fRMsr. MsrA and MsrB are present in all organisms, while fRMsr is present only in unicellular organisms. All three enzymes catalyze the reduction of MetO back to Met; however, each enzyme has a specific stereochemical requirement for its substrate. MsrA requires S-MetO while MsrB requires the R-enantiomer of MetO. fRMsr is the MsrB equivalent in unicellular organisms.[11]

a. MsrA

MsrA is a tetrameric protein which catalyzes the reduction of S-MetO to Met. The crystal structure of the *E. coli* version of the enzyme is shown in Figure 1-7.[12]

Figure 1-7: Crystal structure of a monomer of the *E. coli* MsrA enzyme. The catalytic Cys residues are shown as space filling models with carbon grey, nitrogen blue, oxygen red, and sulfur yellow. α-helices are depicted as purple ribbons and β-sheets are depicted as yellow sheets.[12]

MsrA uses three catalytic Cys residues in its reaction mechanism. Cys 86 reduces the MetO to Met and a sulfenic acid moiety. A regenerating Cys (Cys 198) forms a disulfide bridge with Cys 86 followed by the formation of a second disulfide bridge being formed between Cys 198 and Cys 206. To regenerate the active enzyme, the disulfide bonds are reduced by an NADPH-dependent thioredoxin/thioredoxin reductase system.[11]

b. MsrB

MsrB is a tetrameric protein which catalyzes the reduction of R-MetO to Met. The crystal structure of the monomer of the *Mus musculus* version of the enzyme is shown in Figure 1-8.[13]

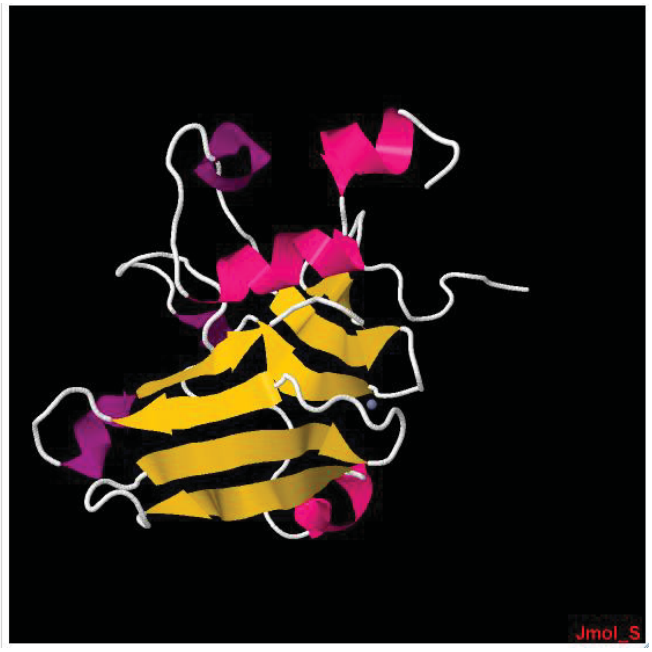

Figure 1-8: Crystal structure of the monomer of the *Mus musculus* MsrB enzyme. Color scheme is the same as in Figure 1-6.[13]

The reaction mechanism of MsrB is similar to MsrA; however, recent evidence has shown that MsrB employs a selenocysteine in its catalytic active site. X-ray crystallography has shown that the selenocysteine is Cys 119 in *Mus musculus*. In mammals, three forms of MsrB exist and are called MsrB1, MsrB2, and MsrB3. MsrB1 exists in the cytosol and nucleus of the cell and exhibits the highest catalytic efficiency due to the presence of selenocysteinine in the active site of the enzyme. MsrB2 is present in the mitochondria of the cell and exhibits less activity relative to MsrB1. MsrB2 can be inhibited by elevated levels of R-MetO. MsrB3 is located on the endoplasmic reticulum and exhibits the lowest activity among the three isoforms. However, its catalytic activity has been shown to increase under conditions of oxidative stress.[11]

Lysozyme

Lysozyme, also called muramidase, is a type of hydrolase that catalyzes the hydrolytic cleavage of the β-(1,4)-glycosidic bond connecting *N*-acetylmuramic acid (NAM) and *N*-

acetylglucosamine (NAG) (Figure 1-9). Since polymers of NAG-NAM are components of bacterial cell membranes, lysozyme can be used as an antimicrobial agent and has been employed as a preservative in the food industry and the pharmaceutical industry.[14]

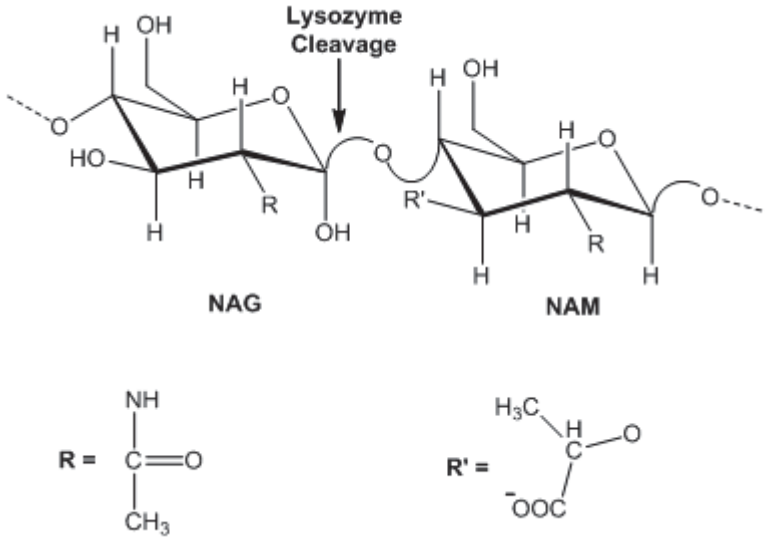

Figure 1-9: Repeating structural unit of NAG-NAM carbohydrate moieties showing where lysozyme cleaves the polymer.[14]

Lysozyme is present in all major taxa of living organisms; however, there are differences between the lysozyme variants in different organisms. In general, there are three major types of lysozyme: chicken or conventional type (c-type lysozyme), goose type (g-type lysozyme), and invertebrate type (i-type lysozyme). All of these different types of lysozyme catalyze the same reaction, but there are several differences between the different types of lysozymes.[14]

a. c-type Lysozyme

c-type lysozyme is the most common variant of lysozyme as most vertebrates produce a c-type lysozyme. A BLAST search reveals that all completely sequenced mammalian genomes contain at least one c-type lysozyme gene. The archetype lysozyme in this class is the hen egg white lysozyme (HEWL). HEWL is a 14.3 kDa, 129-amino acid enzyme whose primary sequence is displayed in Figure 1-10. Note that there are four intramolecular disulfide bridges in the enzyme.

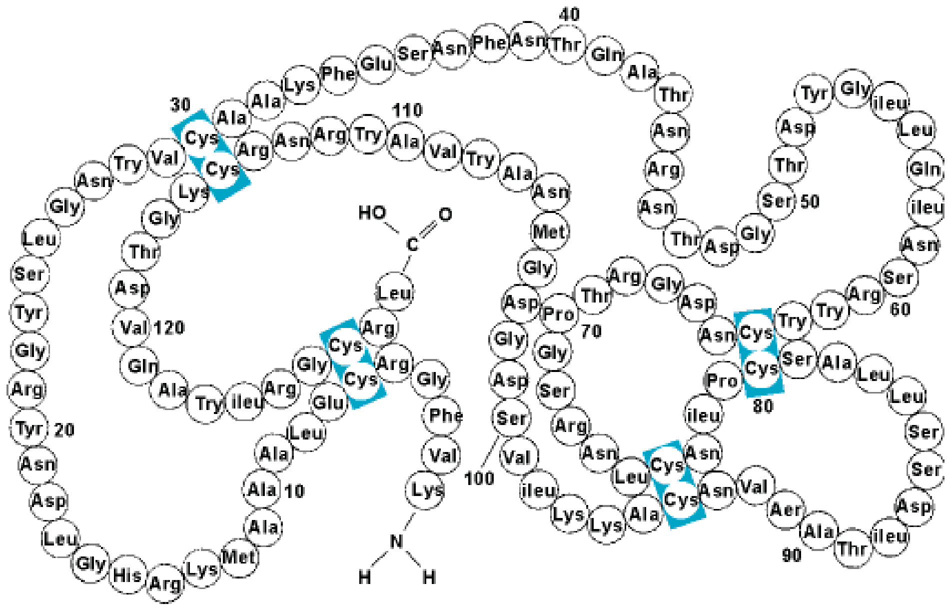

Figure 1-10: Primary sequence of HEWL showing locations of the N- and C-termini as well as locations of disulfide bridges (Cys in blue boxes).[15]

HEWL was the first enzyme to be crystallized and have its structure determined by X-ray crystallography (1966), thus making it an excellent model protein. The crystal structure of HEWL is presented in Figure 1-11 below as a space-filled model. Note how the two catalytic residues, aspartate 52 and glutamate 35, are located in a cleft of the enzyme.[16]

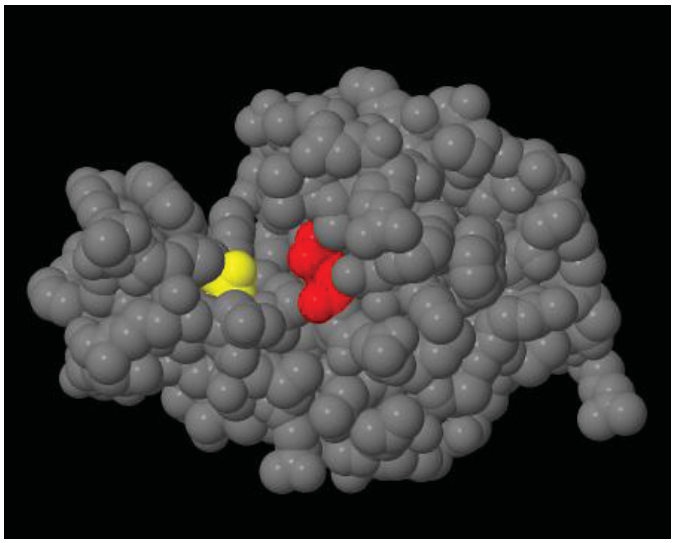

Figure 1-11: Crystal structure of HEWL showing the catalytic residues Asp 52 (yellow) and Glu 35 (red).

Previous research has shown that HEWL can bind up to six sugar residues in its active site. It was noted based on model building-studies, however, that sugar residue D had to be distorted to a half-chair conformation, which made the glycosidic bond connecting residues D and E susceptible to cleavage by the enzyme. After binding in the enzyme active site (step 1, Figure 1-12, page 18), the oxygen atom linking the NAM and NAG residues abstracts a proton from Glu 35 thus breaking the glycosidic bond and forming an oxonium ion transition state that is stabilized by resonance effects (the rest of the larger polysaccharide composing the bacterial cell wall dissociates from the active site of the enzyme) (step 2). In the next step of the mechanism (step 3), the negatively-charged Asp 52 performs a nucleophilic attack on the positively-charged carbon of the oxonium ion intermediate to form a covalent intermediate. To regenerate Glu 35, water enters the active site of the enzyme and the negatively-charged Glu 35 abstracts a proton from water (step 4). Finally, the resulting hydroxide ion attacks the carbon bound to Asp 52, thus breaking the covalent attachment, releasing the resulting NAM moiety, and regenerating the active enzyme (step 5).[17]

b. g-type Lysozyme

g-type lysozyme is the second most common type of lysozyme. This enzyme is present in mammals, birds, fish, and even in some invertebrates. The classical example of a g-type lysozyme is that of goose egg white lysozyme (GEWL). GEWL is a 20.4 kDa, 185 amino acid enzyme whose crystal structure is depicted as a space-filled model in Figure 1-13. Notice how there is no catalytic aspartate in this enzyme.[14]

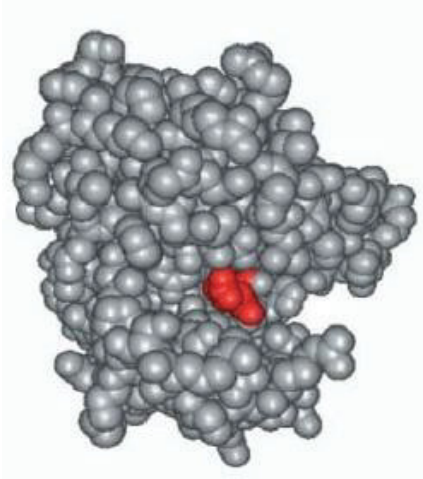

Figure 1-13: Space-filled model of GEWL with the catalytic Glu 73 highlighted in red.[14]

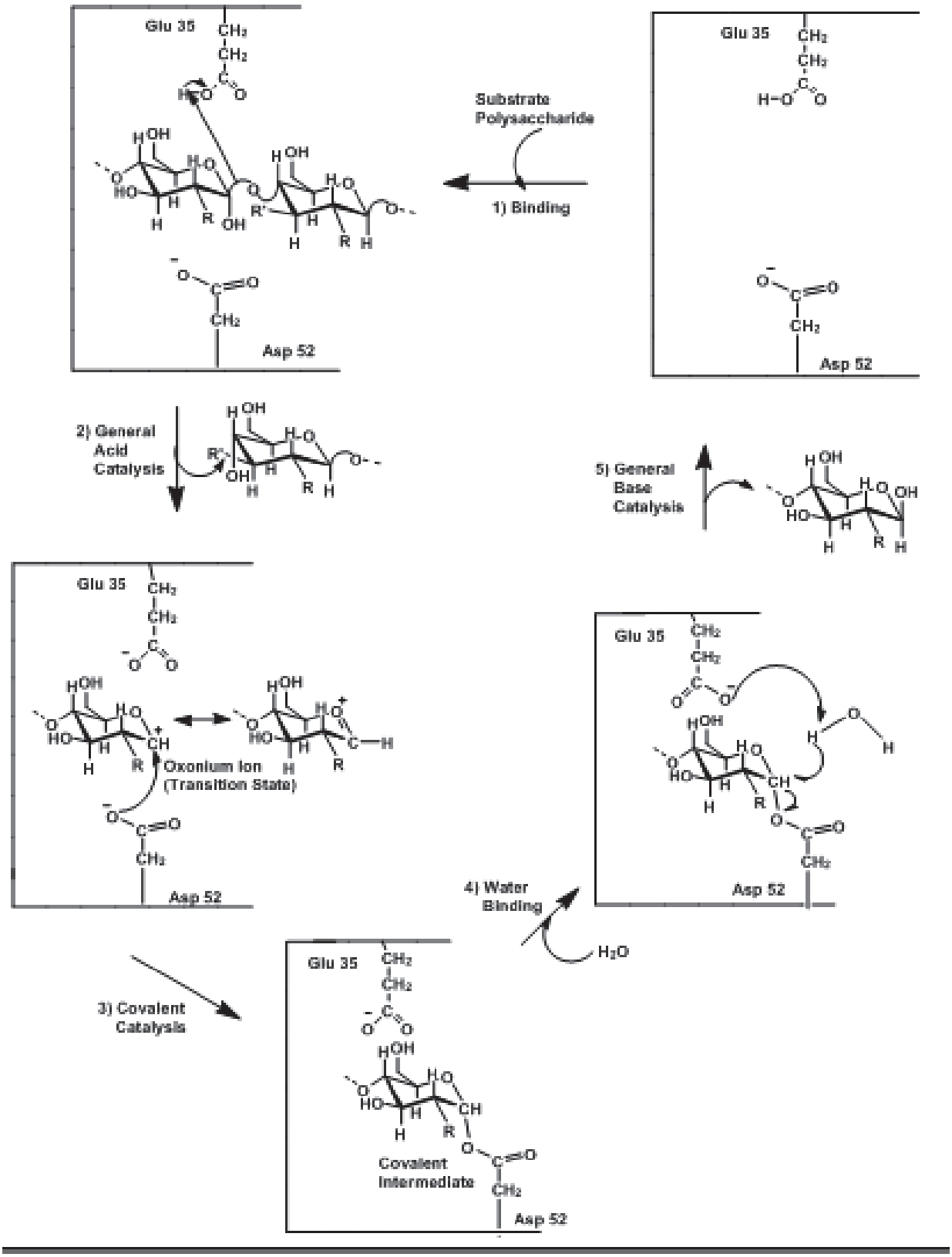

Figure 1-12: Catalytic mechanism of HEWL.[17]

Even though the same reaction is catalyzed by HEWL and GEWL, several differences can be stated. As it was noted above, there is no corresponding catalytic Asp in GEWL like there is in HEWL. However, current research has suggested that GEWL may have invertase characteristics unlike HEWL, meaning that it does not retain chirality in the final product. Analysis of the crystal structure of GEWL shows an Asp 97 which would be at a sufficient distance to catalyze an invertase-like reaction. A final difference between HEWL and GEWL is that the D sugar moiety of the NAG-NAM polymer is not distorted. A possible explanation for this could be that the polysaccharide does not bind as deeply in the active site cleft in GEWL as it does in HEWL.[14]

c. i-type Lysozyme

The third, and least common, type of lysozyme is the i-type lysozyme. This type of lysozyme is prevalent in invertebrates such as members of the phyla Annelida, Arthropoda, Echinodermata, Mollusks, and Porifera. Also, all completely sequenced genomes of insects contain i-type lysozyme gene homologues. The first i-type lysozyme whose amino acid sequence was determined was that of *Tapes japonica* (TjL) in 1999. TjL is a dimer of 13.7 kDa protein monomers that is composed of 123 amino acids. The crystal structure of this enzyme is depicted in Figure 1-14.[14]

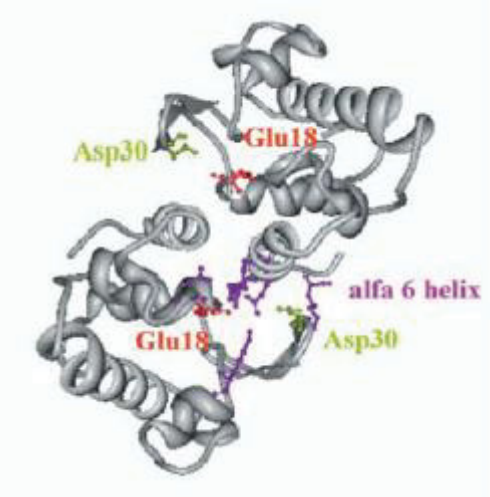

Figure 1-14: Ribbon diagram of the dimer of i-type lysozyme from *Tapes japonica*. The purple amino acid residues are the amino acids involved in associating the two dimers (Asp 95 and Lys 42).[14]

The catalytic mechanism of TjL is very similar to that of HEWL. Glu 18 and Asp 30 corresponds to HEWL's Glu 35 and Asp 52 and function in the same role. An interesting divergence between HEWL and TjL is that with elevated concentrations of sodium chloride, enzymatic activity in TjL increases due to the dissociation of the dimer into two monomers. The dimer is maintained by electrostatic interactions between Glu 18/Asp 30 in one molecule and positively charged residues in the C-terminus (helix 6) of the other molecule. Dimer formation blocks one of the active sites in the enzyme. The increase in activity is due to the availability of more active sites upon dissociation. Since seawater has a high salt content, many sea-dwelling invertebrates have adapted to use this type of lysozyme to take advantage of i-type lysozyme's extra activity.[14]

Research Objective

The purpose of the current project is to isolate and characterize the various oxidized forms of hen egg white lysozyme (HEWL) that have been produced by a copper(II)/H_2O_2 MCO system. The different oxidized forms of lysozyme will be purified and separated using high

performance liquid chromatography (HPLC) and subjected to quadrupole time-of-flight electrospray mass spectrometry to determine which amino acids in each isolated sample of oxidized HEWL were altered. Since methionine 105 and methionine 12, when oxidized, can form two stereoisomers, the enzyme methionine sulfoxide reductase A (MsrA) will be used to examine which stereoisomer is present in the oxidized HEWL samples. A comparison of the activities of each oxidized variant to native lysozyme will also be examined. Finally, crystals of oxidized HEWL will be generated and used to determine the crystal structure of oxidized HEWL. This will allow for a comparison between native HEWL's structure and oxidized HEWL's structure. By generating data on native HEWL's oxidized form, a comparison of the oxidized states of native HEWL and mutated HEWL can be examined to see if primary or tertiary structure is more important in regards to determining the pattern of site-specific oxidation of a protein. This comparison could lead to new insights into the susceptibility of a protein to oxidation by MCO systems.

CHAPTER 2: MATERIALS AND METHODS

Materials and Instrumentation

Lysozyme, 30% H_2O_2, *Micrococcus lysodeikticus* cells, imidazole, thioredoxin, thioredoxin reductase, methionine, and beta-nicotinamide adenine dinucleotide phosphate (β-NADPH) were purchased from Sigma Life Sciences. Ammonium sulfate, catalase, yeast extract, tryptone, isopropyl-β-D-galactopyranoside (IPTG), ampicillin, coomassie brilliant blue G250, wide range protein molecular weight markers, and Blue BANDit™ Coomassie Stain were purchased from Amresco. The centrifuge used was an Avanti J-25I manufactured by Beckman. Potassium phosphate monobasic and dibasic forms, 1 mL quartz cuvette, $CuSO_4$, EDTA, NaCl, 3 mL plastic cuvette, 2 mm magnetic stir bars, and sodium acetate were purchased from Fisher Scientific. All pH measurements were taken using an Accumet digital pH probe purchased from Fisher Scientific. All mass measurements were made using a Mettler AE 100 balance. The 0.45 μm nylon filters were purchased from Micron Separations Inc. The dialysis stirred cell was manufactured by Amicon. The 3000 Da molecular weight filters were purchased from Millipore. The spectrophotometer used was an Agilent 8453 UV-VIS Spectrophotometer manufactured by Hewlett Packard. The data analysis software used to analyze spectrophotometric data was the UV-Visible Chem Station Software suite. The temperature-controlled water bath was purchased from Fisher Scientific. The 0.25 μm nylon filters were purchased from Osmonics Inc. The cation-exchange column used in the HPLC experiments was a PolyCAT A Column manufactured by PolyLC Inc. The HPLC instrument used was a Waters model equipped with a Waters 486 UV Wavelength Detector manufactured by Millipore. HPLC data analysis was performed using Galaxy Chromatography Software written by Varian. Lyophilization was performed using a Freezone 4.5 manufactured by Labconco. Dry ice was purchased from Airgas. Acetone and acetic acid was purchased from

Pharmco-AAPER. The automated temperature controller-magnetic stirrer apparatus consisted of an FE-2 model heating unit manufactured by Haake and a cuvette holder with an internal magnetic stir bar manufactured by Agilent. The coverslips were purchased from Corning GlassWorks. The cell culture plates used as crystallization trays (Corning® Costar® cell culture plates, 24-well) were purchased from Sigma-Aldrich. Polyethylene glycol 6000 was purchased from Fluka Chemika. The light microscope used to visualize the protein crystals was a Zeiss light microscope manufactured by Diagnostic Instruments equipped with an AxioCam MrC digital camera. The software used to process the light microscope images was Axioview written by Diagnostic Instruments. The sonicator used to lyse the bacterial cells was a Microson™ Ultrasonic Cell Disruptor manufactured by Misonix. The transformed M15 *E. coli* cells used were generously provided by Dr. Jackob Moskovitz (The University of Kansas, Department of Pharmacology and Toxicology). The plasmid in the *E. coli* (pQE-30) was produced by Qiagen. The autoclave used was a Tuttnauer 3850M manufactured by Heidolph-Brinkmann. The oven used to grow bacterial cell cultures was purchased from Fisher Scientific. The 37 °C shaking water bath was a C76 Water Bath Shaker manufactured by New Brunswick Scientific. Sodium phosphate (monobasic) was purchased from Merck. Sodium phosphate (dibasic) was purchased from Mallinckrodt. The bovine serum albumin standards and the HisPur™ Ni-NTA resin were purchased from Thermo Scientific. SDS-PAGE gels, the Mini-PROTEAN® II Electrophoresis Cell, PowerPac 300 and protein loading buffer were purchased from Bio-Rad. The microcentrifuge used was an accuSpin™ Micro manufactured by Fisher Scientific. The automated fraction collector was a Model 2110 Fraction Collector manufactured by Bio-Rad. The orbital shaker was manufactured by Cole Parmer.

Ammonium Sulfate Fractionation of Lysozyme

A 5% (w/v) solution of lysozyme, pH 6.7, was prepared in 60 mL of deionized (DI) water. Ammonium sulfate (17.84 g) and water were added slowly, with stirring, until a precipitate was visible and the total volume of the resulting solution reached 100 mL, corresponding to a 50% saturated solution. This solution was stirred for 5.5 hours at 4 °C. Afterwards, the solution was spun in a centrifuge at 10,000 rpm (12,096 x g) for 10 minutes. The supernatant was separated from the pellet and ammonium sulfate (8.61 g) was slowly added to the supernatant with stirring, corresponding to a 75% saturated solution. Afterwards, the solution was stirred for 27 hours at 4 °C. The solution was centrifuged at 10,000 rpm (12,096 x g) for 10 minutes. The pellet was saved and was resuspended in a minimal volume of 10 mM potassium phosphate (KP_i) buffer, pH 7.4. After filtering the resuspended pellet through a 0.45 μm nylon filter, the solution was dialyzed against 200 mL of 10 mM KP_i buffer, pH 7.4, using a stirred cell equipped with a cellulose 3000 Da molecular weight filter at a nitrogen gas pressure of 70 psi.[18]

To determine the concentration of the purified lysozyme, the solution (20 mL) was pipetted out of the apparatus, filtered through a 0.45 μm filter, and its absorbance readings at 277.5 nm, 280 nm, and 290 nm were determined using a spectrophotometer and a 1 mL quartz cuvette. The extinction coefficients of lysozyme have been calculated at these wavelengths since aromatic amino acids, like phenylalanine, tryptophan, and tyrosine, present in the protein absorb UV light at these wavelengths.[19] Using the extinction coefficients of lysozyme calculated at those wavelengths (25.5 at 277.5 nm, 24.7 at 280 nm, and 20.2 at 290 nm), the concentration of purified lysozyme was determined to be 86.7 mg/mL. The purified lysozyme was then placed in a -20 °C freezer for storage.

Oxidation of Lysozyme

18.5 mL of the 86.7 mg/mL lysozyme solution was mixed with 12 mL of 10 mM $CuSO_4$ and 270 mL of 10 mM KP_i buffer (pH 7.4). The oxidation reaction was initiated by adding 100 mL of 200 mM H_2O_2 to the mixture. The reaction was incubated in a 37 °C water bath for 5 minutes. The oxidation reaction was stopped by adding 8 mL of catalase (1 mg/mL, 2600 units/mg) and 40 mL EDTA (50 mM, pH 7.4). After centrifugation (10,000 rpm, 12,096 x g, 10 minutes), the supernatant was separated from the pellet. The supernatant was concentrated using the stirred cell equipped with a 3000 Da molecular weight filter membrane. The concentrated sample was dialyzed against 200 mL of 10 mM KP_i, pH 7.4, buffer and a total volume of 20 mL of solution was recovered. The concentration of the purified oxidized HEWL, as determined through the $E^{1\%}_{280}$ value (24.7), was 49.8 mg/mL. The sample was placed in a -20 °C freezer until needed.

Separation of Oxidized Lysozyme Variants Using HPLC

The oxidized lysozyme was filtered through a 0.25 μm nylon filter prior to HPLC on a PolyCAT A cation-exchange column (100 x 9.4 mm, 3 μm, 1500 Å). The column was first washed with water (3 mL/min, 20 min) then flushed with 40 mM EDTA, pH 7.0, for 20 hours at a flow rate of 0.5 mL/min. Afterwards, the column was washed with Buffer B (20 mM KP_i, 0.4 M NaCl, pH 6.0) for 20 minutes at 3 mL/min, followed by equilibration using a mixture of 44% Buffer B and 56% Buffer A (20 mM KP_i, pH 6.0) for 20 minutes at 3 mL/min. 200 μL of 49.8 mg/mL oxidized lysozyme solution was injected onto the column. The flow rate for the HPLC run was 4.0 mL/min. The HPLC instrument was programmed to perform each run with the following binary gradient at room temperature:

1) Equilibrate column with 44% Buffer B
2) From 0-13 minutes, 44% Buffer B

3) From 13-23 minutes, linear gradient to 50% Buffer B

4) From 23-33 minutes, linear gradient to 60% Buffer B

5) From 33-47 minutes, 60% Buffer B

Five fractions were collected by hand when the absorbance at 280 nm corresponding to a particular oxidized lysozyme peak increased above the baseline reading. This procedure was replicated for the entire oxidized lysozyme sample and five peaks were collected. After each run, the column was equilibrated with 44% Buffer B for 20 minutes at 3 mL/min. All peaks were concentrated and dialyzed against water using the Amicon stirred cell, frozen using a dry ice-acetone bath, and triply lyophilized.

The five peaks collected using the salt gradient were separated a second time by HPLC using an isocratic gradient of 42% Buffer B at either pH 7 (Peak IV) or pH 8 (Peaks I, II, III, and V). In addition, a sample of lysozyme that was purified using ammonium sulfate fractionation, but not subjected to the MCO reaction, was run through the column using the same conditions as were used for the oxidized enzyme. This sample served as the control sample for the activity assays of the collected fractions.

Oxidized HEWL Protein Assays

The activity of each oxidized HEWL variant was examined using visible spectroscopy. The assay used was based on an assay developed by Shugar[20] and modified by Worthington Biochemical Corporation (Freehold, NJ.). A suspension of *Micrococcus lysodeikticus* cells (0.3 mg/mL) was prepared in 0.1 M KP_i, pH 7.0 by suspending 15.0 mg of cells in 50 mL of buffer. The cells were incubated in buffer for 24 hours at 4 °C prior to performing the assays.

The non-lyophilized lysozyme standard was assayed first as a control. To a 3 mL cuvette, 2.9 mL of *Micrococcus lysodeikticus* cell suspension, that was warmed up to room temperature, and three, 2 mm magnetic stir bars were added and allowed to sit in the cuvette

holder for 3-5 minutes in order for the temperature of the suspension to equilibrate to 25 °C. An automated temperature controller-magnetic stirrer apparatus allowed for mixing of the solution in the cuvette. After temperature equilibration, 100 µL of a diluted lysozyme standard was added to the cuvette and the instrument measured the decrease in the absorbance at 450 nm (A_{450}) for 2.5 minutes. After determining the rate of reaction for a particular dilution, the control or oxidized lysozyme protein variant was further diluted to achieve a ΔA_{450}/min between 0.0150-0.0400.

Crystallization of Oxidized HEWL Protein Variants

Each of the peaks that were isolated via HPLC was crystallized using the hanging drop method of protein crystallization. For Peak V, a droplet was prepared (5 µL of Peak V at 15 mg/mL in water plus 5 µL 5% (w/v), pH 10.0, NaCl) on a silanized coverslip. The droplet was inverted and placed over a well containing 1 mL of precipitant (5% (w/v) NaCl, pH 10.0). The tray was placed in a 4 °C cold room for two weeks for crystal development.

The crystallization droplet for Peak III was prepared by mixing 5 µL of Peak III at 20 mg/mL in 1 M sodium acetate buffer, pH 3.0, plus 5 µL of precipitant, which was composed of 6% (w/v) polyethylene glycol 6000 (PEG 6000), 9.5% (w/v) NaCl in 1 M sodium acetate buffer, pH 3.01. The droplet was inverted and placed over a well containing 1 mL of precipitant. The tray was placed in a 4 °C cold room for one week for crystal development. The same procedure was used for Peak IV except that the droplet contained 5 µL of a 20 mg/mL Peak IV solution in 1 M sodium acetate buffer, pH 3.0.

Tandem Mass Spectrometry of Oxidized HEWL

The intact molecular weight of lysozyme was determined on a MaXis 4G (Bruker) ESI mass spectrometer equipped with an electrospray source in positive ion mode. The sample was diluted in a mixture of water:methanol:acetic acid (50:50:2.5) and was infused into the

electrospray source at a flow rate of 3 μL/min. To achieve the optimal electrospray results, the capillary voltage was set at 4500 V and the oven temperature was set at 180 °C. The data was recorded between 100-3000 m/z.

Lysozyme was digested with trypsin prior to tandem MS analysis to identify its oxidation sites. Briefly, lysozyme was diluted into 100 mM ammonium bicarbonate. Dithiotheritol (DTT) solution (5 μL, 5 mg/mL) was added to reduce cysteines after incubating at 60 °C for 15 minutes. Iodoacetamide solution (5 μL, 15 mg/mL) was then added to the sample and incubated with the sample at room temperature in the dark for another 15 minutes to block the reduced cysteines. Sequencing-grade trypsin from Promega was prepared as 20 ng/μL in 50 mM ammonium bicarbonate and was added to the samples with a ratio of 1:20 (enzyme:substrate, w/w). The digestion was carried out at 37 °C for 2 hours before being quenched by adding 5 μL trifluoroacetic acid (TFA, 0.01%).

Capillary-liquid chromatography-nanospray tandem mass spectrometry (Capillary-LC/MS/MS) was performed on a Thermo Finnigan LTQ mass spectrometer equipped with a nanospray source operated in positive ion mode. Samples were separated on a capillary column (0.2 x 150 mm Magic C18AQ 3 μ, 200 Å, Michrom Bioresources Inc.) using an UltiMate^{TM} 3000 HPLC system from LC-Packings A Dionex Co. Each sample was injected into the trapping column and desalted with 50 mM acetic acid for 3 minutes. The injector port was then switched to inject and the peptides were eluted off of the trap onto the column. Mobile Phase A was 0.1% formic acid in water and Mobile Phase B was 0.1% formic acid in acetonitrile. The flow rate for the run was 2 μL/min. The Mobile Phase B was increased from 2% to 50% in 30 minutes; this was then followed by increasing Mobile Phase B from 50% to 80% in 10 minutes, kept at 80% for 2 minutes, and then brought down to 2% in 1 minute. The column was equilibrated at 2% Mobile Phase B for 10 minutes before the next sample

injection. The MS/MS was acquired with a nanospray source operated with a spray voltage of 2 kV and a capillary temperature of 175 °C. The scan sequence of the mass spectrometer was based on the data-dependent TopTen^{TM} method: the analysis was programmed for a full scan recorded between 300-2000 Da and an MS/MS scan to generate the product ion spectra to determine the amino acid sequence in consecutive scans of the ten most abundant peaks in the spectrum. The CID fragmentation energy was set to 35%. Dynamic exclusion was enabled with a repeat count of 30 s, exclusion duration of 350 s, and a low mass width of 0.50 Da and a high mass width of 1.50 Da.

Expression of MsrA

50 μL of M15 *E. coli* stock solution, transformed with the pQE-30 plasmid containing the *Saccharomyces cervisiae* MsrA gene, was plated on fresh Luria-Bertini (LB) agar plates supplemented with ampicillin to a final concentration of 100 μg/mL. The plates were incubated overnight at 37 °C. One colony was selected with a sterile toothpick from each plate and dropped in 3 mL of LB plus ampicillin (100 μg/mL) broth in a sterile 15 mL tube. The tubes were incubated overnight in a 37 °C shaking water bath set at 225 rpm. Two, 2.75 mL aliquots of the overnight growth were used to inoculate two, 500 mL samples of broth. The flasks were placed in a shaking water bath set at 225 rpm for 4.5 hours, and the turbidity of the solution was monitored at 600 nm (OD_{600}) every 15 minutes. When the OD_{600} reached 0.8, 500 μL of 1 M isopropyl-β-D-thiogalacto-pyranoside (IPTG) was added to the flasks, and the flasks were placed in a 37 °C shaking water bath set at 225 rpm for 3.5 hours. The broth was centrifuged at 8,250 rpm (8232.84 x g) for 10 minutes in a centrifuge at 4 °C. The cell pellet was re-suspended in 10 mL of chilled buffer (50 mM NaP_i, 0.3 M NaCl, pH 8.0).[21] Cells were sonicated using the following procedure:

1. Two times for 10 s at Power Setting 4. Cells were placed on ice for 10 s afterwards.

2. Once for 20 s at Power Setting 4. Cells were placed on ice for 20 s afterwards.
3. Once for 30 s at Power Setting 4. Cells were placed on ice for 30 s afterwards.
4. Once for 10 s at Power Setting 8. Cells were placed on ice for 10 s afterwards.

The lysate was centrifuged at 11,250 rpm (15,309 x g) for 10 minutes at 4 °C.

The resulting supernatant was concentrated to 20 mL using an Amicon Stirred Cell equipped with a 3000 Da molecular weight filter. The concentrated solution was filtered three times with 40 mL of buffer (20 mM NaP_i, 300 mM NaCl, 10 mM imidazole, pH 7.40). After determining the concentration of the resulting solution using the Bradford Assay (10.5 mg/mL), the solution was subjected to sodium dodecyl sulfate-polyacrylamide gel electrophoresis (SDS-PAGE). 20 µL of 10-fold diluted protein solution was mixed with 20 µL 2X protein dye loading buffer, heated at 90 °C for 5 minutes, and centrifuged at 10,000 rpm for 30 s in a microcentrifuge. 10 µL of the resulting solution was loaded into each of four wells in a precast gel (4-20% polyacrylamide). 5 µL of the molecular weight marker mixture was loaded into each of two wells in the precast gel. The gel was run at 200 V for 60 minutes. Afterwards, the gel was washed in approximately 30 mL of water by heating in a microwave for one minute. The wash was repeated three times. 25 mL of BlueBANDit® coomassie stain was poured into a container containing the gel, the contents were heated for one minute in a microwave, and then the gel with stain was placed on an orbital shaker at 75 rpm for one hour. The stain was then decanted and 50 mL of water was added as a destain solution. The gel was then allowed to stand for 30 minutes.

Purification of MsrA

MsrA was purified using nickel affinity column chromatography. The MsrA that was expressed from the M15 *E. coli* has a histidine (His) tag on its amino terminus. Histidine has a high affinity for nickel atoms; therefore, it will preferentially bind to the column while other

proteins will elute from the column. The column (12.9 cm x 1.0 cm) was connected to an automated fraction collector, and the storage buffer was allowed to drain from the resin. The column was then equilibrated with three column volumes (30 mL) of Equilibration Buffer (20 mM NaP_i, 300 mM NaCl, 10 mM imidazole, pH 7.40). After determining the binding capacity of the column (60 mg/mL resin x 10 mL = 600 mg total), 5 mL of the protein solution (52.5 mg protein) was loaded onto the column, and the sample was allowed to enter the column. Once the sample had completely entered the column, 25 mL of Wash Buffer (20 mM NaP_i, 300 mM NaCl, 25 mM imidazole, pH 7.40) was passed through the column. Once nearly all wash buffer had entered the column, 25 mL of Elution Buffer (20 mM NaP_i, 300 mM NaCl, 250 mM imidazole, pH 7.40) was passed through the column. During the course of the separation, the A_{280} of the fractions (fraction volume: 2.5 mL) was monitored for protein content. After the Elution Buffer had passed through the column, the column was equilibrated with 25 mL of Equilibration Buffer. This process was repeated for the entire volume of protein solution.[21]

Once the entire protein solution was passed through the column, Wash Buffer fractions that showed above-baseline A_{280} readings were consolidated and concentrated down to 20 mL using an Amicon Stirred Cell equipped with a 3000 Da molecular weight filter. The concentrated solution was then dialyzed with 200 mL of water. This procedure was repeated for the Elution Buffer fractions that showed above-baseline A_{280} readings. 20 mL of collated Wash Buffer fractions and 20 mL of collated Elution Buffer fractions were collected. The concentrations of the collated Wash Buffer fractions and collated Elution Buffer fractions were determined via the Bradford Assay. SDS-PAGE was then used to monitor the extent of purification between the Wash and Elution buffer fractions.

MsrA Activity Assays

To determine if stereoisomers of MetO were present in the oxidized lysozyme variants, a spectrophotometric assay was employed. To a 1 mL cuvette, 100 μL of Assay Buffer (500 mM NaP_i, 20 mM EDTA, pH 7.40), 2 μL of thioredoxin reductase at 0.0229 mM, 14.5 μL of thioredoxin at 0.167 mM, 20 μL of MsrA at 0.0329 mM, 67 μL of NADPH at 2.99 mM, and 510.5 μL of water were added before the addition of 286 μL of 15 mg/mL MetO, Peak III, or Peak V. To assay Peaks I and IV, the same volumes of reagents were added except that 406.5 μL of water were added before the addition of 390 μL of 11 mg/mL Peak I of Peak IV. Before substrate was added, the instrument was blanked and a negative control was run to account for any background activity. Substrate was added to initiate the reaction and the decrease in the A_{340} was monitored for 1 minute.[21]

CHAPTER 3: RESULTS

Separation of Oxidized Lysozyme Variants Using HPLC

The oxidized lysozyme that was prepared as described in the Materials and Methods chapter was subjected to two steps of HPLC on a PolyCAT A cation-exchange column. Figure 3-1 shows the results of the separation.

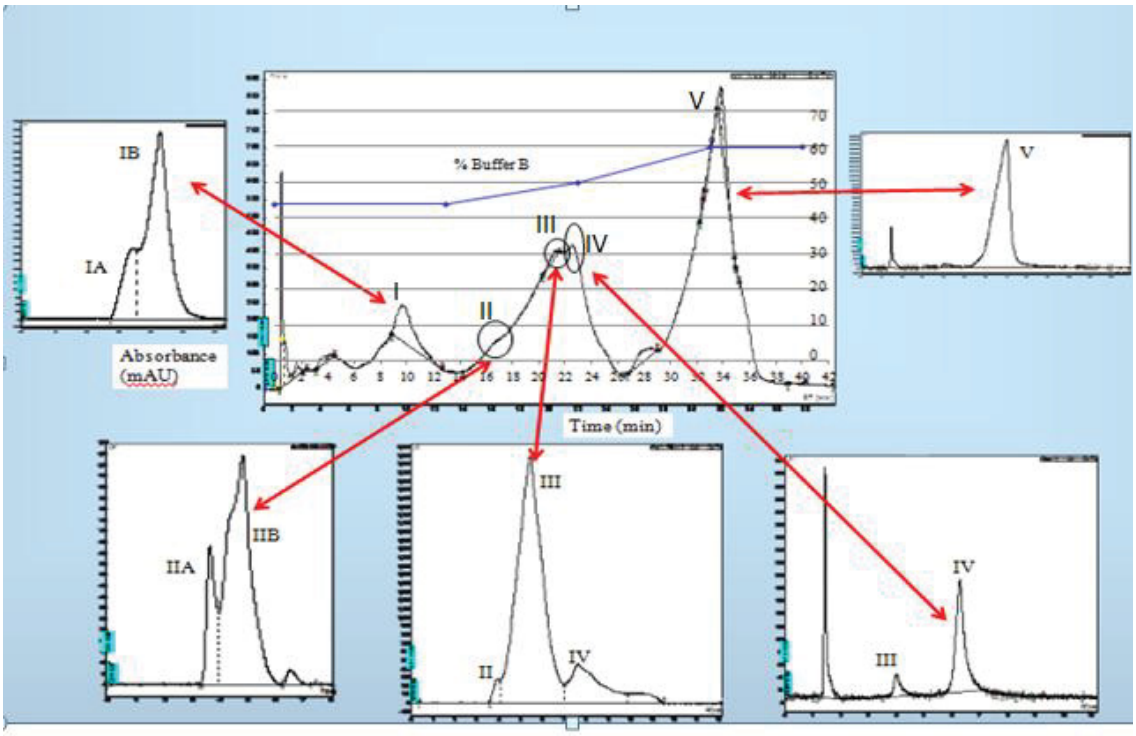

Figure 3-1: HPLC chromatograms showing the separation of oxidized HEWL variants. The central chromatogram shows the separation of oxidized HEWL into five different peaks. The blue line represents the Buffer B (20 mM KP_i, 0.4 M NaCl, pH 6.0) gradient during the elution of the peaks. Chromatograms surrounding the central chromatogram are from the second HPLC separation. Counter-clockwise from top left, Peaks IA and IB, Peaks IIA and IIB, Peak III, Peak IV, and Peak V. Separation of Peaks I, II, III, and V in the second step was performed using an isocratic system of 42% 20 mM KP_i, 0.4 M NaCl, pH 8. Peak IV was further purified using an isocratic system of 42% 20 mM KP_i, 0.4 M NaCl, pH 7.

Oxidized HEWL Protein Activity Assays

The activity of each of the oxidized HEWL peaks was analyzed using a spectroscopic assay. For each activity assay to be counted as valid, the decrease of absorbance at 450 nm

should be linear with the negative slope between 0.015 and 0.04 AU/min. An example of a valid assay is shown in Figure 3-2.

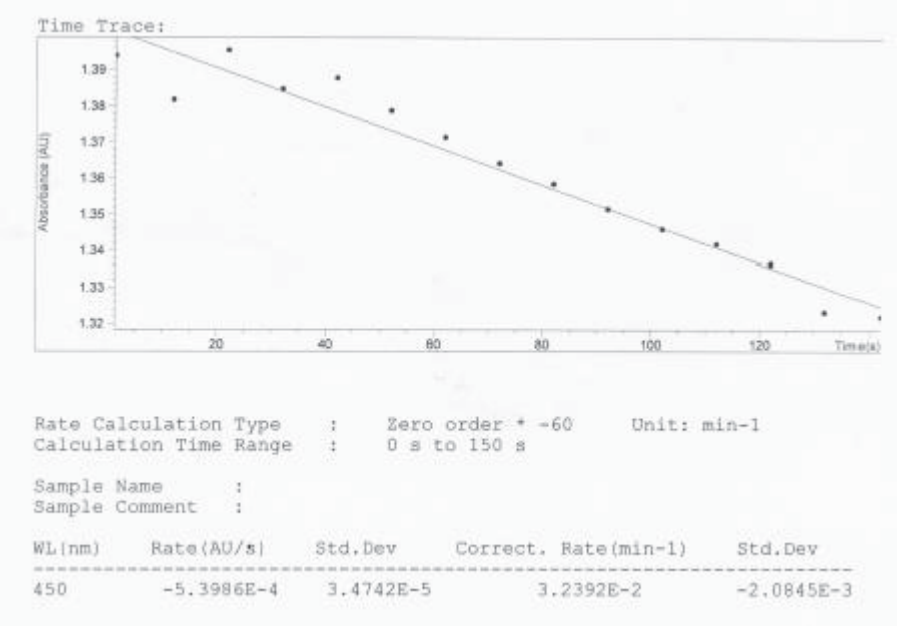

Figure 3-2: Example of a valid activity assay. Note the linearity through most of the 2.5 minute assay and the magnitude of the corrected rate (0.032 AU/min).

The activity of each peak, as well as controls, is summarized in Table 3-1. The protein variant was mixed with *Micrococcus lysodeikticus*, and the A_{450} was measured for 2.5 minutes. Each measurement was performed in triplicate, and the activity reported in the table is the average activity. The negative control represented the assay with no enzyme in the cuvette. Due to the low amount of protein isolated from Peaks IA and IIA, activity assays of these samples could not be performed.

Table 3-1: Results of Activity Assays

Sample	Concentration (mg/mL)	ΔA_{450}/min	Activity (units/mg)	Relative Percent Activity
Negative Control	0.00	2.61×10^{-3} ± 0.00125	N/A	N/A
Lyophilized HEWL	0.0370	0.031 ±0.005	8.45 ± 1.43	100
IB	0.0996	0.026 ±0.003	2.65 ± 0.31	31.4
IIB	0.0600	0.031 ±0.002	5.17 ± 0.38	61.2
III	0.0416	0.030 ±0.002	7.31 ± 0.46	86.5
IV	0.0242	0.044 ±0.004	18.2 ± 1.6	215
V	0.0106	0.024 ±0.001	22.6 ± 0.6	308

The equation used to generate the activity values in Table 3-1 is shown below:

$$Activity\left(\frac{units}{mg}\right) = \frac{\Delta A_{450}/min}{mg\ enzyme\ \ in\ reaction\ \ mix} \qquad \text{Equation 3-1}$$

Crystallization of Oxidized HEWL Protein Variants

Crystals of the oxidized HEWL variants were grown using the procedure outlined in Materials and Methods. Figures 3-3 to 3-5 show images of crystals obtained from Peaks III, IV, and V, respectively.

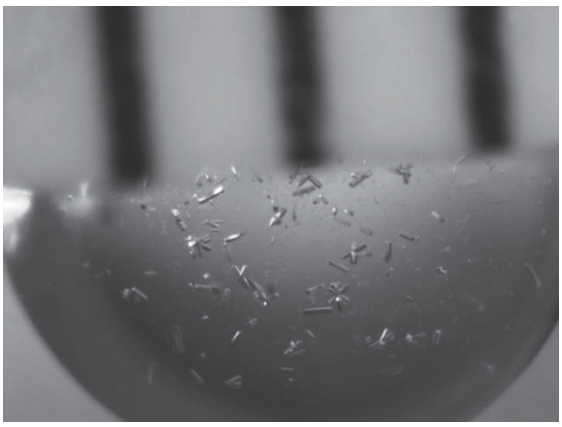

Figure 3-3: Crystals of Peak III. A ruler appears at the top of the figure. The distance from the center of one mark to the center of an adjacent mark represents 1 mm.

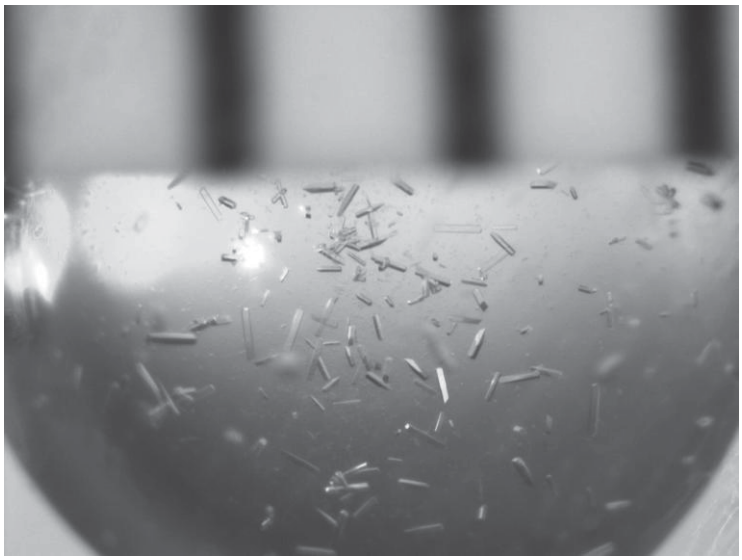

Figure 3-4: Crystals of Peak IV. A ruler appears at the top of the figure. The distance from the center of one mark to the center of an adjacent mark represents 1 mm.

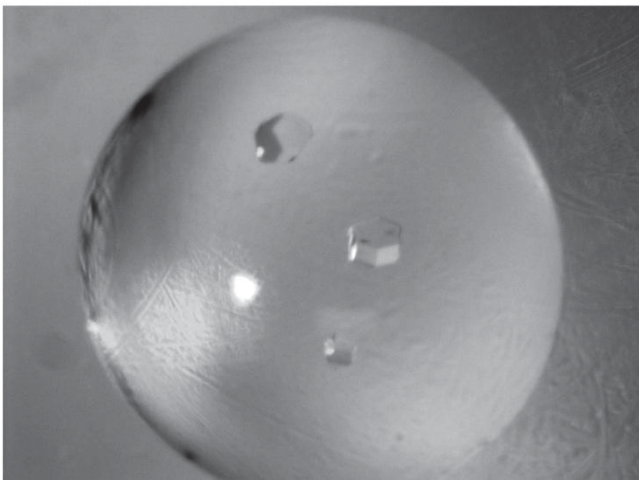

Figure 3-5: Crystals of Peak V. The crystals have an approximate length of 500 μm.

Crystals of Peak IA were also generated during the course of the crystallization procedure; however, due to the fact that the time required to crystallize the variant was not determined, an image of these crystals was not included in this chapter. Attempts to crystallize Peaks IB and IIB were not successful.

Tandem Mass Spectrometry of Oxidized Protein Variants

The primary sequence of each of the oxidized protein variants was examined by tandem mass spectrometry to determine the sites of oxidation. Table 3-2 (page 38) shows which residues were oxidized in each variant.

Expression of MsrA

Bacteria transformed with a recombinant vector containing the *S. cervisiae* MsrA gene were grown using the procedure outlined in the Materials and Methods chapter. The progress of bacterial growth was monitored by measuring the OD_{600} of the culture every 15 minutes. Figure 3-6 shows a graph of the gradually increasing optical density of the solution with time.

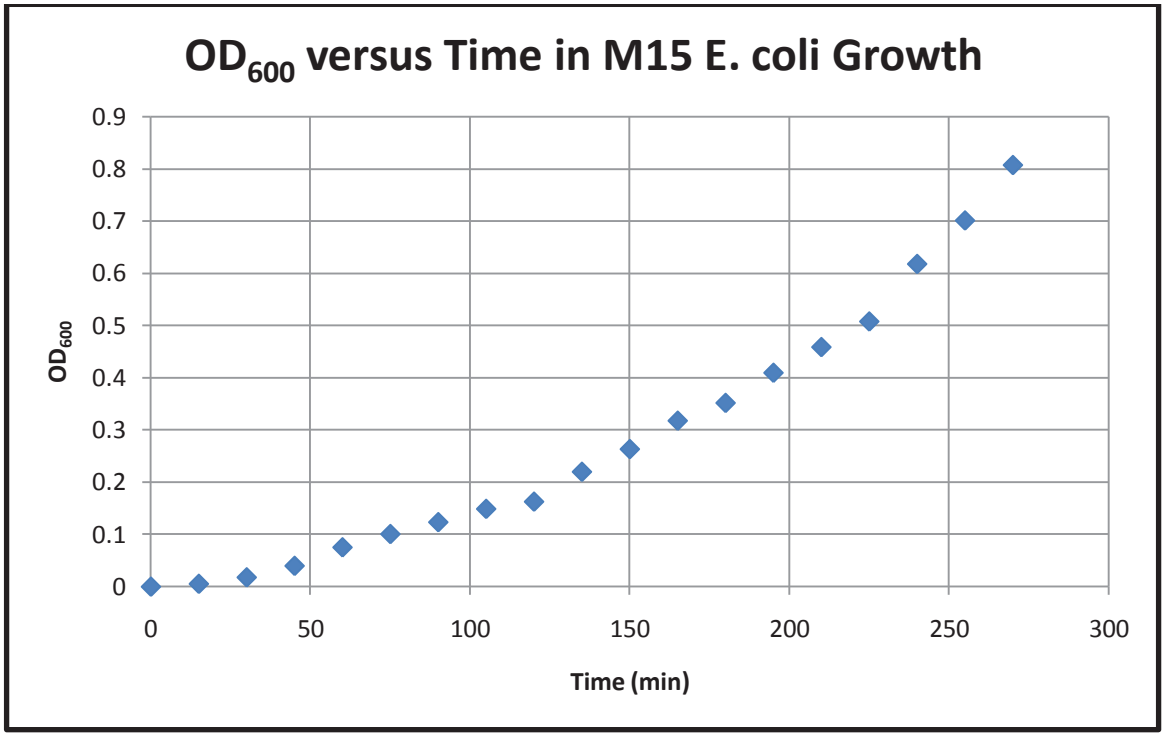

Figure 3-6: Graph showing the growth of the M15 *E. coli* cells as is indicated by the increasing OD_{600} value. IPTG was added when the bacteria were entering the log phase of growth (270 minutes).

Table 3-2: Percent of Oxidized Amino Acids Present in Each Oxidized HEWL Variant

	M12	H15	W28			W62			W63	M105	W108		W123	Two Sites in Same Peptide		
Peak	M12 ox	H15 ox	W28 ox	W28 di-ox	W28 kyn	W62 ox	W62 di-ox	W62 kyn	W63 ox	M105 ox	W108 ox	W108 di-ox	W123 ox	W62 di-ox + W63 ox	M105 ox + W108 ox	M105 ox + W108 di-ox
IA	X	X			X	X	X		X	X	X	X		X	X	
IB	X	X			X	X	X		X	X	X			X		
IIB	X	X		X	X	X	X		X	X	X		X	X	X	
III	X	X		X	X	X	X		X	X	X		X	X		
IV	X	X		X	X	X	X		X	X				X		
V	X	X			X	X	X		X	X			X	X		

*"kyn" means kynurenine, "ox" indicates a single oxidation event while "di-ox" indicates a double oxidation event occurred on the same residue. The two residues with a plus sign between them represents that in a particular fragment of that particular variant, two residues were oxidized together. Percent oxidation of each residue corresponds to color in legend.

100-90% | 79.9-70% | 59.9-50% | 29.9-20% | 9.9-8.0% | 5.9-4.0% | 1.9-0.01%

89.9-80% | 69.9-60% | 39.9-30% | 19.9-10% | 7.9-6.0% | 3.9-2.0%

After letting the bacteria grow for an additional 3.5 hours, the bacterial cells were lysed open and SDS-PAGE was used to analyze the protein content of the bacterial lysate. Figure 3-7 shows the results of the SDS-PAGE analysis.

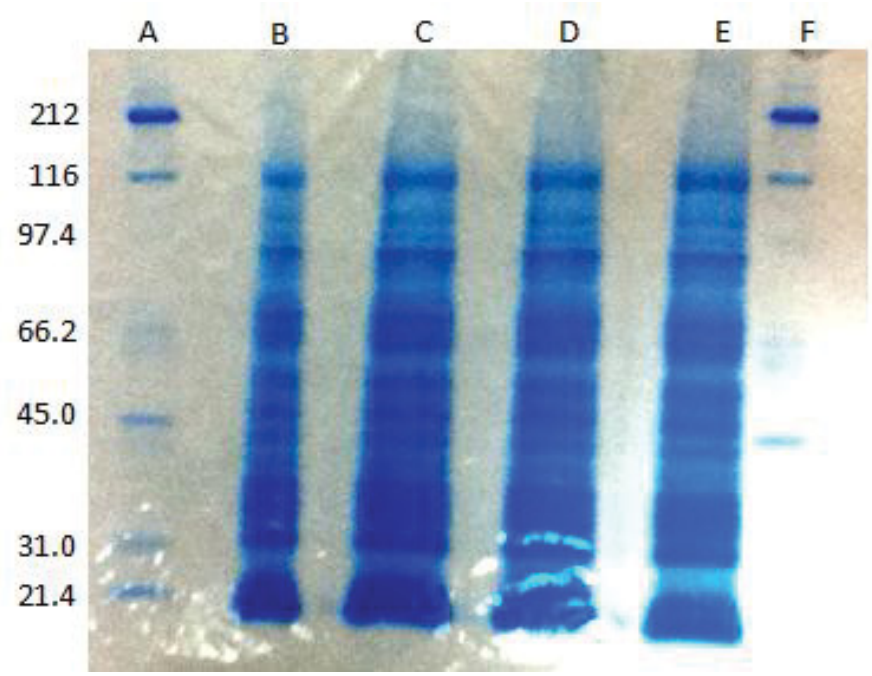

Figure 3-7: SDS-PAGE of bacterial lysate prior to column chromatography. Lanes A and F are molecular weight markers. Lanes B, C, D, and E show the bacterial lysate (10 µL, 1.05 mg/mL lysate). All molecular weight values are in units of kDa. Note the dark band around 21.1 kDa which corresponds to the molecular weight of MsrA.

Purification of MsrA

The bacterial lysate was purified using nickel affinity chromatography. After equilibrating the column with Equillibration Buffer, the bacterial lysate was loaded onto the column and Wash Buffer and Elution Buffer were used to elute contaminating proteins and the protein of interest, respectively. Figure 3-8 shows the elution profile of the lysate upon addition of the Wash Buffer, and Figure 3-9 shows the elution profile of the lysate upon addition of the Elution Buffer.

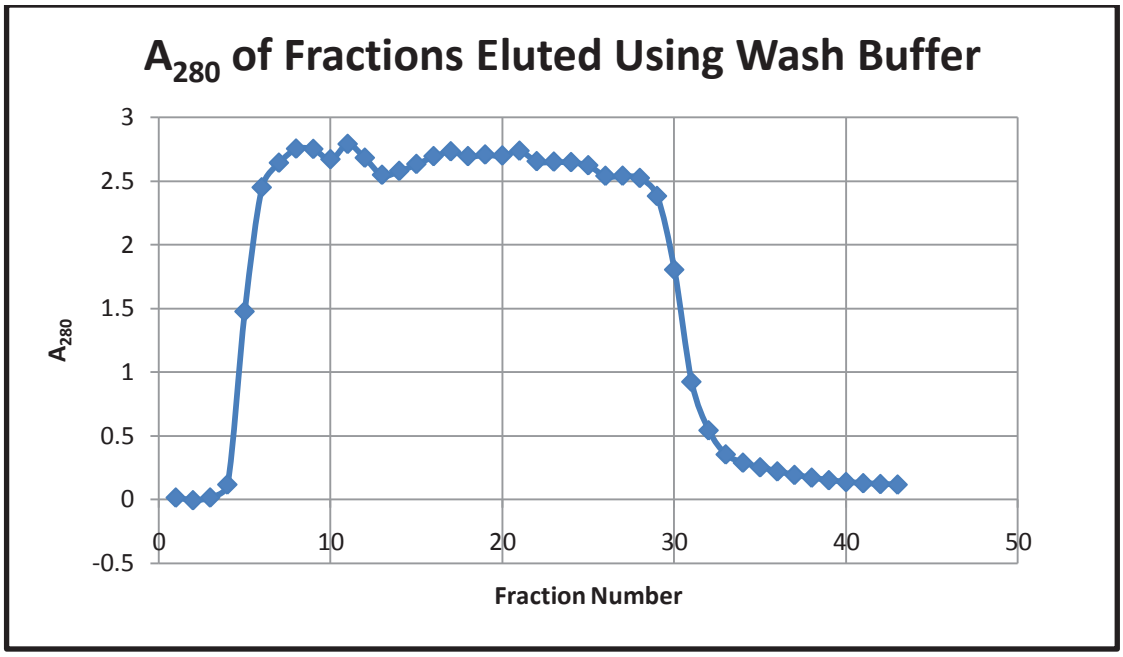

Figure 3-8: Elution profile of the bacterial lysate upon addition of Wash Buffer to the nickel affinity column. Fractions 4-36 were saved for further analysis.

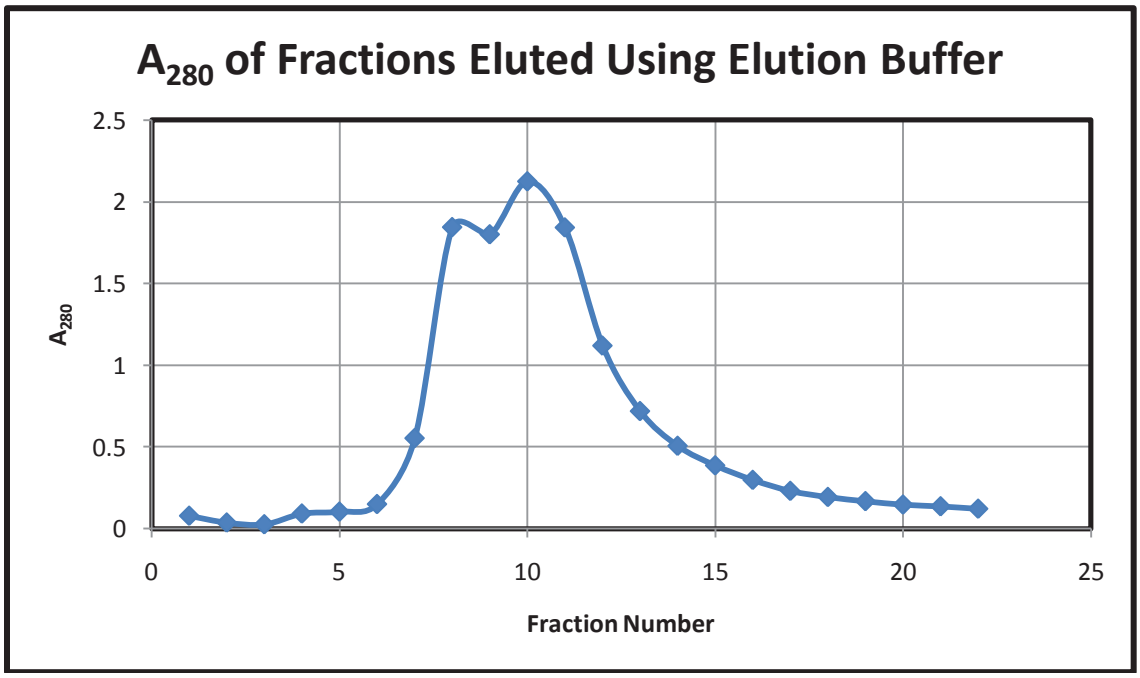

Figure 3-9: Elution profile of the bacterial lysate upon addition of Elution Buffer to the nickel affinity column. Fractions 7-14 were saved for further analysis.

The Bradford Assay was used to determine the concentrations of protein in the fractions collected with Wash Buffer and Elution Buffer (4.24 mg/mL and 4.82 mg/mL, respectively). Figure 3-10 shows an SDS-PAGE gel comparing the protein content of the Wash Buffer and Elution Buffer fractions.

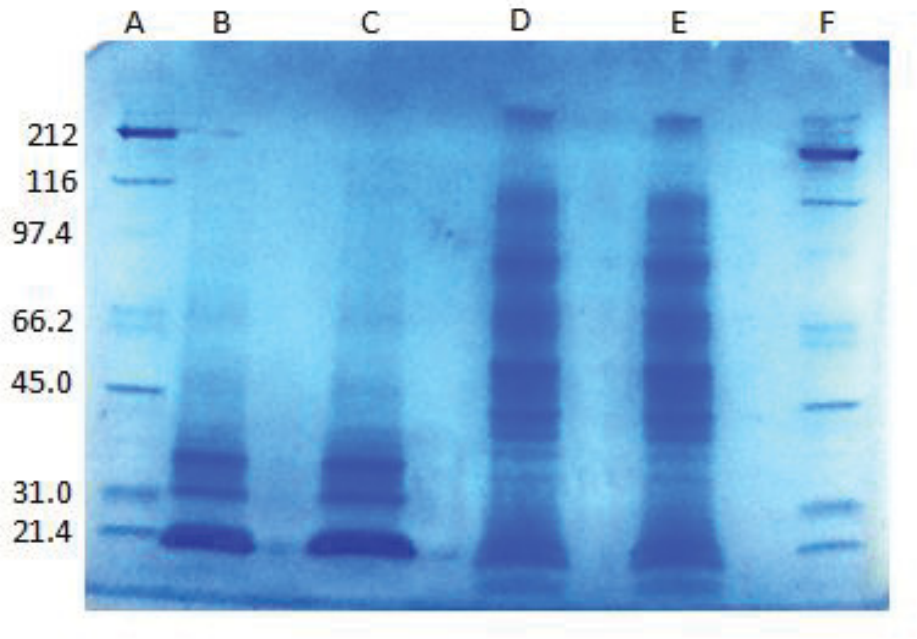

Figure 3-10: SDS-PAGE analysis of the fractions after column chromatography. Lanes A and F are molecular weight markers (all weights reported in kDa). Lanes B and C show the Elution Buffer fractions (20 µL, 4.82 µg/µL). Lanes D and E show the Wash Buffer fractions (20 µL, 4.24 µg/µL).

MsrA Activity Assays

Each of the oxidized lysozyme variants was tested for the presence of S-MetO by using MsrA. Figures 3-11 and 3-12 show graphs of a reaction that contains S-MetO and one that does not contain S-MetO. Note the lack of a linear trend in the reaction that does not contain S-MetO.

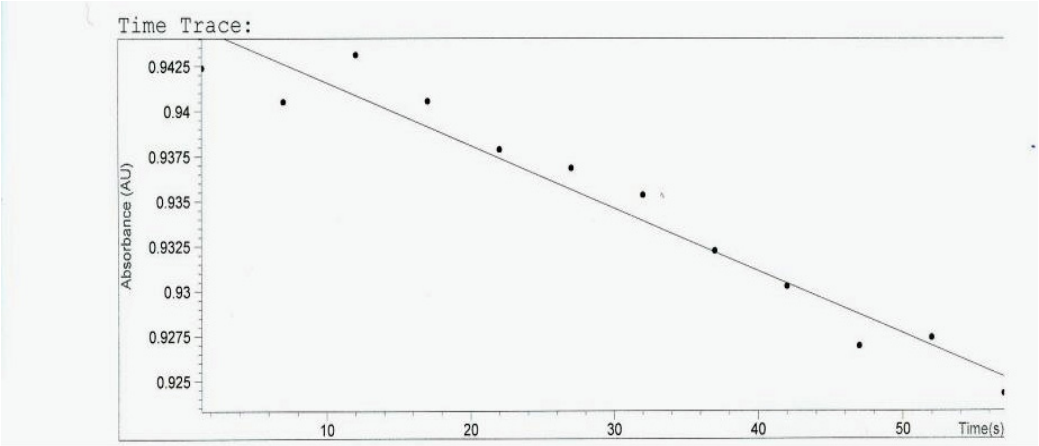

Figure 3-11: Graph plotting A_{340} vs. time (s) for a reaction containing S-MetO. Note the linear trend throughout the graph.

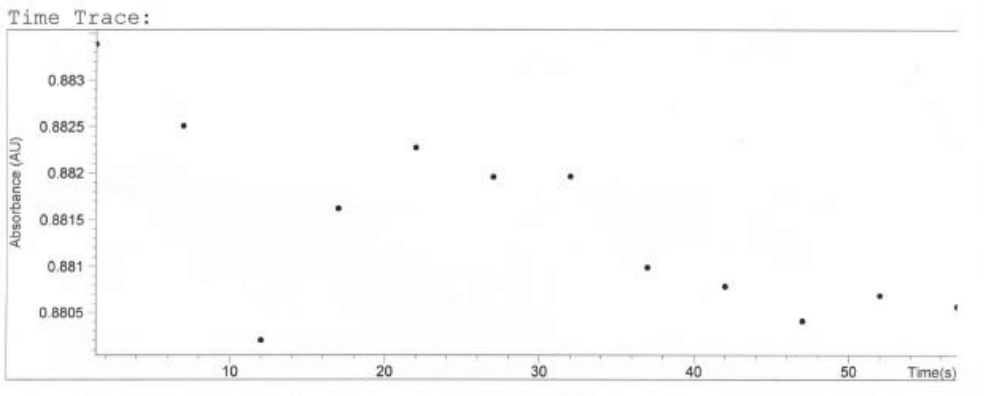

Figure 3-12: Graph plotting A_{340} vs. time (s) for a reaction not containing S-MetO. Note the lack of a linear trend throughout the graph.

Each oxidized HEWL variant was mixed with thioredoxin reductase, thioredoxin, MsrA, NADPH, buffer and water, and the A_{340} was monitored for 60 s. Table 3-3 summarizes the results of the MsrA activity assays.

Table 3-3: Results of the MsrA Assays

Peak*	Concentration (mg/mL)	Average ΔA_{340}/min (AU/min)	Linear?
Blank	0.0	$1.58 \times 10^{-4} \pm 1.3 \times 10^{-5}$	No
Native Lysozyme	15.0	$2.93 \times 10^{-4} \pm 2.2 \times 10^{-5}$	No
MetO	15.0	$2.57 \times 10^{-2} \pm 7.1 \times 10^{-3}$	Yes
Oxidized Lysozyme	15.0	$2.10 \times 10^{-2} \pm 1.7 \times 10^{-3}$	Yes
Peak I	11.0	$4.74 \times 10^{-2} \pm 1.3 \times 10^{-3}$	Yes
Peak IV	11.0	$5.62 \times 10^{-3} \pm 2.5 \times 10^{-4}$	No
Peak III	15.0	$1.25 \times 10^{-2} \pm 2.7 \times 10^{-3}$	Yes
Peak V	15.0	$4.67 \times 10^{-3} \pm 4.4 \times 10^{-4}$	No

* Peak I was assayed prior to its separation into Peaks IA and IB. There was not enough protein in Peak II for the assay.

CHAPTER 4: DISCUSSION

Oxidation of proteins can lead to the alteration of a protein's primary or tertiary structure. These structural changes can lead to inhibition or inactivation of enzymes. Oxidation of proteins has been positively correlated to several diseases including Parkinson's disease, Alzheimer's disease, and cataractogenesis. Oxidation of proteins has also been correlated to the aging process of cells and organisms.

Metal-catalyzed oxidation generates the hydroxyl radical when a metal ion reacts with the superoxide anion or hydrogen peroxide. The hydroxyl radical oxidizes all classes of biological molecules at diffusion-controlled rates. Metal-catalyzed oxidation can be considered site-specific since the hydroxyl radical generated at the metal binding site on a protein (ex: histidyl residues) will react in the immediate vicinity of its site of production.

Hen egg white lysozyme (HEWL) is a 14.3 kDa protein that catalyzes the hydrolysis of the NAM-NAG β(1→4) glycosidic bond found in bacterial cell walls. Lysozyme has been studied extensively since the 1950's, its catalytic mechanism has been elucidated, and its crystal structure is known; therefore, lysozyme makes for an excellent model protein. There is a single histidyl residue, H15, in the primary structure of HEWL. This provides a well-defined site for metal ion binding and can serve as a means to examine site-specific oxidation of the enzyme. By comparing the pattern of oxidation of native HEWL to a suite of site-directed mutants that either lack the H15 residue or have histidyl residues inserted elsewhere in the primary structure, one can see if the primary structure of a protein or its tertiary structure is more important in regards to determining the pattern of site-specific oxidation of a protein.

Figure 3-1 showed the separation of oxidized HEWL into five peaks by HPLC on a cation exchange column. A second separation scheme using 42% Buffer B and pH 8 (pH 7 for Peak IV) was used to achieve better resolution between peaks. Each fraction was analyzed by

electrospray ionization (ESI) and further by tandem mass spectrometry. The ESI data in Appendix B displays signals corresponding to different protein masses in each spectrum. This observation means that each peak isolated from the HPLC separation contains a mixture of proteins that have different modifications (e.g. mono-oxidation and di-oxidation events). The ESI spectrum for native HEWL only shows one prominent peak at 14304 Da, which corresponds with the molecular weight of HEWL. Peak IA had its most intense peak at 14335 Da, which corresponded to a +31 Da increase (two single oxidations or one di-oxidation event). Peak IB had its most intense peak at 14320 Da, which corresponded to a +16 Da increase (single oxidation). Peak IIB had its most intense peak at 14320 Da which corresponded to a +16 Da increase (single oxidation). Peak III had its most intense peak at 14290 Da which corresponded to a -14 Da decrease. This could have resulted from a single oxidation event followed by the liberation of a formaldehyde molecule. Peak IV had its most intense peak at 14321 Da which corresponded with a +17 Da increase (single oxidation within experimental error or the addition of a hydroxyl group). Peak V had its most intense peak at 14306 Da which corresponded to a +2 Da increase. This could have resulted from a double oxidation event followed by the liberation of formaldehyde. Pu *et al.* showed that fragmentation, by mass spectrometry, of serine-containing proteins can liberate formaldehyde molecules.[22] Since the primary structure of lysozyme has 10 Ser residues, it is highly likely that some of these Ser residues would lose formaldehyde during the fragmentation process. In Peaks III and V, M105 is 6.02 Å away from Ser 24, thus oxidation of M105 may promote the loss of formaldehyde during the fragmentation process.

From the results of the tandem mass spectrometry analysis, the number of amino acid residues that were oxidized can be quantified. Several amino acids were oxidized to different extents, but the residues that were most readily oxidized were H15, M105, and W108. A

common feature of all three residues is that they are all partially exposed to the surface and, therefore, they are more susceptible to oxidizing conditions. The other residues that were oxidized were buried and essentially not exposed to solvent, thus accounting for their low percentage of oxidation. However, computational modeling done by Petruk *et al.* showed that intramolecular electron transfer can occur in proteins and peptides that contain redox active side chains. Even though their study focused on Cys and Tyr-rich peptides, they extended their discussion to include the possibility that if the pH and hydrophobicity of the interior of the protein permits electron transfer, and if free radical oxidation occurred, interior residues could become oxidized.[23] Therefore, an electron chain could have developed that transferred the radical from H15 through the protein to W108.

In general, the number of oxidized residues, going from Peak I to Peak V, decreases. This result corresponds to a decrease in the polarity of the oxidized variant going from Peak I to Peak V. Though charge is the key factor in separation by cation-exchange HPLC, oxidation of multiple residues, and thus an increase in polarity of the variant, may lead to tertiary structural changes. This may lead to different affinities for each of the variants for the cation-exchange resin.

The residue that was oxidized to a relatively high extent in all of the protein variants was H15. In Table 3-2, it was shown that H15 had the highest percent oxidation among all the oxidized residues. Histidine has a high affinity for copper ions; therefore, if the protein is subjected to an MCO system, the hydroxyl radical will be in close proximity to the histidyl residue. Oxidation of histidine to 2-oxo histidine results in the addition of a double bonded oxygen atom to the imidazole ring of histidine. Due to the electronegativity of oxygen, it is likely the pK_a of the imidazole ring proton would decrease, thus histidine would become a

stronger acid. This would then lead to histidine becoming more easily deprotonated, which would result in a loss of positive charge to the protein variant and an earlier elution time.

Several other reasons could explain the elution times seen in the HPLC chromatogram. Oxidation of other residues in the variant could lead to the lowering of the pK_a of these residues (ex: Glu 35), which could become deprotonated and result in an earlier elution time. The tandem MS data showed that asparagine is oxidized to aspartic acid (N103D) in Peaks IB, II, and III. This would result in the introduction of negative charge to the protein and would result in an earlier elution time from the cation exchange column. Finally, since each peak obtained from the HPLC separation contains a mixture of proteins with different numbers of oxidation events, this explains why some of the peaks were not symmetrical. Since most of the oxidized residues were buried or only partially exposed, this could be a reason why the variants eluted at roughly the same time.

The results of the activity assay were summarized in Table 3-1. Peaks I, IIB, and III all had a lower activity than native lysozyme while Peaks IV and V showed higher activity than native lysozyme. Correlating these results with the tandem mass spectrometry results, it can be noted that W108 is oxidized in Peaks I, IIB, and III, while it is not oxidized in Peaks IV and V. The role of W108 in HEWL, as was determined by Inoue *et al.*, is to increase the pK_a of Glu 35, stabilize the tertiary structure of HEWL, and assist in substrate binding. Inoue *et al.* showed that substitution of a less hydrophobic amino acid in place of W108, such as tyrosine or glutamine, caused a decrease in the pK_a of Glu 35 by 0.6 pK_a units, dropping the pK_a of Glu 35 from 6.1 to 5.5. This value is still higher than the pK_a of glutamic acid; therefore, the researchers concluded that the electrostatic interaction between Asp 52 and Glu 35 is also involved in elevating the pK_a of Glu 35. The decrease in the pK_a of Glu 35 by 0.6 pK_a units would result in an approximately 5-fold increase in the ease of deprotonation of this residue,

thus lowering the catalytic efficiency of the enzyme which requires a protonated Glu 35 for its mechanism. The researchers also noted that the substitution of a less hydrophobic amino acid for W108 resulted in a loss of 3.4 kcal/mol from the standard free energy of stabilization for lysozyme. This energy loss corresponded entirely to the hydrophobic free energy of W108. Finally, Inoue, *et al.* calculated that the dissociation constant (K_d) increased in the mutant lysozymes as compared to native lysozyme by as much as 300-fold leading them to conclude that W108 is essential in substrate binding. They concluded that the catalytic mechanism of HEWL is dependent on both the catalytic amino acid residues and on maintaining a hydrophobic environment in the substrate binding site of HEWL.[24] Therefore, it is likely that oxidation of W108 plays a central role in the measured loss of activity seen in Peaks I, IIB, and III.

The introduction of negative charge due to the N103D oxidation event could have resulted in reduced activity. N103 is approximately 4 Å from D101. Asp 101 interacts with residues A and B of the NAG-NAM hexasaccharide. Oxidation of Asn 103 to aspartic acid would place two negatively charged residues near each other. This could lead to charge repulsion between the two residues which could lead to tertiary structural changes that decrease the enzyme's affinity for substrate.

As was noted previously, Peaks IV and V did not have W108 oxidized, and these peaks actually had significantly higher activity than native lysozyme. Electrospray ionization (ESI) mass spectrometry did not show large shifts in the molecular weight of the protein that would be apparent through dimerization or cross-linking with protein fragments. Also, an SDS-PAGE gel run after the oxidation reaction (data not shown) revealed no bands at 28.6 kDa or higher. Therefore, only one active site was present in the protein variants. W62 is oxidized to a small extent in protein from Peak IV and to a larger extent in protein from Peak V. Work by

Maenaka *et al.* showed that W62 is involved in interacting with the saccharide ring through van der Waals contact and in maintaining the steric configuration of the lysozyme-sugar interaction.[25] Therefore, oxidation of this residue could lead to an increase in the binding affinity of HEWL to substrate through new interactions that could increase the turnover number of the enzyme, thus accounting for the increase in activity.

Figures 3-3 to 3-5 showed images of crystals of Peaks III, IV, and V, respectively. Some of the crystals were less than 100 μm in length; however, they were still sufficiently large enough to attempt a determination of the crystal structure of these oxidized proteins. Using the instrumentation at the Cleveland Center for Membrane and Structural Biology, the crystals of Peaks III, IV, and V were analyzed. Upon data analysis, though, the crystals appeared to be those of the native enzyme. This result could have been due to the fact that the samples that were analyzed were not one pure variant. Looking at the chromatogram in Figure 3-1, one can see that the separation between Peaks IA and IB was not baseline separation; therefore, mixing between the two variants could have occurred. The separation between Peaks IIA and IIB was also not baseline. Finally, Peak V was not symmetrical meaning that more than one protein could be represented by that peak. Data from the ESI spectra (Appendix B) show that all of the peaks are mixtures of more than one protein variant. By having more than one protein in each peak, the modifications could "average" each other out, thus getting a crystal structure that does not show the electron density of the modifications, or there could be preferential crystallization of the most lightly modified oxidized variant.[26]

Another reason why the modifications to the oxidized residues did not show up in the crystal structure could be due to the flexibility of the protein. If the modified residues undergo thermal vibrations, then the electron density would be smeared over the actual location of the

modification. Due to the low intensity of the electron density in this region of the structure, the modification would not be detectable.[26]

A final reason why the crystal structure of the protein variants could not be determined is due to the low percent of appearance of each of the oxidized residues in each protein variant. Table 3-2 showed the residues that were oxidized in each variant and the percentage of their appearance. In all the protein variants, the only residue that was oxidized to a large extent was H15; oxidation of the other residues occurred in low percentages. If these residues are only oxidized in a small number of molecules present in each variant, then the crystals that were produced would show very weak electron density corresponding to the modifications; therefore, the crystal structure would not show the modified residues. Arenas *et al.* generated oxidized lysozyme after letting the oxidation system react with the protein for 60 – 180 minutes.[27] Longer reaction times (60 – 120 minutes) have also been used to generate oxidized lysozyme by Jimenez *et al.*[28] Both studies showed evidence that the longer the protein is exposed to oxidizing conditions, the greater the extent of oxidation that occurred in the protein. Increasing the length of time that HEWL is exposed to the MCO system may increase the percentage of protein molecules that show the oxidized residues.

The enzyme MsrA was purified from M15 *E. coli* cells in order to investigate whether stereoisomers of MetO were generated. Figure 3-10 shows one prominent band at 21.1 kDa which corresponds to the molecular weight of MsrA. The two additional bands that are above the band corresponding to MsrA are likely proteins that also have a high affinity for nickel, thus they bound to the column with an equal affinity as did the His-tagged MsrA. These additional proteins did not appear to interfere with the MsrA activity assays.

Table 3-3 showed the results of the MsrA activity assays. The assays performed with native lysozyme showed very little activity, indicating that the native lysozyme has no S-

MetO. The assays with MetO showed significant activity and a linear relationship between the decrease in the A_{340} with time. Interestingly, assays with Peak I as substrate showed higher activity than with MetO as substrate. An explanation for this result could be found in the way MetO was prepared. The MetO used in the assay was prepared by using a reaction that likely generated a racemic mixture of MetO. Since MsrA only reacts with S-MetO, not all of the substrate MetO may have been S-MetO; therefore, the enzyme may not have reacted with all of the substrate. Peak I has two Met residues that were oxidized, M12 and M105, however, M12 is only oxidized to a small extent (less than 2% in all samples). M105 may be the S-enantiomer, thus accounting for the higher activity. Peak III also has M12 and M105 oxidized; however, it showed a lower activity than Peak I. One reason for this observation could be due to the fact that one of the oxidized Met residues could be the R-enantiomer or there is a mixture of R- and S-enantiomers since metal-catalyzed oxidation does not produce only one enantiomer. MsrA would not recognize this enantiomer, so the activity would be lower with Peak III as a substrate. Also, the Peak I that was assayed was a mixture of Peaks IA and IB which had a percent oxidation of M105 (or W108) of 30.66% and 69.86%, respectively, while Peak III had a percent oxidation of M105 (or W108) of 35.89%. Due to the higher percent oxidation in Peak IB, there could have been more substrate available for MsrA, thus accounting for the higher activity. Table 3-3 also showed that when Peaks IV and V were used as substrate for MsrA, the enzymatic activity decreased by about an order of magnitude, as compared to the MetO standard, and adopted a non-linear relationship. This could be due to the fact that Peaks IV and V contain the R-enantiomer for both M12 and M105. Also, the percent oxidation of M12 and M105 is lower than in Peaks I and III, thus there is less substrate available for the enzyme. Since there was little or no S-MetO present, MsrA would not use this protein as substrate, and thus would show no activity.

Since enantiomers of MetO were generated and formed in different protein peaks, this could be another reason for the observed separation seen in the HPLC chromatogram. Separation by HPLC is dependent on surface interactions between the protein or molecule and the resin. With enantiomers of MetO, the resin can see two possible "faces" of the protein: a face showing the oxygen atom of the sulfur-oxygen double bond or the lone pair of electrons on the sulfur. An oxygen atom would be much more polar than a lone pair of electrons; therefore, protein variants with the electron pair facing the resin would elute earlier than protein variants with the oxygen atom facing the resin.[29]

CHAPTER 5: CONCLUSION

Due to the availability of metal ions present in organisms, metal-catalyzed oxidation is a modification that proteins and other biological molecules are constantly susceptible to. How the primary or tertiary structure of a protein affects the pattern of oxidation seen in proteins is an avenue of research that could lead to a better understanding of their role in Parkinson's disease, Alzheimer's disease, cancer, and other chronic diseases.

Upon oxidation and purification of HEWL, the amino acid residues that were oxidized in the protein were determined by tandem MS. In all the protein variants, H15 was oxidized and in the highest percentage. This provides evidence that oxidation was largely site-specific. The activity of each variant was examined, and it was seen that the activity of Peaks I-III decreased upon oxidation while the activity of Peaks IV and V increased upon oxidation. Crystals of Peaks IB, III, IV, and V were grown, but attempts at determining the crystal structure of these variants were unsuccessful.

Future work should include exposing HEWL to the oxidation reaction for extended periods of time to examine if this longer exposure will increase the percent oxidation of some of the residues in the protein variants. This should be followed with the development of a better HPLC separation scheme to purify the protein variants to obtain one pure form. Solving the crystal structures of each variant would allow one to see how the oxidized residues affect the tertiary structure of HEWL, and this could lead to a possible explanation for the increased activity of Peaks IV and V. Finally, mutagenesis studies, including the removal of H15 and placing a histidine residue in other regions of the protein could provide further insight on how the relationship between primary sequence and tertiary structure affects the pattern of oxidation.

CHAPTER 6: REFERENCES

1) Bandyopadhya, U.; Das, D.; and Banerjee, R. K. *Curr. Sci. India*. **1999**, *77*, 658-666.

2) Hussain, S. P., Aguilar, F., Amstad, P. and Cerutti, P. *Oncogene*. **1994**, *9*, 2277-2281.

3) Berlett, B. S. and Stadtman, E. R. *J. Biol. Chem*. **1997**, *272*, 20313-20316.

4) Stadtman, E. R. and Berlett, B. S. *Chem. Res. Toxicol.* **1997**, *10*, 485-494.

5) Stohs, S. J. and Bagchi, D. *Free Radical Bio. Med*. **1995**, *18*, 321-336.

6) Fenton, H. J. H. *J. Chem. Soc. Trans*. **1894**, *65*, 899-911.

7) Stadtman, E. R. and Levine, R. L. *Amino Acids*. **2003**, *25*, 207-218.

8) Davies, M. J. *Biochim. Biophys.Acta*. **2005**, 1703, 93-109.

9) Vogt, W. *Free Radical Bio. Med*. **1995**, *18*, 93-105.

10) Moskovitz, J., Poston, J. M., Berlett, B. S., Nosworthy, N. J., Szczepanowski, R., and Stadtman, E. R. *J Biol. Chem.* **2000**, *275*, 14167-14172.

11) Sreekumar, P. G., Hinton, D. R., and Kannan, R. *World J. Biol. Chem*. **2011**, *2*, 184-192.

12) Tete-Favier, F.; Cobessi, D.; Boschi-Muller, S.; Azza, S.; Branlant, G.; and Aubry, A. *Structure Fold Des.* **2000**, *8*, 1167-1178.

13) Aachmann, F. L.; Del Conte, R.; Kwak, G.; Kim, H.; Gladyshew, V. N.; and Dikiy, A. *Proteins*. **2011**, *79*, 3123-3131.

14) Callewaert, L. and Michiels, C. W. *J. Biosci.* **2010**, *35*, 127-160.

15) Canfield, R. E. and Liu, A. K. *J. Biol. Chem.* **1965**, *240*, 1997-2002.

16) Diamond, R.; Phillips, D. C.; Blake, C. C. F.; and North, A. C. T. *J. Mol. Biol.* **1974**, *82*, 371-391.

17) Blake, C. C. F.; Johnson, L. N.; Mair, G. A.; North, A. C. T.; Phillips, D. C.; and Sarma, U. R. *Proc. R. Soc. London Ser. B*. **1967**, *167*, 378-388.

18) Sophianopoulous, A. J.; Rhodes, C. K.; Holcomb, D. N.; and Van Holde, K. E. *J. Biol. Chem.* **1962**, *237*, 1107-1112.

19) Fasman, G. D. and Cox, M. "Practical Handbook of Biochemistry and Molecular Biology." Taylor and Francis Inc. **1989**, 281-282.

20) Shugar, D. *Biochimica et Biophysica Acta.* **1952**, *8*, 302-309.

21) Moskovitz, J.; Berlett, B. S.; Poston, J. M.; and Stadtman, E. R. *Proc. Natl. Acad. Sci. USA*. **1997**, *94*, 9585-9589.

22) Pu, D. and Cassady, C. J. *Rapid Commun. Mass Spectrom*. **2008**, *22*, 91-100.

23) Petruk, A. A.; Bartesaghi, S.; Trujillo, M.; Estrin, D. A.; Murgida, D.; Kalyanaraman, B.; Marti, M. A.; and Radi, R. *Arch. Biochem. Biophys.* **2012**, 525, 82-91.

24) Inoue, M.; Yamada, H.; Yasukochi, T.; Kuroki, R.; Miki, T.; Horiuchi, T.; and Imoto, T. *Biochemistry*. **1992**, *31*, 5545-5553.

25) Maenaka, K., Kawai, G., Watanabe, K., Sunada, F., and Kumagai, I. *J. Biol. Chem.* **1994**, *269*, 7070-7075.

26) Yee, V. Personal Communication. **2013**.

27) Arenas, A., Alarcón, C. L., Kogan, M., Lissi, E., Davies, M. J., and Silva, E. *Chem. Res. Toxicol.* **2013**, *26*, 67-77.

28) Jiménez, I., Lissi, E. A., and Speisky, H. *Arch. Biochem. Biophys.* **2000**, *381*, 247-252.

29) Alpert, A. Personal Communication. **2013**.

Appendix A

HPLC Chromatographs

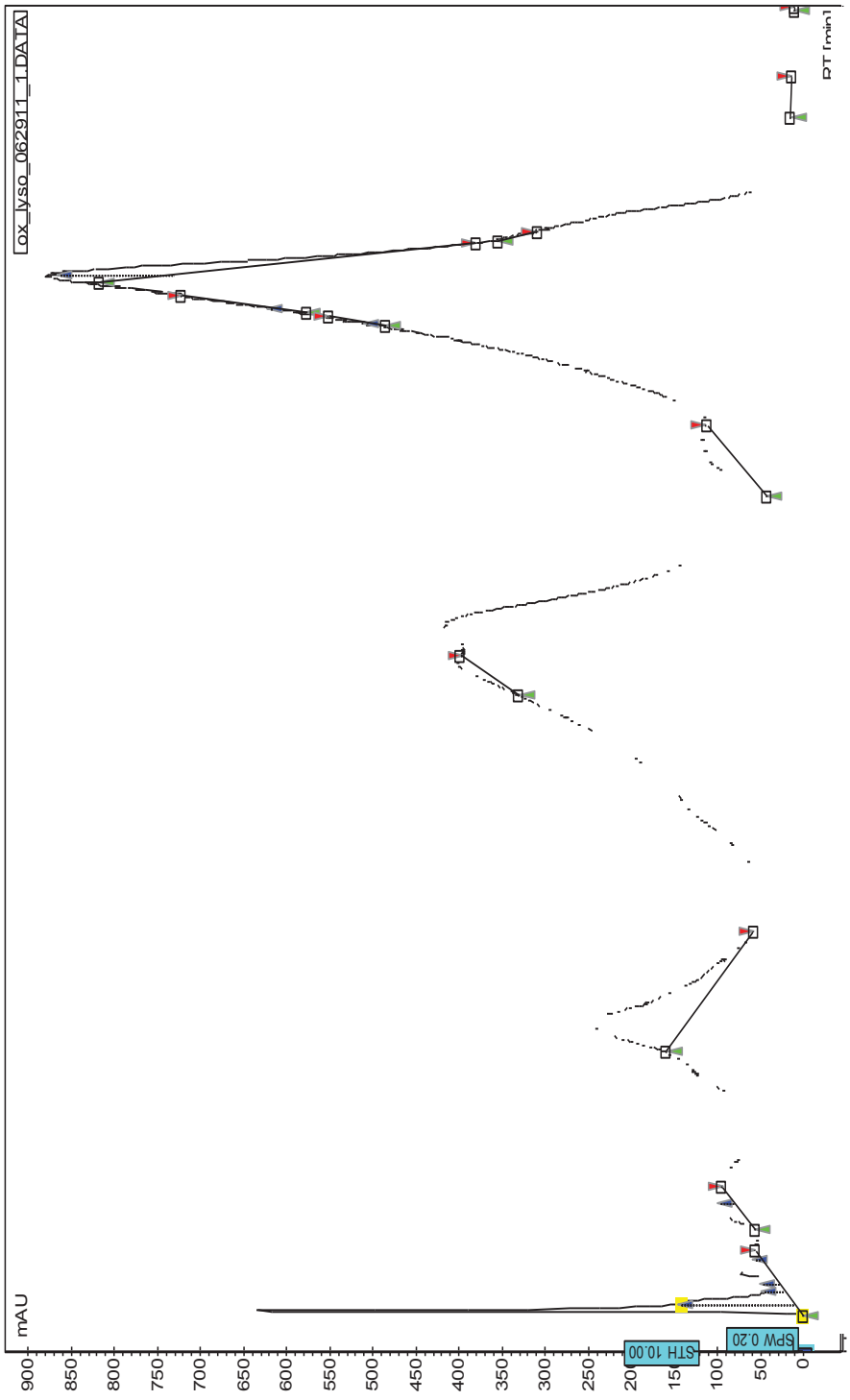

Figure A-1: Initial chromatograph of crude oxidized HEWL. See main text for the details on the separation scheme

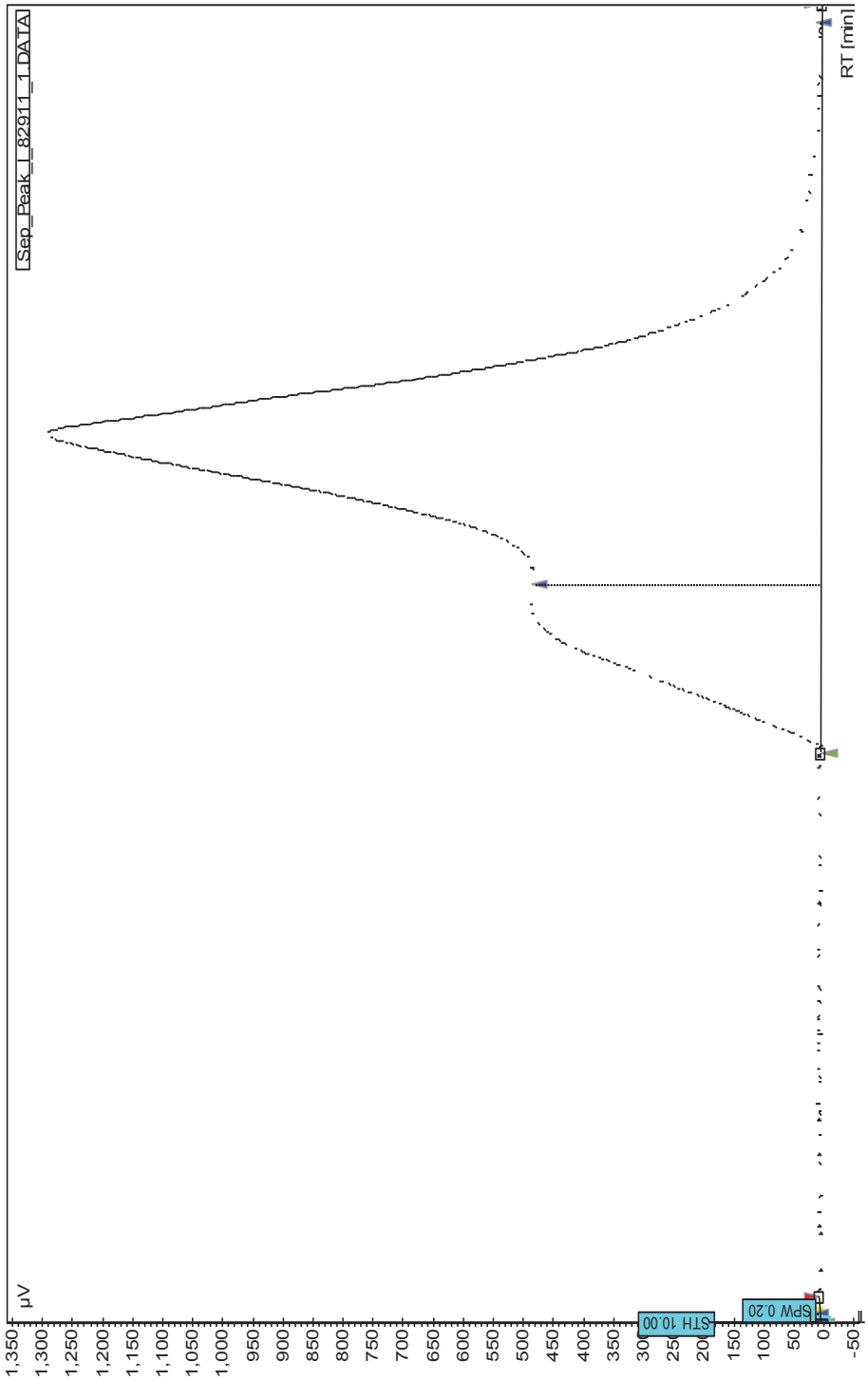

Figure A-2: Separation of Peak I into IA and IB. See main text for separation scheme.

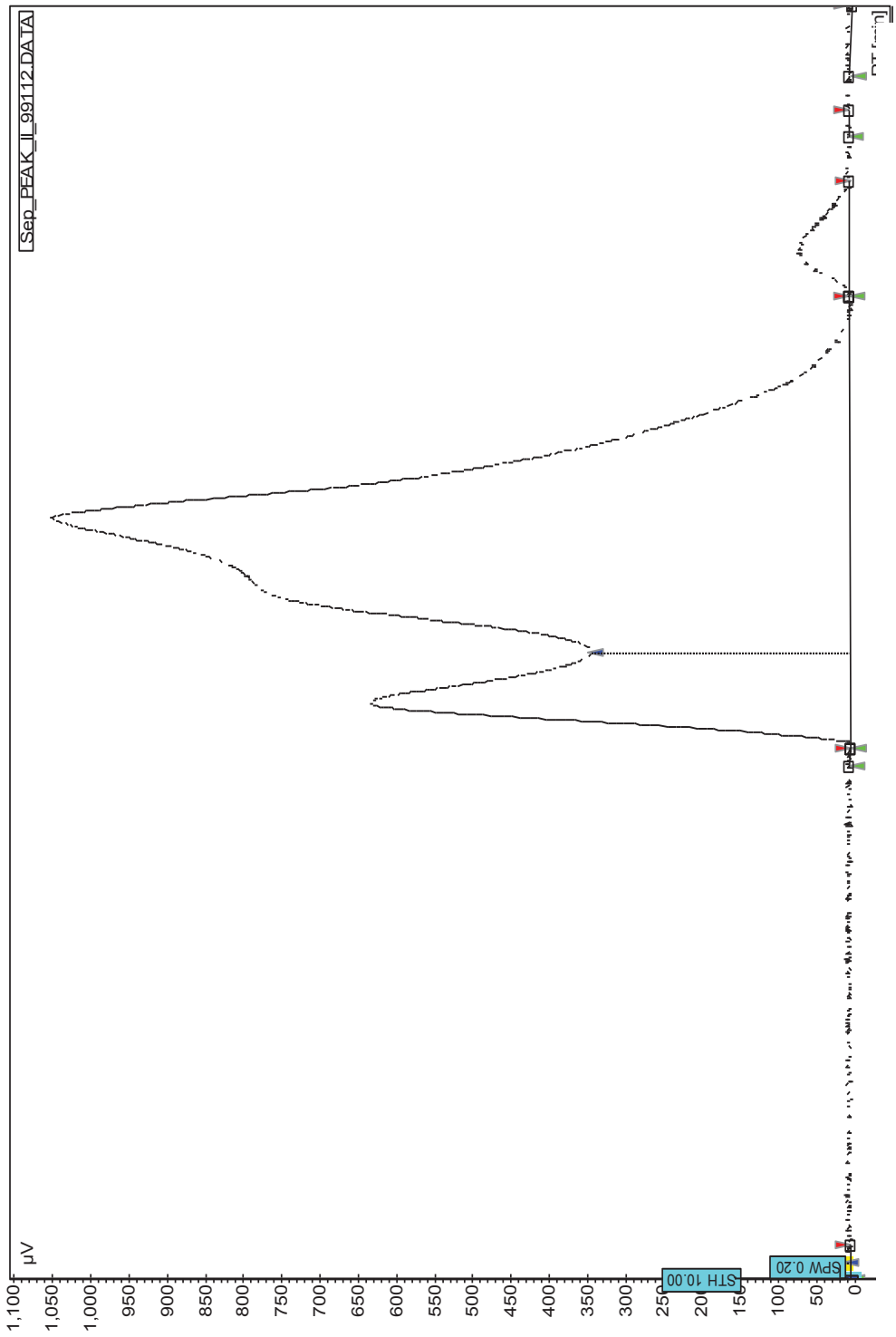

Figure A-3: Separation of Peak II into IIA and IIB. See main text for separation scheme.

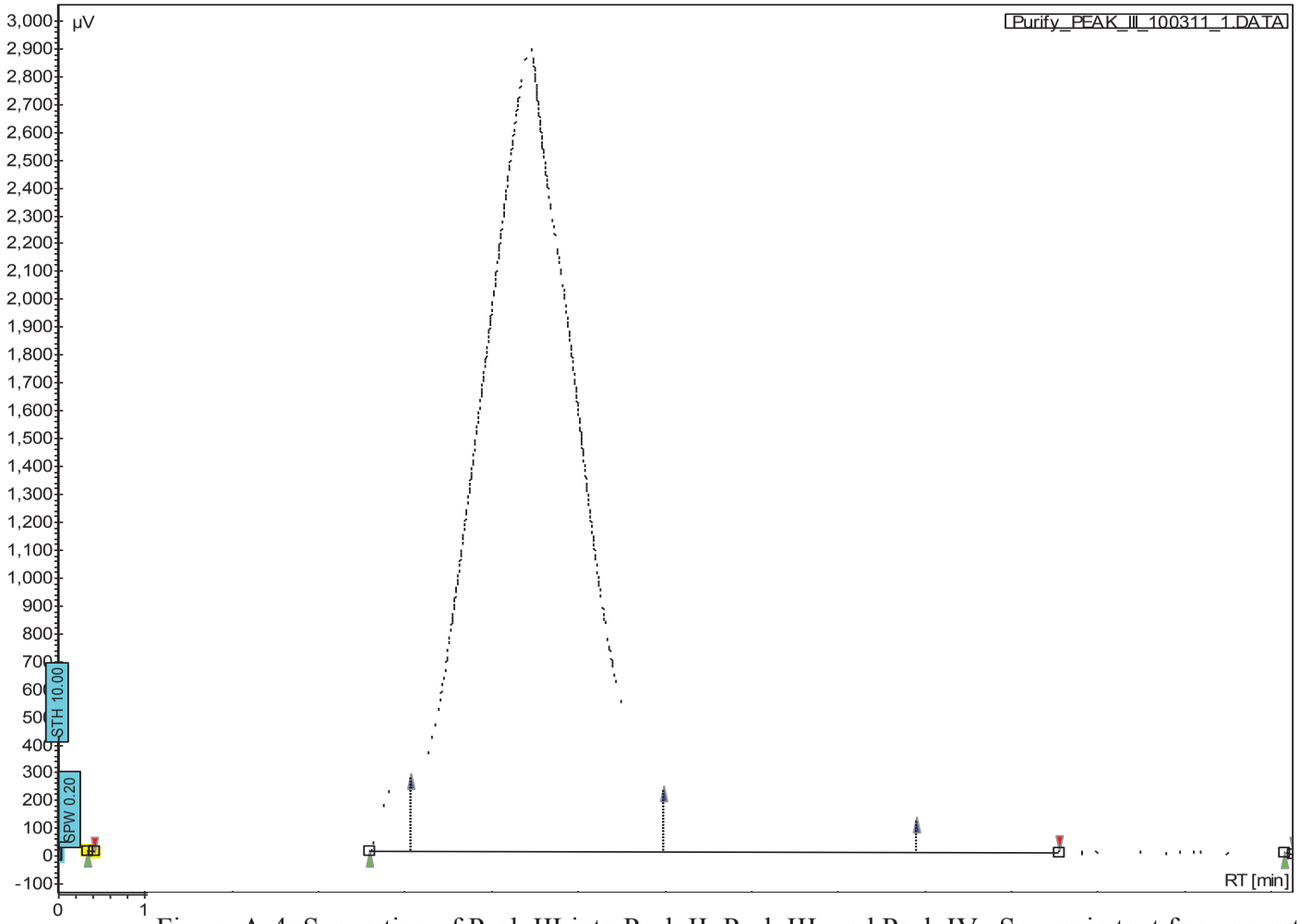

Figure A-4: Separation of Peak III into Peak II, Peak III, and Peak IV. See main text for separation scheme.

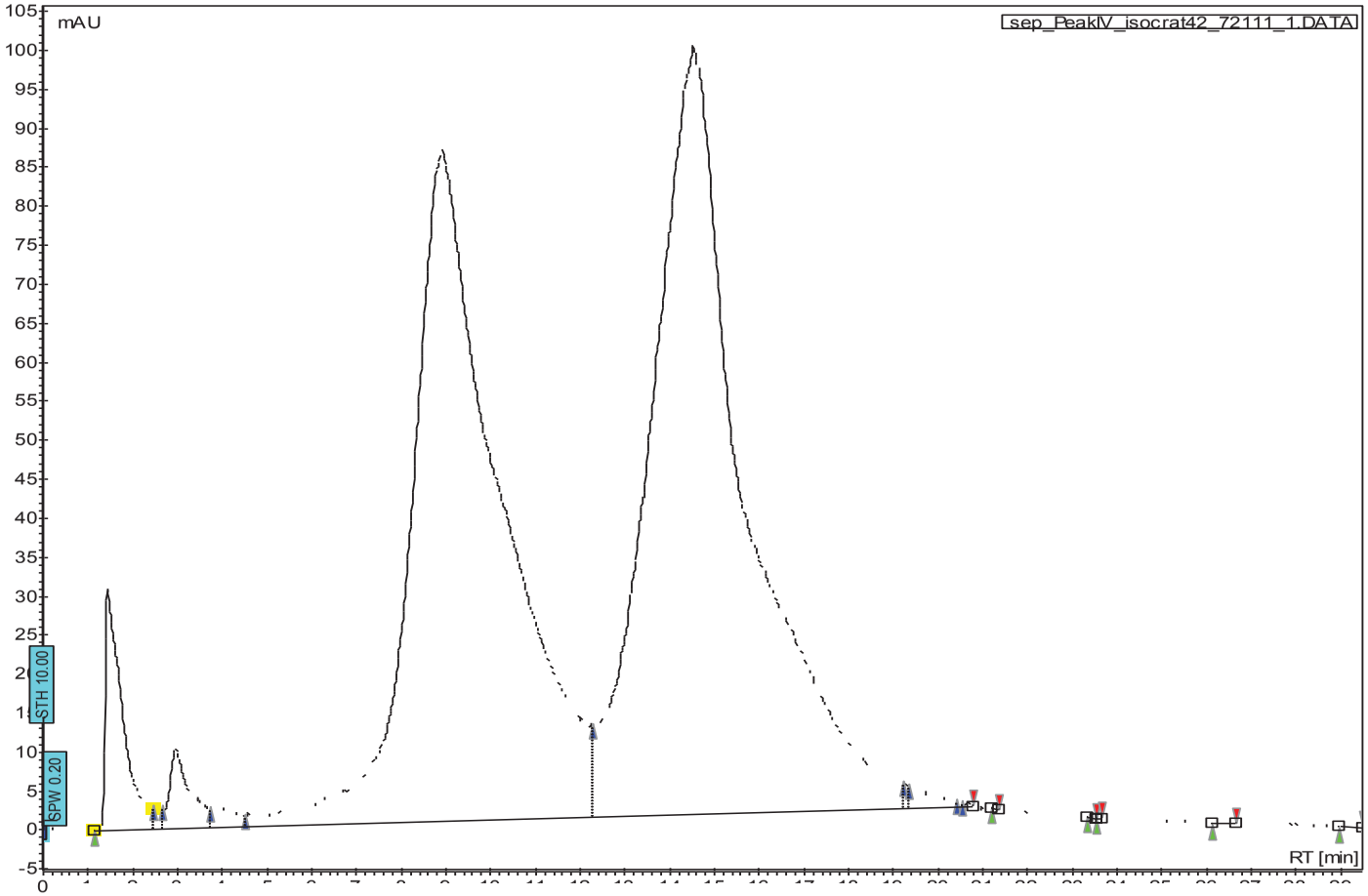

Figure A-5: Separation of Peak IV into Peak III and Peak IV. See main text for separation scheme.

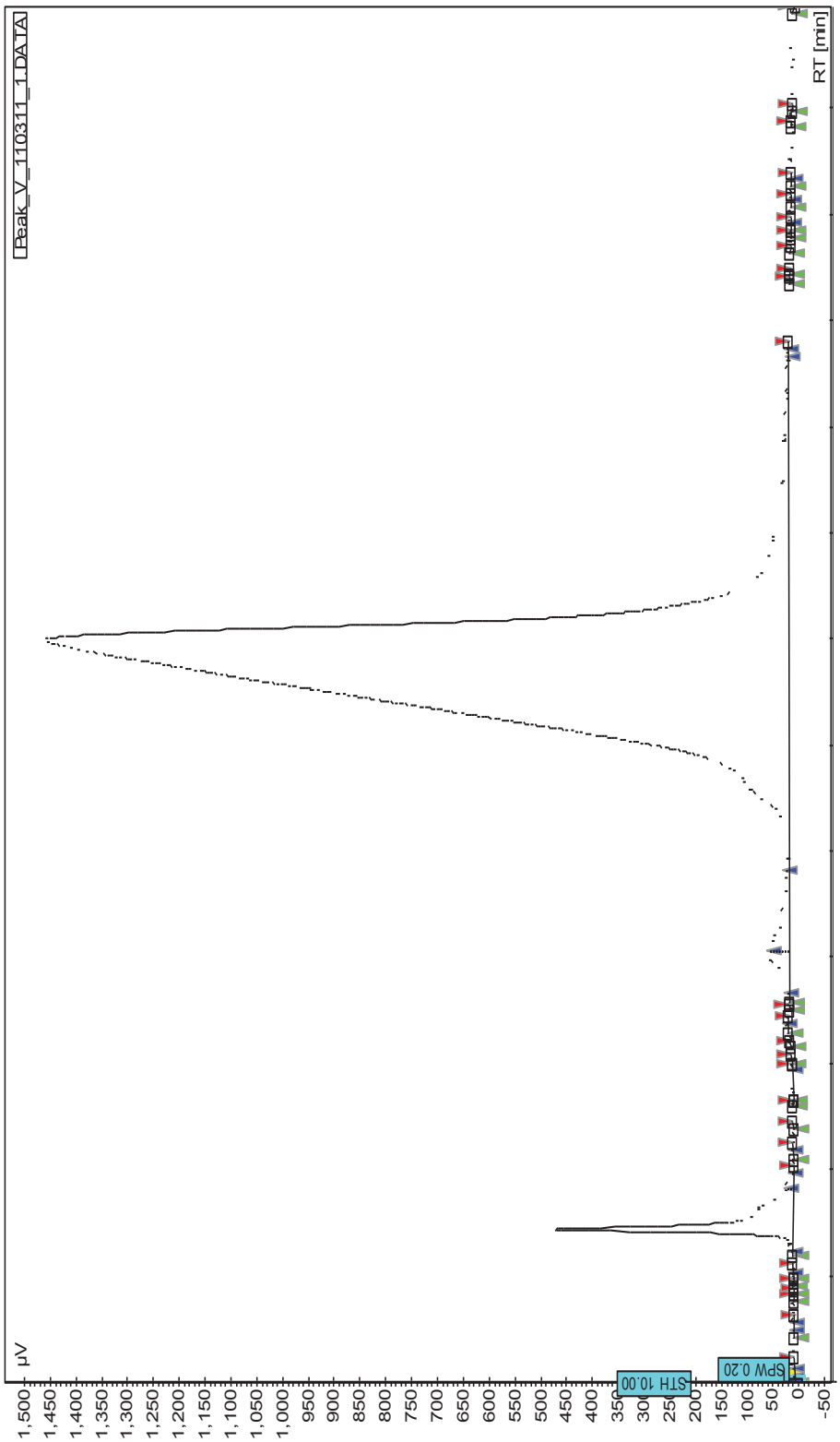

Figure A-6: Separation of Peak V. See main text for separation scheme.

Appendix B

ESI Mass Spectra

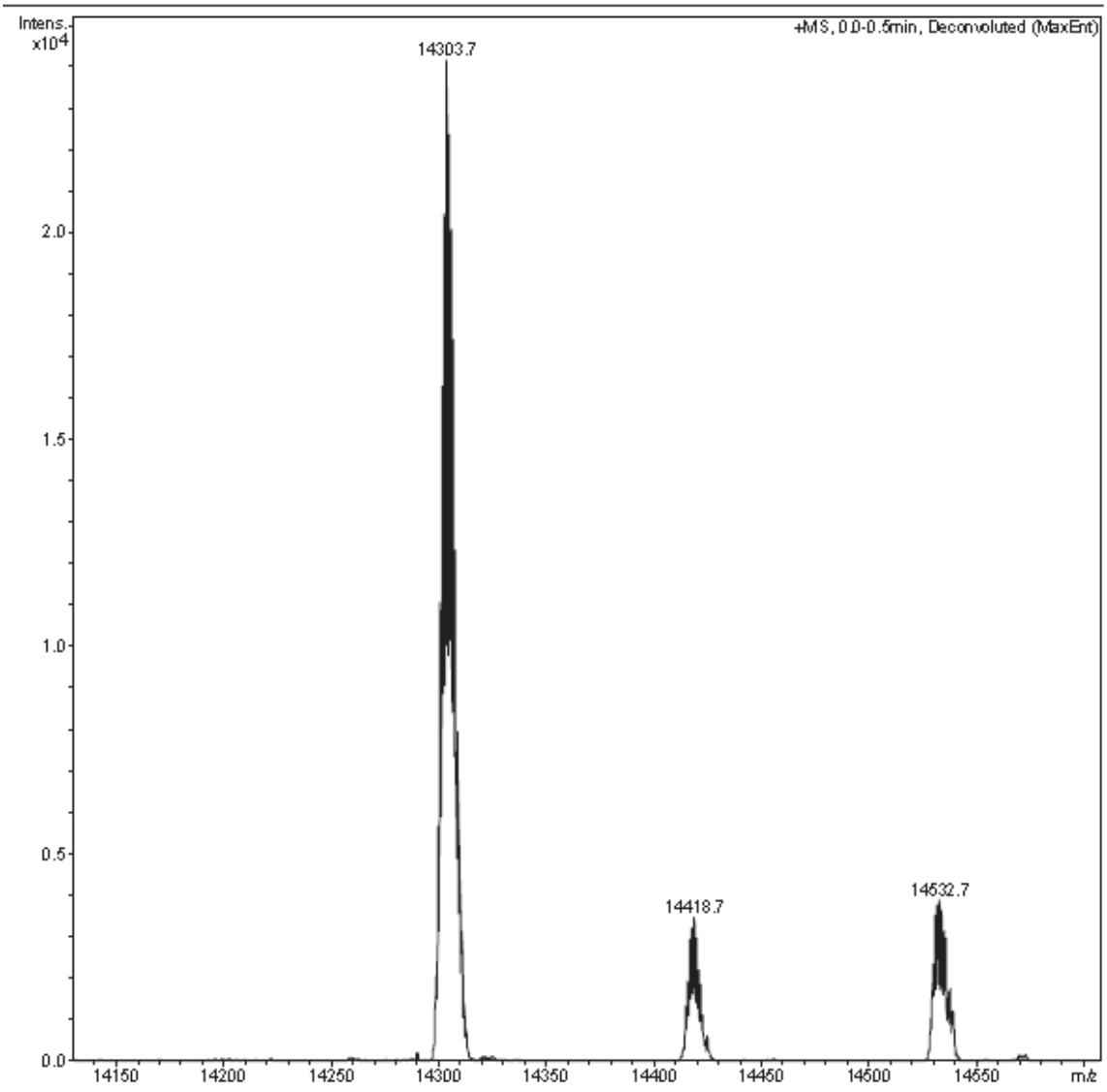

Figure B-1: ESI spectrum of native HEWL.

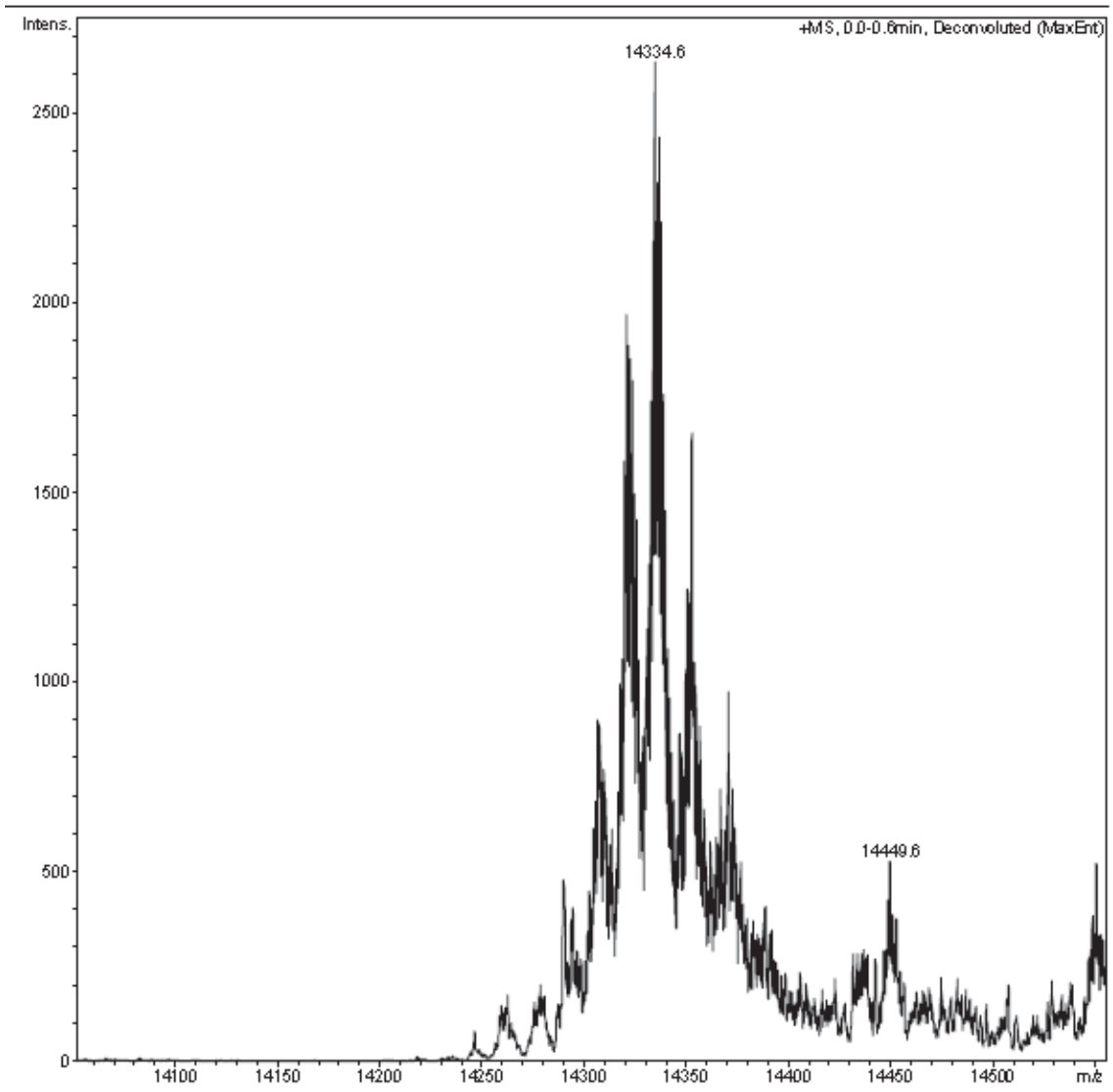

Figure B-2: ESI spectrum of Peak IA.

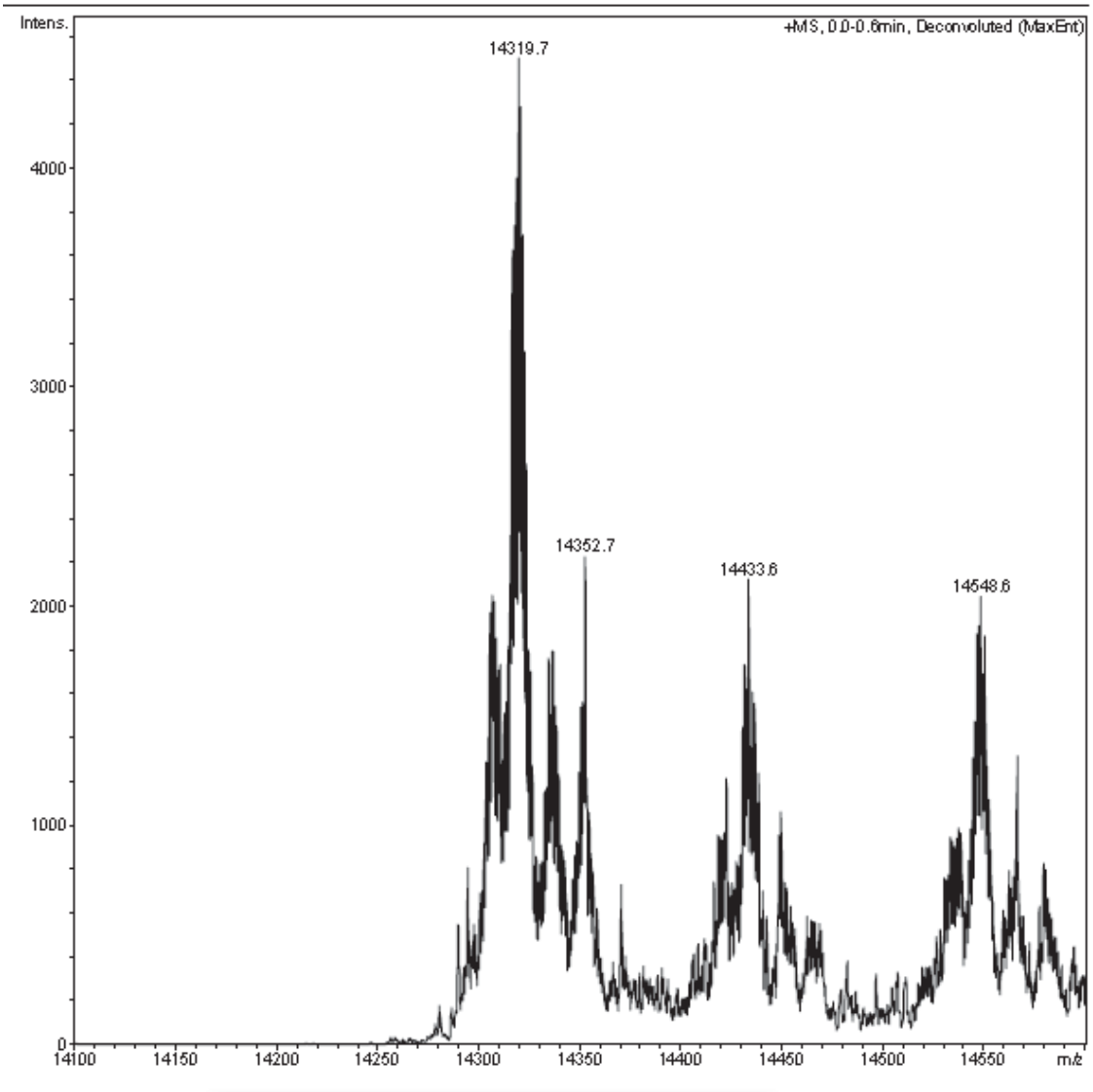

Figure B-3: ESI spectrum of Peak IB.

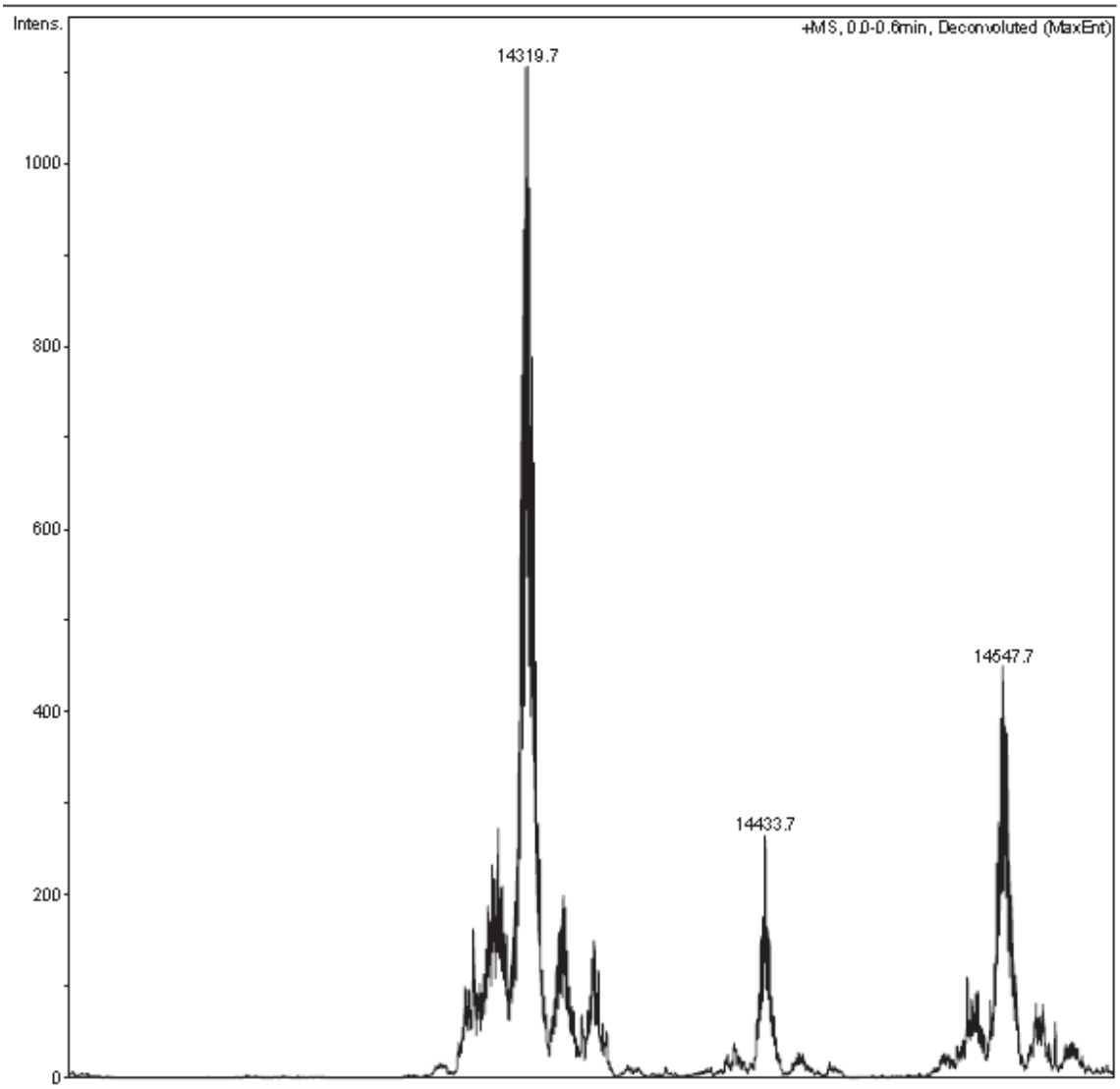

Figure B-4: ESI spectrum of Peak IIB.

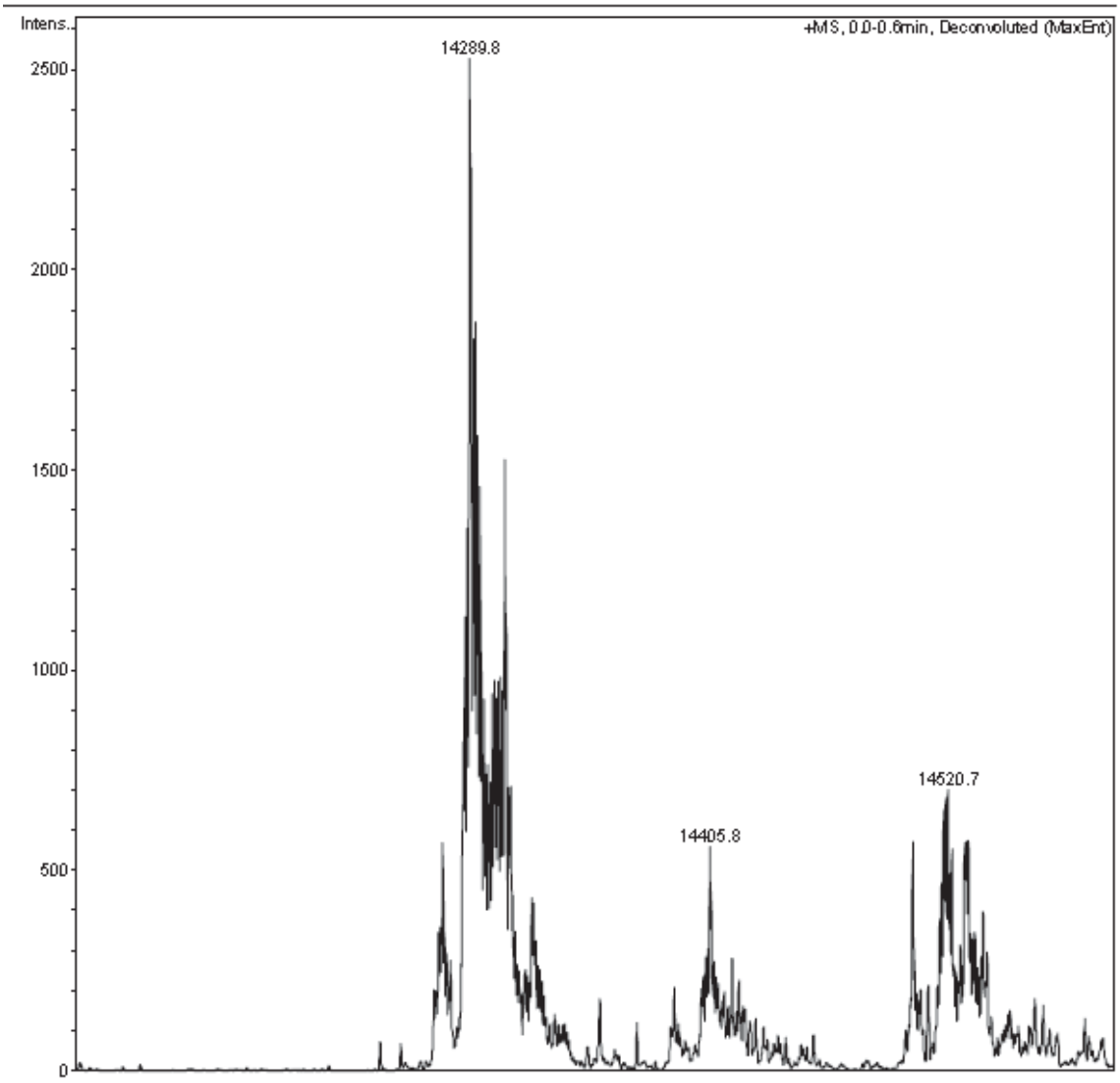

Figure B-5: ESI spectrum of Peak III.

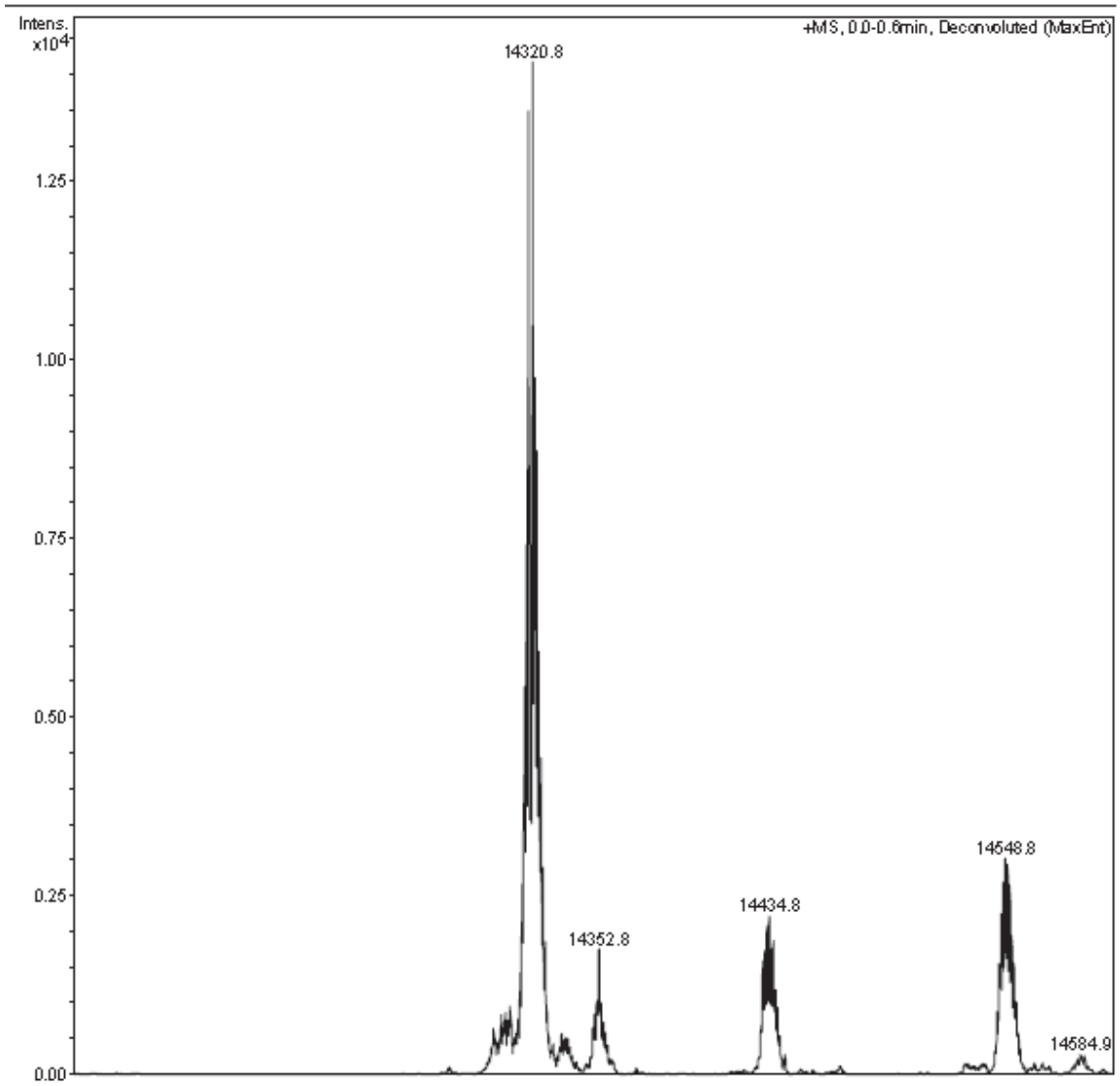

Figure B-6: ESI spectrum of Peak IV.

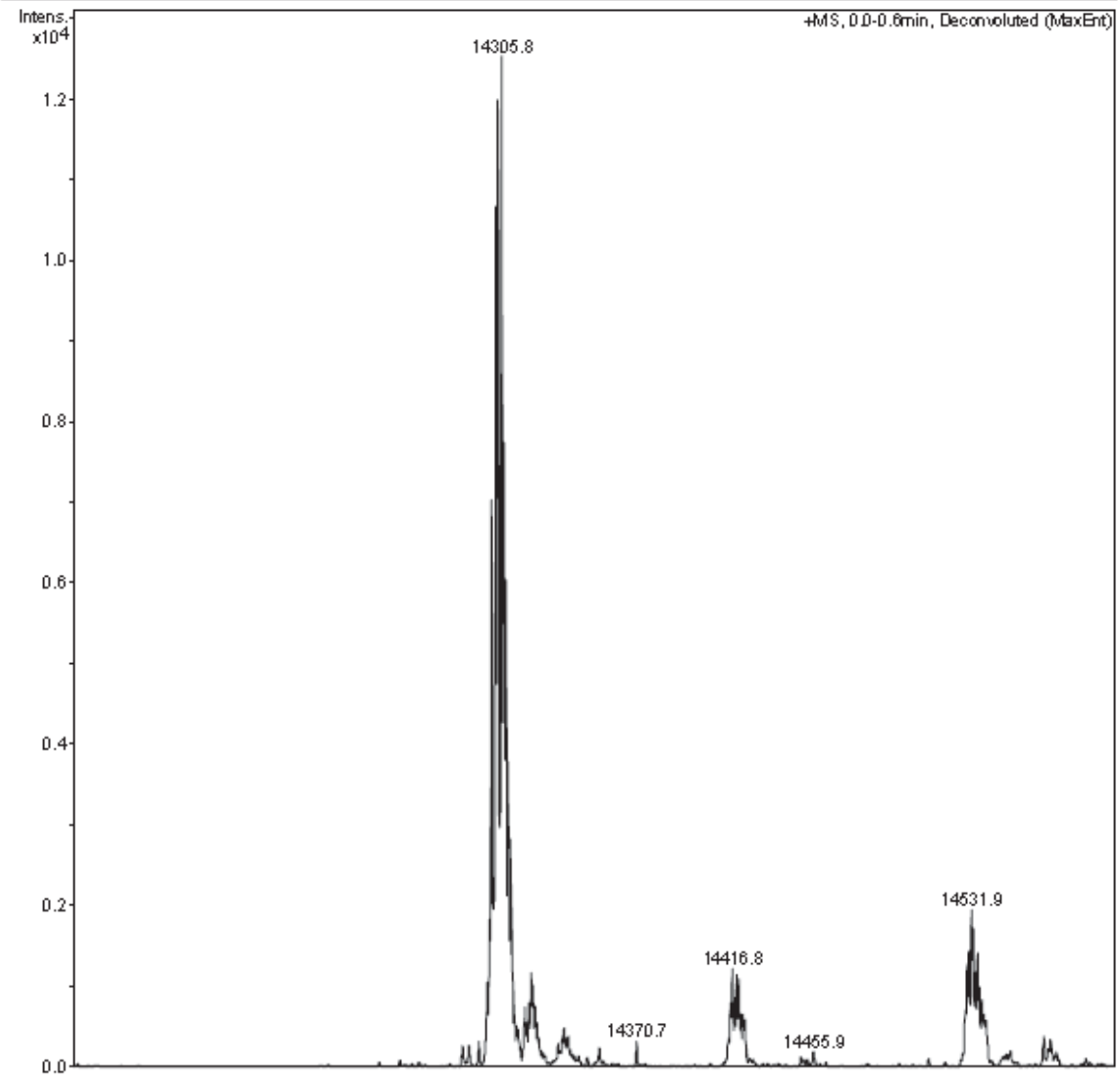

Figure B-7: ESI spectrum of Peak V

Appendix C

Tandem Mass Spectrometry Data

When digested with trypsin, one peak at 455.57^{2+} was observed, this peak was sequenced as $_6C_{(CAM)}ELAAAM_{(OX)}K_{13}$, C6 was carbamidomethylated and M12 was Oxidized.

Table C-1: Ion Labeling for Peak at 455.57^{2+}

Measured m/z	Theoretical m/z	Ion name
146.97	147.1128	$\mathbf{y_1}$
290.03	290.0805	$\mathbf{b_2}$
294.25	294.1482	$\mathbf{y_2}$
365.21	365.1853	$\mathbf{y_3}$
403.18	403.1646	$\mathbf{b_3}$
436.27	436.2224	$\mathbf{y_4}$
474.14	474.2017	$\mathbf{b_4}$
507.23	507.2595	$\mathbf{y_5}$
545.20	545.2388	$\mathbf{b_5}$
616.29	616.2759	$\mathbf{b_6}$
620.34	620.3436	$\mathbf{y_6}$
749.39	749.3862	$\mathbf{y_7}$
763.22	763.3113	$\mathbf{b_7}$

Table C-2: Detailed MS/MS Map of $_6C_{(CAM)}ELAAAM_{(OX)}K_{13}$

Δm between y-n and yn-1	Fragment Ion	Measured m/z	Sequence	Measured m/z	Fragment Ion	Δm between b-n and bn-1
			$Cys_{(CAM)}$			
129.05	$\mathbf{y_7}$	749.39	Glu	290.03	$\mathbf{b_2}$	
113.11	$\mathbf{y_6}$	620.34	Leu	403.18	$\mathbf{b_3}$	113.15
70.96	$\mathbf{y_5}$	507.23	Ala	474.14	$\mathbf{b_4}$	70.96
71.06	$\mathbf{y_4}$	436.27	Ala	545.20	$\mathbf{b_5}$	71.06
70.96	$\mathbf{y_3}$	365.21	Ala	616.29	$\mathbf{b_6}$	71.09
147.28 (131+16)	$\mathbf{y_2}$	294.25	**$Met_{(OX)}$**	763.22	$\mathbf{b_7}$	**146.93 (131+16)**
	$\mathbf{y_1}$	146.97	Lys			

This peptide was observed in sample IA (scan #2058, 2120), IB (scan #1735, 1737), II (scan #1673), III (scan #1968, 1966), IV (scan #1697, 1695) and V (scan #1805, 1803).

When digested with trypsin, one peak at 890.41.$^{1+}$ was observed, this peak was sequenced as $_{15}H(_{OX})GLDNYR_{24}$, H15 was oxidized.

Table C-3: Ion Labeling for Peak at 890.41^{1+}

Measured m/z	Theoretical m/z	Ion name
175.01	175.1190	$\mathbf{y_1}$
211.01	211.0826	$\mathbf{b_2}$
324.13	324.1666	$\mathbf{b_3}$
338.18	338.1823	$\mathbf{y_2}$
439.24	439.1936	$\mathbf{b_4}$
452.30	452.2252	$\mathbf{y_3}$
553.23	553.2365	$\mathbf{b_5}$
567.29	567.2522	$\mathbf{y_4}$
680.37	680.3362	$\mathbf{y_5}$
716.26	716.2998	$\mathbf{b_6}$
737.37	737.3577	$\mathbf{y_6}$

Table C-4: Detailed MS/MS Map of $_{15}H(_{OX})GLDNYR_{24}$

Δm between y-n and yn-1	Fragment Ion	Measured m/z	Sequence	Measured m/z	Fragment Ion	Δm between b-n and bn-1
			$His_{(OX)}$			
57	$\mathbf{y_6}$	737.37	Gly	211.01	$\mathbf{b_2}$	
113.08	$\mathbf{y_5}$	680.37	Leu	324.13	$\mathbf{b_3}$	113.12
114.99	$\mathbf{y_4}$	567.29	Asp	439.24	$\mathbf{b_4}$	115.11
114.12	$\mathbf{y_3}$	452.30	Asn	553.23	$\mathbf{b_5}$	113.99
163.17	$\mathbf{y_2}$	338.18	Tyr	716.26	$\mathbf{b_6}$	163.03
	$\mathbf{y_1}$	175.01	Arg			

This peptide was observed in sample IA (scan #2135, 2147, 2139), IB (scan #1826, 1831), II (scan #1752, 1757), III (scan #2095, 2098), IV (scan #1787, 1774, 1780, 1781) and V (scan #2020, 2025).

When digested with trypsin, one peak at 671.68^{2+} was observed, this peak was sequenced as $_{22}GYSLGNW_{(OX)}VC_{(CAM)}AAK_{33}$, C30was carbamidomethylated and W28 was Oxidized.

Table C-5: Ion Labeling for Peak at 671.68^{2+}

Measured m/z	Theoretical m/z	Ion name
218.10	218.1499	$\mathbf{y_2}$
221.00	221.0921	$\mathbf{b_2}$
289.31	289.1870	$\mathbf{y_3}$
308.08	308.1241	$\mathbf{b_3}$
421.23	421.2082	$\mathbf{b_4}$
449.22	449.2177	$\mathbf{y_4}$
478.36	478.2296	$\mathbf{b_5}$
548.30	548.2861	$\mathbf{y_5}$
592.25	592.2726	$\mathbf{b_6}$
750.30	750.3603	$\mathbf{y_6}$
794.54	794.3468	$\mathbf{b_7}$
864.39	864.4032	$\mathbf{y_7}$
893.36	893.4152	$\mathbf{b_8}$
921.33	921.4247	$\mathbf{y_8}$
$1034.54/517.92^{+2}$	$1034.5088/517.7580^{+2}$	$\mathbf{y_9}$
1053.39	1053.4458	$\mathbf{b_9}$
$1121.45/561.44^{+2}$	$1121.5408/561.2740^{+2}$	$\mathbf{y_{10}}$
1124.40	1124.4830	$\mathbf{b_{10}}$
1195.45	1195.5201	$\mathbf{b_{11}}$

Table C-6: Detailed MS/MS Map of $_{22}GYSLGNW_{(OX)}VC_{(CAM)}AAK_{33}$

Δm between y-n and yn-1	Fragment Ion	Measured m/z	Sequence	Measured m/z	Fragment Ion	Δm between b-n and bn-1
			Gly			
			Tyr	221.00	$\mathbf{b_2}$	
86.91	1121.45	$\mathbf{y_{10}}$	Ser	308.08	$\mathbf{b_3}$	87.08
113.21	1034.54	$\mathbf{y_9}$	Leu	421.23	$\mathbf{b_4}$	113.15
56.94	921.33	$\mathbf{y_8}$	Gly	478.36	$\mathbf{b_5}$	57.13
114.09	864.39	$\mathbf{y_7}$	Asn	592.25	$\mathbf{b_6}$	113.89
202 (186+16)	750.30	$\mathbf{y_6}$	**$Trp_{(OX)}$**	794.54	$\mathbf{b_7}$	**202.29 (186+16)**
99.08	548.30	$\mathbf{y_5}$	Val	893.36	$\mathbf{b_8}$	98.82
159.91 (103+57)	449.22	$\mathbf{y_4}$	$Cys_{(CAM)}$	1053.39	$\mathbf{b_9}$	160.03 (103+57)
71.21	289.31	$\mathbf{y_3}$	Ala	1124.40	$\mathbf{b_{10}}$	71.01
	218.10	$\mathbf{y_2}$	Ala	1195.45	$\mathbf{b_{11}}$	71.05
			Lys			

This peptide was observed in sample II (scan #1619), also detected in sample IV (scan #1439) with much lower intensity.

When digested with trypsin, one peak at 697.44^{2+} was observed, this peak was sequenced as $_{22}GYSLGNW_{(2OX)}VC_{(CAM)}AAK_{33}$, C30was carbamidomethylated and W28 was di-oxidized.

Table C-7: Ion Labeling for Peak at 697.44^{2+}

Measured m/z	Theoretical m/z	Ion name
218.15	218.1499	$\mathbf{y_2}$
220.97	221.0921	$\mathbf{b_2}$
289.20	289.1870	$\mathbf{y_3}$
308.14	308.1241	$\mathbf{b_3}$
421.21	421.2082	$\mathbf{b_4}$
449.29	449.2177	$\mathbf{y_4}$
478.29	478.2296	$\mathbf{b_5}$
548.36	548.2861	$\mathbf{y_5}$
766.30	766.3552	$\mathbf{y_6}$
810.43	810.3417	$\mathbf{b_7}$
880.47	880.3982	$\mathbf{y_7}$
937.39	937.4196	$\mathbf{y_8}$
1050.49	1050.5037	$\mathbf{y_9}$
1069.49	1069.4408	$\mathbf{b_9}$
1137.43	1137.5357	$\mathbf{y_{10}}$
1140.59	1140.4779	$\mathbf{b_{10}}$
1211.39	1211.5150	$\mathbf{b_{11}}$

Table C-8: Detailed MS/MS Map of $_{22}GYSLGNW_{(2OX)}VC_{(CAM)}AAK_{33}$

Δm between y-n and yn-1	Fragment Ion	Measured m/z	Sequence	Measured m/z	Fragment Ion	Δm between b-n and bn-1
			Gly			
			Tyr	220.97	$\mathbf{b_2}$	
86.94	$\mathbf{y_{10}}$	1137.43	Ser	308.14	$\mathbf{b_3}$	87.17
113.1	$\mathbf{y_9}$	1050.49	Leu	421.21	$\mathbf{b_4}$	113.07
56.92	$\mathbf{y_8}$	937.39	Gly	478.29	$\mathbf{b_5}$	57.08
114.17	$\mathbf{y_7}$	880.47	Asn			
217.94 (186+32)	$\mathbf{y_6}$	766.30	**$Trp_{(2OX)}$**	810.43	$\mathbf{b_7}$	**332.14 (114+186+32)**
99.07	$\mathbf{y_5}$	548.36	Val			
160.09	$\mathbf{y_4}$	449.29	$Cys_{(CAM)}$	1069.49	$\mathbf{b_9}$	259.06 (99+103+57)
71.05	$\mathbf{y_3}$	289.20	Ala	1140.59	$\mathbf{b_{10}}$	71.10
	$\mathbf{y_2}$	218.15	Ala	1211.39	$\mathbf{b_{11}}$	70.80
			Lys			

This peptide was observed in sample II (scan #1609), also detected in sample IV (scan #1441).

When digested with trypsin, one peak at 665.70^{2+} was observed, this peak was sequenced as $_{22}$GYSLGNW$_{(Kynurenin)}$VC$_{(CAM)}$AAK$_{33}$, C30was carbamidomethylated and W28 was Oxidized and then lose a C to form Kynurenine.

Table C-9: Ion Labeling of Peak at 665.70^{2+}

Measured m/z	Theoretical m/z	Ion name
218.12	218.1499	$\mathbf{y_2}$
221.06	221.0921	$\mathbf{b_2}$
289.19	289.1870	$\mathbf{y_3}$
308.01	308.1241	$\mathbf{b_3}$
421.16	421.2082	$\mathbf{b_4}$
449.27	449.2177	$\mathbf{y_4}$
478.17	478.2296	$\mathbf{b_5}$
548.34	548.2861	$\mathbf{y_5}$
592.21	592.2726	$\mathbf{b_6}$
738.35	738.3603	$\mathbf{y_6}$
782.47	782.3468	$\mathbf{b_7}$
852.40	852.4032	$\mathbf{y_7}$
881.44	881.4152	$\mathbf{b_8}$
909.41	909.4247	$\mathbf{y_8}$
1022.42	1022.5088	$\mathbf{y_9}$
1041.49	1041.4458	$\mathbf{b_9}$
1109.57	1109.5408	$\mathbf{y_{10}}$
1112.51	1112.4830	$\mathbf{b_{10}}$
1183.42	1183.5201	$\mathbf{b_{11}}$

Table C-10: Detailed MS/MS Map of $_{22}$GYSLGNW$_{(Kynurenin)}$VC$_{(CAM)}$AAK$_{33}$

Δm between y-n and yn-1	Fragment Ion	Measured m/z	Sequence	Measured m/z	Fragment Ion	Δm between b-n and bn-1
			Gly			
			Tyr	221.06	$\mathbf{b_2}$	
87.15	$\mathbf{y_{10}}$	1109.57	Ser	308.01	$\mathbf{b_3}$	86.95
113.01	$\mathbf{y_9}$	1022.42	Leu	421.16	$\mathbf{b_4}$	113.15
57.01	$\mathbf{y_8}$	909.41	Gly	478.17	$\mathbf{b_5}$	57.01
114.05	$\mathbf{y_7}$	852.40	Asn	592.21	$\mathbf{b_6}$	114.04
190.01 (186+4)	$\mathbf{y_6}$	738.35	**Trp$_{(Kynurenin)}$**	782.47	$\mathbf{b_7}$	**190.26 (186+4)**
99.07	$\mathbf{y_5}$	548.34	Val	881.44	$\mathbf{b_8}$	98.97
160.08	$\mathbf{y_4}$	449.27	Cys$_{(CAM)}$	1041.49	$\mathbf{b_9}$	160.05
71.07	$\mathbf{y_3}$	289.19	Ala	1112.51	$\mathbf{b_{10}}$	71.02
	$\mathbf{y_2}$	218.12	Ala	1183.42	$\mathbf{b_{11}}$	70.91
			Lys			

This peptide was observed in sample IA (scan #2566), also detected in sample II(scan #2099) and III (scan # 2442). We observed multiple loss of H in fragment ions.

When digested with trypsin, one peak at 499.34^{2+} was observed, this peak was sequenced as $_{62}W_{(Kynurenin)}WC_{(CAM)}NDGR_{68}$, C64 was carbamidomethylated and W62 was Oxidized and then lose a C to form Kynurenine (+4Da).

Table C-11: Ion Labeling of Peak at 499.34^{2+}

Measured m/z	Theoretical m/z	Ion name
175.08	175.1190	$\mathbf{y_1}$
232.09	232.1404	$\mathbf{y_2}$
347.07	347.1674	$\mathbf{y_3}$
377.08	377.1608	$\mathbf{b_2}$
461.25	461.2103	$\mathbf{y_4}$
537.35	537.1915	$\mathbf{b_3}$
622.30	621.2409	$\mathbf{y_5}$
766.25	766.2613	$\mathbf{b_5}$
807.33	807.3202	$\mathbf{y_6}$

Table C-12: Detailed MS/MS Map of $_{62}W_{(Kynurenin)}WC_{(CAM)}NDGR_{68}$

Δm between y-n and yn-1	Fragment Ion	Measured m/z	Sequence	Measured m/z	Fragment Ion	Δm between b-n and bn-1
			$\mathbf{Trp_{(Kynurenin)}}$			
186.06	$\mathbf{y_6}$	807.33	Trp	377.08	$\mathbf{b_2}$	
160.02 (103+57)	$\mathbf{y_5}$	621.27	$Cys_{(CAM)}$	537.35	$\mathbf{b_3}$	160.27 (103+57)
114.18	$\mathbf{y_4}$	461.25	Asn			
114.98	$\mathbf{y_3}$	347.07	Asp	766.25	$\mathbf{b_5}$	228.9 (114+115)
57.01	$\mathbf{y_2}$	232.09	Gly			
	$\mathbf{y_1}$	175.08	Arg			

This peptide was observed in sample IA (scan #2307), also detected in sample IB(scan #1978) and V(scan # 2149). We observed multiple loss of H in fragment ions.

When digested with trypsin, one peak at 506.13^{2+} was observed, this peak was sequenced as $_{62}W_{(OX)}WC_{(CAM)}NDGR_{68}$, C64 was carbamidomethylated and W62 was Oxidized.

Table C-13: Ion Labeling for Peak A at 506.13^{2+}

Measured m/z	Theoretical m/z	Ion name
175.10	175.1190	$\mathbf{y_1}$
232.10	232.1404	$\mathbf{y_2}$
347.23	347.1674	$\mathbf{y_3}$
389.11	389.1608	$\mathbf{b_2}$
461.27	461.2103	$\mathbf{y_4}$
549.18	549.1915	$\mathbf{b_3}$
621.25	621.2409	$\mathbf{y_5}$
663.46	663.2344	$\mathbf{b_4}$
778.22	778.2613	$\mathbf{b_5}$
807.30	807.3202	$\mathbf{y_6}$

Table C-14: Detailed MS/MS Map of $_{62}W_{(OX)}WC_{(CAM)}NDGR_{68}$

Δm between y-n and yn-1	Fragment Ion	Measured m/z	Sequence	Measured m/z	Fragment Ion	Δm between b-n and bn-1
			$\mathbf{Trp_{(OX)}}$			
186.05	$\mathbf{y_6}$	807.30	Trp	389.11	$\mathbf{b_2}$	
159.98 (103+57)	$\mathbf{y_5}$	621.25	$Cys_{(CAM)}$	549.18	$\mathbf{b_3}$	160.07 (103+57)
114.04	$\mathbf{y_4}$	461.27	Asn	663.46	$\mathbf{b_4}$	114.28
115.13	$\mathbf{y_3}$	347.23	Asp	778.22	$\mathbf{b_5}$	114.76
57.00	$\mathbf{y_2}$	232.10	Gly			
	$\mathbf{y_1}$	175.10	Arg			

This peptide was observed in sample IA (scan #2289), sample IB(scan #1966), sample II (scan #1871, 1878, 1854), sample III (scan #2221), sample IV (scan #1904) and sample V(scan # 2117).

When digested with trypsin, one peak at 506.13^{2+} was observed, this peak was sequenced as $_{62}WW_{(OX)}C_{(CAM)}NDGR_{68}$, C64 was carbamidomethylated and W63 was Oxidized.

Table C-15: Ion Labeling for Peak B at 506.13^{2+}

Measured m/z	Theoretical m/z	Ion name
175.00	175.1190	$\mathbf{y_1}$
232.07	232.1404	$\mathbf{y_2}$
347.15	347.1674	$\mathbf{y_3}$
389.15	389.1608	$\mathbf{b_2}$
461.26	461.2103	$\mathbf{y_4}$
549.21	549.1915	$\mathbf{b_3}$
621.31	621.2409	$\mathbf{y_5}$
663.14	663.2344	$\mathbf{b_4}$
778.23	778.2613	$\mathbf{b_5}$
823.31	823.3152	$\mathbf{y_6}$

Table C-16: Detailed MS/MS Map of $_{62}WW_{(OX)}C_{(CAM)}NDGR_{68}$

Δm between y-n and yn-1	Fragment Ion	Measured m/z	Sequence	Measured m/z	Fragment Ion	Δm between b-n and bn-1
			Trp			
202.00 (186+16)	$\mathbf{y_6}$	823.31	**$Trp_{(OX)}$**	389.15	$\mathbf{b_2}$	
160.05 (103+57)	$\mathbf{y_5}$	621.31	$Cys_{(CAM)}$	549.21	$\mathbf{b_3}$	160.06 (103+57)
114.11	$\mathbf{y_4}$	461.26	Asn	663.14	$\mathbf{b_4}$	113.93
115.08	$\mathbf{y_3}$	347.15	Asp	778.23	$\mathbf{b_5}$	115.09
57.07	$\mathbf{y_2}$	232.07	Gly			
	$\mathbf{y_1}$	175.00	Arg			

This peptide was observed in sample IA (scan #2267), sample III (scan #2240), sample IV (scan #1890) and sample V (scan # 2152).

When digested with trypsin, one peak at 513.42^{2+} was observed, this peak was sequenced as $_{62}W_{(2OX)}W\ C_{(CAM)}NDGR_{68}$, C64 was carbamidomethylated and W62 was di-oxidized.

Table C-17: Ion Labeling for Peak at 513.42^{2+}

Measured m/z	Theoretical m/z	Ion name
175.11	175.1190	$\mathbf{y_1}$
232.11	232.1404	$\mathbf{y_2}$
347.18	347.1674	$\mathbf{y_3}$
387.11	387.1451	$\mathbf{b_2\text{-}H_2O}$
405.16	405.1557	$\mathbf{b_2}$
461.25	461.2103	$\mathbf{y_4}$
547.11	547.1758	$\mathbf{b_3\text{-}H_2O}$
565.33	565.1864	$\mathbf{b_3}$
621.25	621.2409	$\mathbf{y_5}$
661.10	661.2187	$\mathbf{b_4\text{-}H_2O}$
679.21	679.2293	$\mathbf{b_4}$
776.23	776.2457	$\mathbf{b_5\text{-}H_2O}$
794.20	794.2563	$\mathbf{b_5}$
807.32	807.3202	$\mathbf{y_6}$
833.25	833.2671	$\mathbf{b_6\text{-}H_2O}$
851.63	851.2777	$\mathbf{b_6}$

Table C-18: Detailed MS/MS Map of $_{62}W_{(2OX)}WC_{(CAM)}NDGR_{68}$

Δm between y-n and yn-1	Fragment Ion	Measured m/z	Sequence	Measured m/z	Fragment Ion	Δm between b-n and bn-1
			$\mathbf{Trp_{(2OX)}}$			
186.07	$\mathbf{y_6}$	807.32	Trp	405.16	$\mathbf{b_2}$	
160 (103+57)	$\mathbf{y_5}$	621.25	$Cys_{(CAM)}$	565.33	$\mathbf{b_3}$	160.17 (103+57)
114.07	$\mathbf{y_4}$	461.25	Asn	679.21	$\mathbf{b_4}$	113.89
115.07	$\mathbf{y_3}$	347.18	Asp	794.20	$\mathbf{b_5}$	114.99
57	$\mathbf{y_2}$	232.11	Gly	851.63	$\mathbf{b_6}$	57.43
	$\mathbf{y_1}$	175.11	Arg			

This peptide was observed in sample IA (scan #2224, 2280, 2306), sample IB (scan # 1904), sample II (scan # 1819, 1850, 1730, 1734), sample III (scan #2072, 2069), sample IV (scan #1912, 1853) and sample V(scan # 2144, 1944, 2138).

When digested with trypsin, one peak at 521.53^{2+} was observed, this peak was sequenced as $_{62}W_{(2OX)}W\ C_{(CAM)}NDGR_{68}$, C64 was carbamidomethylated, W62 was di-oxidized and W63 was oxidized.

Table C-19: Ion Labeling for Peak at 521.53^{2+}

Measured m/z	Theoretical m/z	Ion name
174.98	175.1190	$\mathbf{y_1}$
232.04	232.1404	$\mathbf{y_2}$
347.18	347.1674	$\mathbf{y_3}$
421.17	421.1506	$\mathbf{b_2}$
461.23	461.2103	$\mathbf{y_4}$
581.23	581.1813	$\mathbf{b_3}$
621.27	621.2409	$\mathbf{y_5}$
695.20	695.2242	$\mathbf{b_4}$
810.29	810.2512	$\mathbf{b_5}$
823.32	823.3152	$\mathbf{y_6}$

Table C-20: Detailed MS/MS Map of $_{62}W_{(2OX)}W_{(OX)}C_{(CAM)}NDGR_{68}$

Δm between y-n and yn-1	Fragment Ion	Measured m/z	Sequence	Measured m/z	Fragment Ion	Δm between b-n and bn-1
			$Trp_{(2OX)}$			
202.05 (186+16)	$\mathbf{y_6}$	823.32	**$Trp_{(OX)}$**	421.17	$\mathbf{b_2}$	
160.04 (103+57)	$\mathbf{y_5}$	621.27	$Cys_{(CAM)}$	581.23	$\mathbf{b_3}$	160.06(103 +57)
114.05	$\mathbf{y_4}$	461.23	Asn	695.20	$\mathbf{b_4}$	113.97
115.14	$\mathbf{y_3}$	347.18	Asp	810.29	$\mathbf{b_5}$	115.09
57.06	$\mathbf{y_2}$	232.04	Gly			
	$\mathbf{y_1}$	174.98	Arg			

This peptide was observed in sample sample II (scan # 1755), sample III (scan #2102) and sample V(scan # 2014, 2021).

When digested with trypsin, one peak at 846.73^{2+} was observed, this peak was sequenced as $_{98}$IVSDGNGM$_{(OX)}$NAWVAWR$_{112}$, M105 was Oxidized.

Table C-21: Ion Labeling for Peak at 846.73^{2+}

Measured m/z	Theoretical m/z	Ion name
300.23	300.1918	$\mathbf{b_3}$
361.18	361.1983	$\mathbf{y_2}$
415.30	415.2187	$\mathbf{b_4}$
432.27	432.2354	$\mathbf{y_3}$
472.33	472.2402	$\mathbf{b_5}$
531.35	531.3038	$\mathbf{y_4}$
586.26	586.2831	$\mathbf{b_6}$
643.37	643.3046	$\mathbf{b_7}$
717.42	717.3831	$\mathbf{y_5}$
788.42	788.4202	$\mathbf{y_6}$
790.33	790.3400	$\mathbf{b_8}$
902.50	902.4631	$\mathbf{y_7}$
904.38	904.3829	$\mathbf{b_9}$
975.39	975.4200	$\mathbf{b_{10}}$
1049.41	1049.4985	$\mathbf{y_8}$
1106.48	1106.5200	$\mathbf{y_9}$
1161.40	1161.4993	$\mathbf{b_{11}}$
1220.48	1220.5629	$\mathbf{y_{10}}$
1260.39	1260.5677	$\mathbf{b_{12}}$
$1277.51/639.30^{+2}$	$1277.5844/639.2958^{+2}$	$\mathbf{y_{11}}$
1331.46	1331.6049	$\mathbf{b_{13}}$
$1392.52/697.06^{+2}$	$1392.6113/696.8093^{+2}$	$\mathbf{y_{12}}$
$1479.54/740.38^{+2}$	$1479.6434/740.3253^{+2}$	$\mathbf{y_{13}}$
1517.45	1517.6842	$\mathbf{b_{14}}$

Table C-22: Detailed MS/MS Map of $_{98}$IVSDGNGM$_{(OX)}$NAWVAWR$_{112}$

Δm between y-n and yn-1	Fragment Ion	Measured m/z	Sequence	Measured m/z	Fragment Ion	Δm between b-n and bn-1
			Ile			
			Val			
87.02	y_{13}	1479.54	Ser	300.23	b_3	
115.01	y_{12}	1392.52	Asp	415.30	b_4	115.07
57.03	y_{11}	1277.51	Gly	472.33	b_5	57.03
114	y_{10}	1220.48	Asn	586.26	b_6	113.93
57.07	y_9	1106.48	Gly	643.37	b_7	57.11
146.91 (131+16)	y_8	1049.41	**Met$_{(OX)}$**	790.33	b_8	**146.96 (131+16)**
114.08	y_7	902.50	Asn	904.38	b_9	114.05
71	y_6	788.42	Ala	975.39	b_{10}	71.01
186.07	y_5	717.42	Trp	1161.40	b_{11}	186.01
99.08	y_4	531.35	Val	1260.39	b_{12}	98.99
71.09	y_3	432.27	Ala	1331.46	b_{13}	71.07
	y_2	361.18	Trp	1517.45	b_{14}	185.99
			Arg			

This peptide was observed in sample IA (scan #2576), IB (scan #2263), II (scan #2102), III (scan #2452) and V (scan #2349).

When digested with trypsin, one peak at 846.67^{2+} was observed, this peak was sequenced as $_{98}IVSDGNGMNAW_{(OX)}VAWR_{112}$, W108 was Oxidized.

Table C-23: Ion Labeling for Peak at 846.67^{2+}

Measured m/z	Theoretical m/z	Ion name
299.29	300.1918	$\mathbf{b_3}$
361.22	361.1983	$\mathbf{y_2}$
415.25	415.2187	$\mathbf{b_4}$
432.30	432.2354	$\mathbf{y_3}$
472.22	472.2402	$\mathbf{b_5}$
531.30	531.3038	$\mathbf{y_4}$
586.28	586.2831	$\mathbf{b_6}$
643.31	643.3046	$\mathbf{b_7}$
733.48	733.3781	$\mathbf{y_5}$
774.44	774.3451	$\mathbf{b_8}$
804.47	804.4151	$\mathbf{y_6}$
888.31	888.3880	$\mathbf{b_9}$
918.45	918.4581	$\mathbf{y_7}$
959.35	959.4251	$\mathbf{b_{10}}$
1049.48	1049.4985	$\mathbf{y_8}$
1106.43	1106.5200	$\mathbf{y_9}$
1161.32	1161.4993	$\mathbf{b_{11}}$
1220.48	1220.5629	$\mathbf{y_{10}}$
1260.40	1260.5677	$\mathbf{b_{12}}$
$1277.51/639.40^{+2}$	$1277.5844/639.2958^{+2}$	$\mathbf{y_{11}}$
1331.42	1331.6049	$\mathbf{b_{13}}$
$1392.53/697.05^{+2}$	$1392.6113/696.8093^{+2}$	$\mathbf{y_{12}}$
$1479.49/740.54^{+2}$	$1479.6434/740.3253^{+2}$	$\mathbf{y_{13}}$
1517.55	1517.6842	$\mathbf{b_{14}}$
$1578.58/789.8595^{+2}$	$1578.58/789.8595^{+2}$	$\mathbf{y_{14}}$

Table C-24: Detailed MS/MS Map of $_{98}$IVSDGNGMNAW$_{(OX)}$VAWR$_{112}$

Δm between y-n and yn-1	Fragment Ion	Measured m/z	Sequence	Measured m/z	Fragment Ion	Δm between b-n and bn-1
			Ile			
99.09	**y_{14}**	1578.58	Val			
86.96	**y_{13}**	1479.49	Ser	299.29	**b_3**	
115.02	**y_{12}**	1392.53	Asp	415.25	**b_4**	115.96
57.03	**y_{11}**	1277.51	Gly	472.22	**b_5**	56.97
114.05	**y_{10}**	1220.48	Asn	586.28	**b_6**	114.06
56.95	**y_9**	1106.43	Gly	643.31	**b_7**	57.03
131.03	**y_8**	1049.48	Met	774.44	**b_8**	131.13
113.98	**y_7**	918.45	Asn	888.31	**b_9**	113.87
70.99	**y_6**	804.47	Ala	959.35	**b_{10}**	71.04
202.18 (186+16)	**y_5**	733.48	**Trp$_{(OX)}$**	1161.32	**b_{11}**	**201.97 (186+16)**
99	**y_4**	531.30	Val	1260.40	**b_{12}**	99.08
71.08	**y_3**	432.30	Ala	1331.42	**b_{13}**	71.02
	y_2	361.22	Trp	1517.55	**b_{14}**	186.13
			Arg			

This peptide was observed in sample IA (scan #2591).

When digested with trypsin, one peak at 846.91^{2+} was observed, this peak was sequenced as $_{98}$IVSDGDGM$_{(OX)}$NAWVAWR$_{112}$, M105 was Oxidized.

Table C-25: Ion Labeling for Peak at 846.91^{2+}

Measured m/z	Theoretical m/z	Ion name
300.21	300.1918	$\mathbf{b_3}$
361.20	361.1983	$\mathbf{y_2}$
415.24	415.2187	$\mathbf{b_4}$
432.29	432.2354	$\mathbf{y_3}$
472.33	472.2402	$\mathbf{b_5}$
531.35	531.3038	$\mathbf{y_4}$
587.30	587.2671	$\mathbf{b_6}$
644.40	644.2886	$\mathbf{b_7}$
717.44	717.3831	$\mathbf{y_5}$
791.29	791.3240	$\mathbf{b_8}$
788.44	788.4202	$\mathbf{y_6}$
902.46	902.4631	$\mathbf{y_7}$
905.43	905.3669	$\mathbf{b_9}$
976.31	976.4040	$\mathbf{b_{10}}$
1049.44	1049.4985	$\mathbf{y_8}$
1106.50	1106.5200	$\mathbf{y_9}$
1162.43	1162.4833	$\mathbf{b_{11}}$
1221.45	1221.5470	$\mathbf{y_{10}}$
1261.41	1261.5518	$\mathbf{b_{12}}$
1278.54	1278.5684	$\mathbf{y_{11}}$
1332.49	1332.5889	$\mathbf{b_{13}}$
$1393.50/697.36^{+2}$	$1393.5954/697.3013^{+2}$	$\mathbf{y_{12}}$
$1480.53/741.10^{+2}$	$1480.6274/740.8173^{+2}$	$\mathbf{y_{13}}$
1518.44	1518.6682	$\mathbf{b_{14}}$
790.51^{+2}	$1579.6958/790.3515^{+2}$	$\mathbf{y_{14}}$

Table C-26: Detailed MS/MS Map of $_{98}$IVSDGDGM$_{(OX)}$NAWVAWR$_{112}$

Δm between y-n and yn-1	Fragment Ion	Measured m/z	Sequence	Measured m/z	Fragment Ion	Δm between b-n and bn-1
			Ile			
99.49	y_{14}	790.51^{+2}	Val			
87.03	y_{13}	1480.53	Ser	300.21	b_3	
114.96	y_{12}	1393.50	Asp	415.24	b_4	115.03
57.09	y_{11}	1278.54	Gly	472.33	b_5	57.09
114.95	y_{10}	1221.45	Asp	587.30	b_6	114.97
57.06	y_9	1106.50	Gly	644.40	b_7	57.1
146.98 (131+16)	y_8	1049.44	**Met$_{(OX)}$**	791.29	b_8	**146.89 (131+16)**
114.02	y_7	902.46	Asp	905.43	b_9	114.14
71	y_6	788.44	Ala	976.31	b_{10}	70.88
186.09	y_5	717.44	Trp	1162.43	b_{11}	186.12
99.06	y_4	531.35	Val	1261.41	b_{12}	98.98
71.09	y_3	432.29	Ala	1332.49	b_{13}	71.08
	y_2	361.20	Trp	1518.44	b_{14}	185.95
			Arg			

This peptide was observed in sample III (scan #2517 and 2452), also detected in sample IB (scan #2296) and II (scan # 2132 and 2154) with less purity.

When digested with trypsin, one peak at 854.77^{2+} was observed, this peak was sequenced as $_{116}$IVSDGNGM$_{(OX)}$NAW$_{(OX)}$VAWR$_{130}$, M105 and W108 were Oxidized.

Table C-27: Ion Labeling for Peak at 854.77^{2+}

Measured m/z	Theoretical m/z	Ion name
300.12	300.1918	$\mathbf{b_3}$
361.29	361.1983	$\mathbf{y_2}$
415.27	415.2187	$\mathbf{b_4}$
432.28	432.2354	$\mathbf{y_3}$
472.36	472.2402	$\mathbf{b_5}$
531.34	531.3038	$\mathbf{y_4}$
586.40	586.2831	$\mathbf{b_6}$
643.51	643.3046	$\mathbf{b_7}$
733.43	733.3780	$\mathbf{y_5}$
790.30	790.3400	$\mathbf{b_8}$
918.58	918.4581	$\mathbf{y_7}$
904.61	904.3829	$\mathbf{b_9}$
975.17	975.4200	$\mathbf{b_{10}}$
1065.46	1065.4935	$\mathbf{y_8}$
1122.43	1122.5149	$\mathbf{y_9}$
1177.32	1177.4942	$\mathbf{b_{11}}$
1236.53	1236.5579	$\mathbf{y_{10}}$
1276.50	1276.5627	$\mathbf{b_{12}}$
1293.45	1293.5793	$\mathbf{y_{11}}$
1347.49	1347.5998	$\mathbf{b_{13}}$
1408.58	1408.6063	$\mathbf{y_{12}}$
$1495.584/740.38^{+2}$	$1495.6383/748.3228^{+2}$	$\mathbf{y_{13}}$
1533.53	1533.6791	$\mathbf{b_{14}}$

Table C-28: Detailed MS/MS Map of $_{98}$IVSDGNGM$_{(OX)}$NAW$_{(OX)}$VAWR$_{112}$

Δm between y-n and yn-1	Fragment Ion	Measured m/z	Sequence	Measured m/z	Fragment Ion	Δm between b-n and bn-1
			Ile			
			Val			
87	y_{13}	1495.58	Ser	300.12	b_3	
115.13	y_{12}	1408.58	Asp	415.27	b_4	115.15
56.92	y_{11}	1293.45	Gly	472.36	b_5	57.09
114.1	y_{10}	1236.53	Asn	586.40	b_6	114.04
56.97	y_9	1122.43	Gly	643.51	b_7	57.11
146.88 (131+16)	y_8	1065.46	**Met$_{(OX)}$**	790.30	b_8	**146.79 (131+16)**
185.16 (114+71)	y_7	918.58	Asn	904.61	b_9	114.31
			Ala	975.17	b_{10}	70.56
202.09 (186+16)	y_5	733.43	**Trp$_{(OX)}$**	1177.32	b_{11}	**202.15 (186+16)**
99.06	y_4	531.34	Val	1276.50	b_{12}	99.18
70.99	y_3	432.28	Ala	1347.49	b_{13}	70.99
	y_2	361.29	Trp	1533.53	b_{14}	186.04
			Arg			

This peptide was observed in sample IA (scan #2534) and II (scan #2133).

When digested with trypsin, one peak at 854.70^{2+} was observed, this peak was sequenced as $_{98}$IVSDGNGMNAW$_{(2OX)}$VAWR$_{112}$, W108 were di-oxidized.

Table C-29: Ion Labeling for Peak at 854.70^{2+}

Measured m/z	Theoretical m/z	Ion name
300.15	300.1918	$\mathbf{b_3}$
361.22	361.1983	$\mathbf{y_2}$
415.22	415.2187	$\mathbf{b_4}$
432.29	432.2354	$\mathbf{y_3}$
472.31	472.2402	$\mathbf{b_5}$
531.34	531.3038	$\mathbf{y_4}$
586.22	586.2831	$\mathbf{b_6}$
643.24	643.3046	$\mathbf{b_7}$
749.47	749.3729	$\mathbf{y_5}$
774.20	774.3451	$\mathbf{b_8}$
820.46	820.4100	$\mathbf{y_6}$
888.28	888.3880	$\mathbf{b_9}$
934.47	934.4530	$\mathbf{y_7}$
959.40	959.4251	$\mathbf{b_{10}}$
1065.47	1065.4935	$\mathbf{y_8}$
1122.48	1122.5149	$\mathbf{y_9}$
1177.32	1177.4942	$\mathbf{b_{11}}$
1236.48	1236.5579	$\mathbf{y_{10}}$
1276.48	1276.5627	$\mathbf{b_{12}}$
$1293.53/647.52^{+2}$	$1293.5793/647.2933^{+2}$	$\mathbf{y_{11}}$
1347.53	1347.5998	$\mathbf{b_{13}}$
$1408.47/704.73^{+2}$	$1408.6063/704.8068^{+2}$	$\mathbf{y_{12}}$
$1495.52/748.60^{+2}$	$1495.6383/748.3228^{+2}$	$\mathbf{y_{13}}$
1533.42	1533.6791	$\mathbf{b_{14}}$

Table C-30: Detailed MS/MS Map of $_{98}$IVSDGNGMNAW$_{(2OX)}$VAWR$_{112}$

Δm between y-n and yn-1	Fragment Ion	Measured m/z	Sequence	Measured m/z	Fragment Ion	Δm between b-n and bn-1
			Ile			
			Val			
87.05	$\mathbf{y_{13}}$	1495.52	Ser	300.15	$\mathbf{b_3}$	
114.94	$\mathbf{y_{12}}$	1408.47	Asp	415.22	$\mathbf{b_4}$	115.07
57.05	$\mathbf{y_{11}}$	1293.53	Gly	472.31	$\mathbf{b_5}$	57.09
114	$\mathbf{y_{10}}$	1236.48	Asn	586.22	$\mathbf{b_6}$	113.91
57.01	$\mathbf{y_9}$	1122.48	Gly	643.24	$\mathbf{b_7}$	57.02
131	$\mathbf{y_8}$	1065.47	Met	774.20	$\mathbf{b_8}$	130.96
114.01	$\mathbf{y_7}$	934.47	Asn	888.28	$\mathbf{b_9}$	114.08
70.99	$\mathbf{y_6}$	820.46	Ala	959.40	$\mathbf{b_{10}}$	71.12
218.13 (186+32)	$\mathbf{y_5}$	749.47	**Trp$_{(2OX)}$**	1177.32	$\mathbf{b_{11}}$	**217.92 (186+32)**
99.05	$\mathbf{y_4}$	531.34	Val	1276.48	$\mathbf{b_{12}}$	99.16
71.07	$\mathbf{y_3}$	432.29	Ala	1347.53	$\mathbf{b_{13}}$	71.05
	$\mathbf{y_2}$	361.22	Trp	1533.42	$\mathbf{b_{14}}$	185.89
			Arg			

This peptide was observed in sample IA (scan #2613).

When digested with trypsin, one peak at 862.71^{2+} was observed, this peak was sequenced as $_{98}$IVSDGNGMNAW$_{(2OX)}$VAWR$_{112}$, M105 was oxidized and W108 were di-oxidized.

Table C-31: Ion Labeling for Peak at 862.71^{2+}

Measured m/z	Theoretical m/z	Ion name
300.16	300.1918	**b_3**
361.29	361.1983	**y_2**
415.27	415.2187	**b_4**
432.35	432.2354	**y_3**
472.32	472.2402	**b_5**
531.40	531.3038	**y_4**
586.28	586.2831	**b_6**
749.29	749.3729	**y_5**
772.39	772.3294	**b_8 –H2O**
790.25	790.3400	**b_8**
820.49	820.4100	**y_6**
934.45	934.4530	**y_7**
975.24	975.4200	**b_{10}**
1081.39	1081.4884	**y_8**
1138.59	1138.5098	**y_9**
1193.29	1193.4891	**b_{11}**
1252.39	1252.5528	**y_{10}**
1292.45	1292.5576	**b_{12}**
1309.55	1309.5742	**y_{11}**
1363.51	1363.5947	**b_{13}**
1549.24	1549.6740	**b_{14}**

Table C-32: Detailed MS/MS Map of $_{98}$IVSDGNGM$_{(OX)}$NAW$_{(2OX)}$VAWR$_{112}$

Δm between y-n and yn-1	Fragment Ion	Measured m/z	Sequence	Measured m/z	Fragment Ion	Δm between b-n and bn-1
			Ile			
			Val			
			Ser	300.16	**b_3**	
			Asp	415.27	**b_4**	115.11
57.16	**y_{11}**	1309.55	Gly	472.32	**b_5**	57.05
113.8	**y_{10}**	1252.39	Asn	586.28	**b_6**	113.96
57.2	**y_9**	1138.59	Gly			
146.94 (131+16)	**y_8**	1081.39	**Met$_{(OX)}$**	790.25	**b_8**	**203.97 (57+131+16)**
113.96	**y_7**	934.45	Asn			
71.2	**y_6**	820.49	Ala	975.24	**b_{10}**	184.99 (114+71)
217.89 (186+32)	**y_5**	749.29	**Trp$_{(2OX)}$**	1193.29	**b_{11}**	**218.05 (186+32)**
99.05	**y_4**	531.40	Val	1292.45	**b_{12}**	99.16
71.06	**y_3**	432.35	Ala	1363.51	**b_{13}**	71.06
	y_2	361.29	Trp	1549.24	**b_{14}**	185.73
			Arg			

This peptide was observed in sample IB (scan #2088).

When digested with trypsin, one peak at 531.64^{2+} was observed, this peak was sequenced as $_{117}$GTDVQAW$_{(OX)}$IR$_{125}$, W123 was Oxidized.

Table C-33: Ion Labeling for Peak at 531.64^{2+}

Measured m/z	Theoretical m/z	Ion name
158.96	159.0764	$\mathbf{b_2}$
175.03	175.1190	$\mathbf{y_1}$
274.18	274.1034	$\mathbf{b_3}$
288.17	288.2030	$\mathbf{y_2}$
373.17	373.1718	$\mathbf{b_4}$
490.37	490.2772	$\mathbf{y_3}$
501.18	501.2304	$\mathbf{b_5}$
561.38	561.3144	$\mathbf{y_4}$
572.27	572.2675	$\mathbf{b_6}$
689.39	689.3729	$\mathbf{y_5}$
774.36	774.3417	$\mathbf{b_7}$
788.34	788.4413	$\mathbf{y_6}$
887.43	887.4258	$\mathbf{b_8}$
$903.43/452.06^{+2}$	$903.4683/452.2378^{+2}$	$\mathbf{y_7}$

Table C-34: Detailed MS/MS Map of $_{117}$GTDVQAW$_{(OX)}$IR$_{125}$

Δm between y-n and yn-1	Fragment Ion	Measured m/z	Sequence	Measured m/z	Fragment Ion	Δm between b-n and bn-1
			Gly			
			Thr	158.96	$\mathbf{b_2}$	
115.09	$\mathbf{y_7}$	903.43	Asp	274.18	$\mathbf{b_3}$	115.22
98.95	$\mathbf{y_6}$	788.34	Val	373.17	$\mathbf{b_4}$	98.99
128.01	$\mathbf{y_5}$	689.39	Gln	501.18	$\mathbf{b_5}$	128.01
71.01	$\mathbf{y_4}$	561.38	Ala	572.27	$\mathbf{b_6}$	71.09
202.20 (186+16)	$\mathbf{y_3}$	490.37	**Trp$_{(OX)}$**	774.36	$\mathbf{b_7}$	**202.09 (186+16)**
113.14	$\mathbf{y_2}$	288.17	Ile	887.43	$\mathbf{b_8}$	113.07
	$\mathbf{y_1}$	175.03	Arg			

This peptide was observed in sample II (scan #1662).

Table C-35: Percent Oxidation of M12 in Peptide Fragment CELAAAMK

Sample	Peak Area of Un-oxidized Fragment	Peak Area of Oxidized Fragment	Total Peak Area	Percent Oxidation of M12
IA	461363864	1.91×10^5	4.62×10^8	0.04
IB	119381908	3.11×10^5	1.20×10^8	0.26
IIB	26299024	4.13×10^5	2.67×10^7	1.55
III	83207829	1.61×10^5	8.34×10^7	0.19
IV	27031969	1.22×10^5	2.72×10^7	0.45
V	276705505	1.15×10^5	2.77×10^8	0.04

Table C-36: Percent Oxidation of H15 in Peptide Fragment HGLDNYR

Sample	Peak Area of Un-oxidized Fragment	Peak Area of Oxidized Fragment	Total Peak Area	Percent Oxidation of H15
IA	9165753	1.32×10^8	1.41×10^8	93.51
IB	19245227	1.25×10^8	1.45×10^8	86.69
IIB	2967539	4.31×10^6	7.27×10^6	59.20
III	7613298	2.46×10^6	1.01×10^7	24.45
IV	432429	2.52×10^8	2.52×10^8	99.83
V	1495718	2.58×10^6	4.08×10^6	63.30

Table C-37: Percent Single Oxidation of W28 in Peptide Fragment GYSLGNWVCAAK

Sample	Peak Area of Un-oxidized Fragment	Peak Area of Oxidized Fragment	Total Peak Area*	Percent Single Oxidation of W28
IA	1.13×10^9	0	1.13×10^9	0
IB	1.26×10^8	0	1.30×10^8	0
IIB	2.61×10^7	0	2.79×10^7	0
III	7.49×10^8	0	7.51×10^8	0
IV	3.33×10^6	0	4.29×10^6	0
V	2.08×10^8	9.28×10^3	2.08×10^8	0

*Total Peak Area includes all areas of peaks for different oxidation events, not just the event of interest and the un-oxidized fragment areas.

Table C-38: Percent Di-oxidation of W28 in Peptide Fragment GYSLGNWVCAAK

Sample	Peak Area of Un-oxidized Fragment	Peak Area of Di-oxidized Fragment	Total Peak Area	Percent Di-oxidation of W28
IA	1.13×10^9	0	1.13×10^9	0
IB	1.26×10^8	0	1.30×10^8	0
IIB	2.61×10^7	3.69×10^5	2.79×10^7	1.32
III	7.49×10^8	9.60×10^5	7.51×10^8	0.13
IV	3.33×10^6	2.35×10^5	4.29×10^6	5.48
V	2.08×10^8	0	2.08×10^8	0

Table C-39: Percent Kynureinination of W28 in Peptide Fragment GYSLGNWVCAAK

Sample	Peak Area of Un-oxidized Fragment	Peak Area of Kynureininated Fragment	Total Peak Area	Percent Kynureninination of W28
IA	1.13×10^9	1.43×10^6	1.13×10^9	0.13
IB	1.26×10^8	3.95×10^6	1.30×10^8	3.05
IIB	2.61×10^7	1.43×10^6	2.79×10^7	5.12
III	7.49×10^8	9.50×10^5	7.51×10^8	0.13
IV	3.33×10^6	7.25×10^5	4.29×10^6	16.90
V	2.08×10^8	5.43×10^5	2.08×10^8	0.26

Table C-40: Percent Single Oxidation of W62 or W63* in Peptide Fragment WWCNDGR

Sample	Peak Area of Un-oxidized Fragment	Peak Area of Oxidized Fragment	Total Peak Area	Percent Oxidation of W62 or W63
IA	292865398	1.20×10^6	3.29×10^8	0.36
IB	470468234	6.29×10^6	4.82×10^8	1.30
IIB	166992114	4.08×10^6	1.79×10^8	2.28
III	193996588	7.90×10^6	2.11×10^8	3.74
IV	484189094	3.79×10^6	4.90×10^8	0.77
V	19193233	5.24×10^6	3.09×10^7	16.98

*Detector could not discern between single oxidations of the two residues due to co-elution.

Table C-41: Percent Di-oxidation of W62 in Peptide Fragment WWCNDGR

Sample	Peak Area of Un-oxidized Fragment	Peak Area of Di-oxidized Fragment	Total Peak Area	Percent Di-oxidation of W62
IA	292865398	1.08×10^7	3.29×10^8	3.29
IB	470468234	2.99×10^6	4.82×10^8	0.62
IIB	166992114	2.10×10^6	1.79×10^8	1.17
III	193996588	8.01×10^5	2.11×10^8	0.38
IV	484189094	1.08×10^6	4.90×10^8	0.22
V	19193233	4.33×10^6	3.09×10^7	14.01

Table C-42: Percent Di-oxidation of W62 and Single Oxidation of W63 in Peptide Fragment WWCNDGR

Sample	Peak Area of Un-oxidized Fragment	Peak Area of Triply Oxidized Fragment	Total Peak Area	Percent Di-oxidation of W62 and Single Oxidation of W63
IA	292865398	2.44×10^7	3.29×10^8	7.40
IB	470468234	2.72×10^6	4.82×10^8	0.56
IIB	166992114	5.63×10^6	1.79×10^8	3.15
III	193996588	8.57×10^6	2.11×10^8	4.06
IV	484189094	1.09×10^6	4.90×10^8	0.22
V	19193233	2.12×10^6	3.09×10^7	6.88

Table C-43: Percent Single Oxidation of M105 or W108* in Peptide Fragment IVSDGN(D)GMNAWVAWR

Sample	Peak Area of Un-oxidized Fragment	Peak Area of Oxidized Fragment	Total Peak Area	Percent Oxidation of M105 or W108
IA	289122439	1.36×10^8	4.43×10^8	30.66
IB	50064548	1.16×10^8	1.66×10^8	69.86
IIB	250289769	9.81×10^6	2.72×10^8	3.61
III	68992880	3.86×10^7	1.08×10^8	35.89
IV	15434767	1.66×10^6	1.71×10^7	9.69
V	77258970	1.80×10^7	9.53×10^7	18.93

*Detector could not discern between single oxidations of the two residues due to co-elution.

Table C-44: Percent Di-oxidation of W108 in Peptide Fragment IVSDGNGMNAWVAWR

Sample	Peak Area of Un-oxidized Fragment	Peak Area of Di-oxidized Fragment	Total Peak Area	Percent Di-oxidation of W108
IA	289122439	4.58×10^6	4.43×10^8	1.03
IB	50064548	0	1.66×10^8	0
IIB	250289769	0	2.72×10^8	0
III	68992880	0	1.08×10^8	0
IV	15434767	0	1.71×10^7	0
V	77258970	0	9.53×10^7	0

Table C-45: Percent Single Oxidation of M105 and W108 in Peptide Fragment IVSDGNGMNAWVAWR

Sample	Peak Area of Un-oxidized Fragment	Peak Area of Oxidized Fragment	Total Peak Area	Percent Oxidation of M105 and W108
IA	289122439	1.34×10^7	4.43×10^8	3.02
IB	50064548	0	1.66×10^8	0
IIB	250289769	1.19×10^7	2.72×10^8	4.37
III	68992880	0	1.08×10^8	0
IV	15434767	0	1.71×10^7	0
V	77258970	0	9.53×10^7	0

Table C-46: Percent Single Oxidation of W123 in Peptide Fragment GTDVQAWIR

Sample	Peak Area of Un-oxidized Fragment	Peak Area of Oxidized Fragment	Total Peak Area	Percent Oxidation of W123
IA	41249143	0	4.12×10^7	0
IB	14474910	0	1.45×10^7	0
IIB	26302057	1.74×10^6	2.80×10^7	6.19
III	8173664	6.13×10^5	8.79×10^6	6.98
IV	4689574	0	4.69×10^6	0
V	1063287	2.80×10^4	1.09×10^6	2.57